Interference Characterization and Suppression for Multiuser Direct-sequence Spread-spectrum System

BARKER
MASSACHUSETTS INSTITUTE OF TECHNOLOGY
JUL 31 2002
LIBRARIES

by

Mingxi Fan

Submitted to the Department of Electrical Engineering and Computer Science
in partial fulfillment of the requirements for the degree of

Doctor of Philosophy

at the

MASSACHUSETTS INSTITUTE OF TECHNOLOGY

June 2002

© Massachusetts Institute of Technology 2002. All rights reserved.

Author .....
Department of Electrical Engineering and Computer Science
May 3, 2002

Certified by .....
Kai-Yeung Siu
Associate Professor
Thesis Supervisor

Accepted by .....
Arthur C. Smith
Chairman, Department Committee on Graduate Students

Interference Characterization and Suppression for Multiuser Direct-sequence Spread-spectrum System

by

Mingxi Fan

Submitted to the Department of Electrical Engineering and Computer Science
on May 3, 2002, in partial fulfillment of the
requirements for the degree of
Doctor of Philosophy

Abstract

In this thesis we investigate efficient modulation and detection techniques for the uplink (i.e. transmission from mobile to base station) of a DS-CDMA network. Specifically, the thesis contains three parts. In the first part, we focus on the mobile transmitter. In particular, we evaluate and compare the spectral efficiency of two promising variable rate DS-CDMA transmission techniques, multicode (MCD) and variable-spreading-gain (VSG), under the presence of multiple-access (user-to-user) interferences (MAI) and multipath interferences. The uniqueness of our study is that in bit-error-rate evaluation, instead of approximating the interference as Gaussian noise (which has been done in most of the previous studies), we incorporate both power and distribution of interferences into consideration. We show where the Gaussian assumption may give misleading answers and how our results in these cases are different from those obtained in the past. In part two and three of the thesis, we focus on the base station receiver. Specifically, we present effective joint detection techniques that have good performance-complexity tradeoff. Part two of the thesis introduces a class of novel multistage parallel interference cancellation algorithms based on stage-by-stage minimum mean-squared error (MMSE) optimization. We show that this scheme is capable of achieving significantly better performance than other algorithms with similar complexity. Part three of the thesis presents a low-complexity dual-mode multiuser detector that dynamically switches its detection mode between the matched-filter receiver and the decorrelator. We show that this detector is capable of achieving the performance of a decorrelator but with significant savings in processing power and complexity.

Thesis Supervisor: Kai-Yeung Siu
Title: Associate Professor

Acknowledgments

First, I would like to thank my advisor, Prof. Kai-Yeung (Sunny) Siu for his dedicated and enlightening guidance during the course of my doctoral study. I have always enjoyed the many-hour per week discussions (even in late night sometimes) with Prof. Siu on various research related topics. His inspirational advice not only improved my analytical skills but also constantly broadened my vision in communications research. In addition, he also taught me how to effectively express my ideas through both writing and presentation. Many times, he would go through my paper drafts word by word to improve my technical writing skills. I really appreciate all his help and guidance throughout my graduate study at MIT, and I don't think I could have completed this thesis without him.

Next, my special thanks go to Prof. David Staelin and Prof. Franz Kaertner for spending many hours of their valuable time to be on my doctoral committee. Their generous support and insightful suggestions have been a great help and an integral part in improving the quality of the thesis. It has been a great pleasure and privilege for me to have them on my thesis committee. In addition, I would also like to thank many other MIT faculty who have taught me, advised me, and provided me valuable insights on a wide range of subjects, in particular Prof. Dave Forney (my master thesis supervisor), Prof. Mildred Dresselhaus (my undergraduate advisor), Prof. Munther Dahleh (my graduate counselor), Prof. Arthur Smith, Prof. Alan Willsky, Prof. Gregory Wornell, and Prof. Muriel Medard.

Another special person that I would like to thank is my colleague Thit Minn. Being a more senior graduate student than me, Thit has always been a great friend and mentor, especially when I just started exploring CDMA. Thit seems to know everything there is about wireless communications and has a very unique and fundamental vision on CDMA related technologies. Whenever I talk to him, I not only learn something new and interesting but also start to think more analytically and critically about various aspects of my own research. His amazing insights really helped me to find the key problems and to progress through my research, and I really enjoyed

working with him. In fact, results outlined in chapter 2 of the thesis is a joint work between Thit and myself.

I also would like to thank my friends and colleagues who have supported and helped me throughout my graduate study. In terms of research, I have always enjoyed and benefited from technical discussions and/or working with Changqing Zheng, Albert Chan, Chanvee Chong, Irina Medvedev, Anne Pak, Frank Wang, Boris Bartolome, Nancy Neigus, Michael Parr, Vanu Bose, Andrew Chiu, Alok Shah, Romeo Velearde, Derek Chan, Alfred Ebrahim, On-Wa Yeung, and many others. I also want to thank friends (with so many of them and so limited space, I apologize that I cannot list them one by one) who have supported me mentally and lightened my mood when I was in deep stress. I would not have made it through MIT without them.

At last, but not the least, my deepest appreciation goes to my family, as home is always where I can find the most support, comfort, and motivation. I would like to thank my Dad and Mom for their consistent support, understanding, advice, and love throughout all these years. I am very lucky to have such special and caring parents. I would also like to thank my grandparents, in particular my incredible grandmother, for their love, care and wise advice. I want thank my younger sister, Mingyan, who is going through MIT undergraduate study right now, for her love and for always providing her beautifully written poems and funny stories to lighten me up in the most stressful times. And finally, I want to thank my wife, Jun, for her dearest love and support. I really appreciate her understanding and patience as I have always been so busy. Without her quietly taking care of our everything besides my research even during her pregnancy, there is no way I could have completed this thesis on time.

Contents

List of Figures

Chapter 1

Introduction

Direct-sequence spread-spectrum (DSSS) modulation technique has been developed since the 1950's [52]. The initial applications were primarily military related such as anti-jamming tactical communications, guidance systems, and experimental anti-multipath systems [59, 69]. With the surge of personal wireless communication systems in the last one and half decade, DSSS modulation became the foundation of the physical layer of a widely adopted multiuser wireless communication system known as the direct-sequence code-division multiple-access (DS-CDMA) system. In this thesis, we investigate practical physical-layer modulation and detection techniques for wireless DS-CDMA system that exhibit robust performance in the presence of interference. In this chapter, we first provide some essential background information on DS-CDMA system in section 1.1. Those who are familiar with CDMA can skip over this section and go to section 1.2, where we describe the problems addressed by the thesis and summarize our key contributions.

1.1 Background

1.1.1 DSSS modulation and its application to multiuser communication networks

Direct-sequence spread-spectrum (DSSS) system is a digital transmission technique in which the signal occupies a bandwidth in excess of the minimum necessary to send the information [52]. The bandwidth expansion is accomplished through the so-called "direct-sequence" spreading modulation, in which a fast, data-independent code sequence, defined as the spreading code, causes rapid phase transitions in the data-bearing carrier. Each element of the code sequence is referred to as a chip, and hence the rate that the spreading code is running at during DSSS modulation is referred to as the chip rate. The ratio between the chip rate and the data (symbol) rate (before spreading) is called the processing gain, or the spreading gain, which measures the amount of bandwidth expansion due to the spreading process. An illustration of DSSS modulation in both time and frequency domains is illustrated in figure 1-1. To recover the data of a DSSS user, the receiver normally employs matched-filter detection that correlates the received signal with the spreading code in each symbol interval.

In essence, DSSS modulation trades power for bandwidth to combat interferences. One of the main original motivations of DSSS modulation is to enhance the anti-jamming capability of a power-limited single-user communication system by providing the user additional degrees of freedom (or dimensions) after spreading [59]. DSSS modulation can be viewed as a process that projects a low dimensional (i.e. narrow frequency-band) data signal onto a high dimensional (i.e. wide frequency-band) signal space. The total number of dimensions in the system after spreading is typically N times that before spreading, where N is the processing gain. The philosophy is that since the user data only occupies one of the N available dimensions, a large N will give the jammer a hard time to guess where to concentrate the energy of its jamming signal in the signal space.

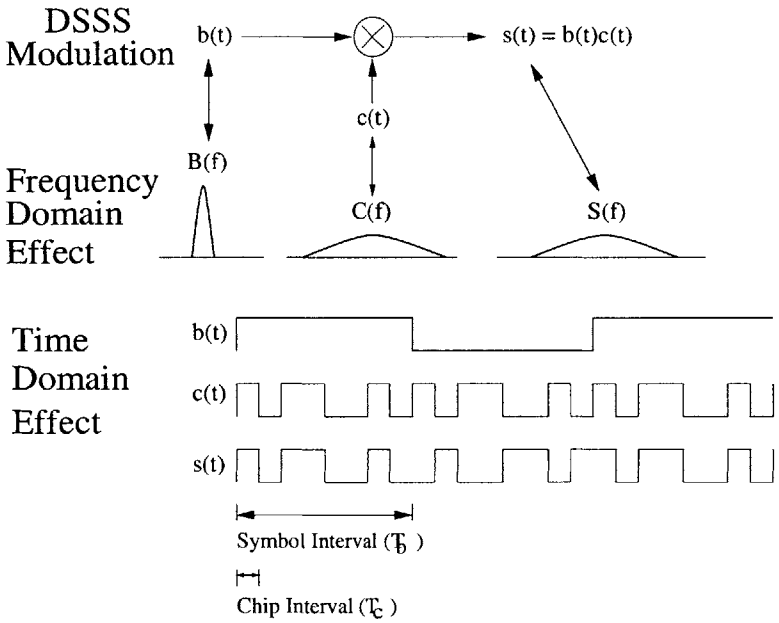

Figure 1-1: Direct-sequence spread-spectrum modulation illustration

Interestingly, these extra dimensions also turn out to be very useful for multiplexing subscribers in a multiuser communication system. Theoretically, by assigning different users different spreading codes, we have mapped each user onto a unique "code" dimension in the system, which then allows all users to simultaneous transmit over the same frequency band without significantly interfering each other. The total number of available dimensions in the system is determined by the spreading gain. This is exactly the principle behind the well-known direct-sequence code-division multiple-access (DS-CDMA) system that is widely used in cellular communications today. In a DS-CDMA system, the data of each user is spread via DSSS modulation with a user-specific spreading code, which is also used by the receiver to "de-spread" or demodulate the data for the desired user. The spreading codes are typically designed to have low cross-correlations to minimize interferences between different users. There are many benefits for using DS-CDMA for mobile radio communication, which we discuss next.

1.1.2 Why use DS-CDMA for mobile communication?

Cellular perspective

Before showing the advantages of using DS-CDMA for mobile communications, we first introduce briefly the cellular concept, which is the foundation of mobile radio networks today. Prior to the deployment of cellular networks, the design objective of early mobile radio system was to achieve a large coverage area by using a single, high powered transmitter with an antenna mounted on a tall tower [58]. While this indeed achieves good coverage, the total number of users that the system can accommodate is extremely limited due to scarcity of the available wireless spectrum, which has to be shared among all users over a very large geographical region.

The birth of cellular concept was a major breakthrough in solving the spectral-congestion problem [4, 20]. Instead of having a single, high-powered transmitter, a cellular network uses many small base stations (cell site) with relatively low transmit power, each serving a small geographical area (i.e. a cell). Since propagation loss of the radio signal is proportional to the nth power of the propagation distance, where n is between 2 and 6 depending on the environment (large for urban area and indoors and small for rural and light-of-sight connections)[58], the same frequency spectrum can be reused at distant cells without causing much interference among each other. The concept of frequency reuse essentially enables the network to serve an unlimited number of users using finite spectrum, since, if the user population increases beyond the capacity of the existing cell, a new cell site can always be built to accommodate the demand.

The frequency reuse pattern of a typical cellular network is illustrated in figure 1-2. The hexagonal cell shape shown in the figure is a conceptual and simplistic model of the radio coverage for each base station. In a typical cellular network, the overall available spectrum is divided equally into R disjoint frequency bands, each of which is reused in every R cells that are far apart enough from each other to minimize intercell interferences. In figure 1-2, we have $R = 3$. R is called the frequency reuse factor, and its value depends on the cell size, distance between the cells, error performance target

of the system, and the spectrum-sharing strategy used within each cell. A smaller R implies a more spectrally efficient system, as well as easier frequency planning.

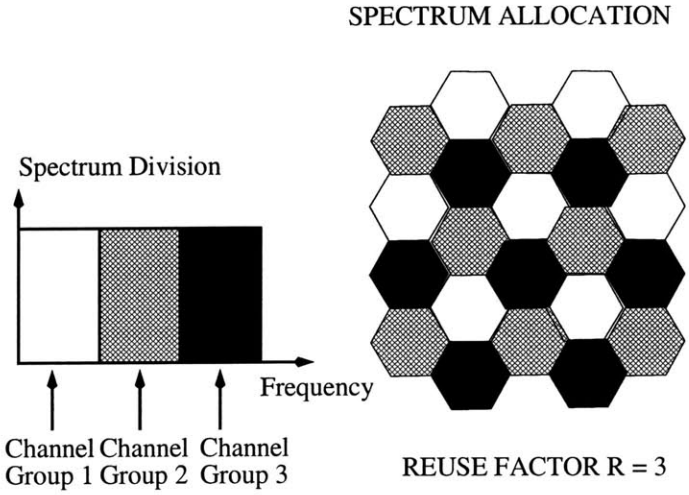

Figure 1-2: Frequency assignment in a cellular network, reuse factor = 3

Within each cell, all users make calls through the base station positioned at the center of the cell. The transmission link from the base station to user terminals is called the forward link or the downlink, while communication from user terminals to the base station is named the reverse link or the uplink. A key design consideration for the cellular network is how to let users share the available spectrum within each cell to communicate with the base station in both links. One method is to divide the total spectrum within the cell into small disjoint bands and assign one frequency band to each user. This is the well-known frequency-division multiple-access (FDMA) concept. The first generation (analog) cellular systems are mostly FDMA-based. For instance, the first U.S. cellular telephone system – Advance Mobile Phone Service (AMPS)[87], developed by AT&T Bell Labs in the 1970s and first deployed in 1983 in Chicago, is a FDMA system that assigns a 30 KHz band to each user in both up- and downlink. The 30 KHz band was later reduced to 10 KHz in the N-AMPS standard (developed by Motorola) using digital techniques to increase the spectral efficiency [58]. The first cellular system in Europe, the European Total Access Communication System (ETACS), developed in the 1980's, was also FDMA-based and in fact almost

identical to AMPS, except that the bandwidth for each user is 25 KHz per link [38]. The advantage of FDMA system is its low cost and simplicity. Its major drawback, however, is the low spectral efficiency due to large spectral gaps between adjacent frequency bands [58]. Since the analog bandpass filter used in practical FDMA systems often does not have a sharp cutoff, these gaps are necessary to prevent severe cross-talks or adjacent-channel interferences.

With the aid of digital technology, a second spectrum-sharing mechanism, time-division multiple-access (TDMA), was proposed to increase the spectral efficiency. In TDMA, the spectrum within a cell is divided into a number of wider frequency bands, each shared by several users. Within each band, every user is assigned a time slot and therefore transmits only a fraction of the time. With wider frequency bands, the waste of bandwidth due to the spectral gaps in TDMA is much less than that in analog FDMA systems, even though a guard-time needs to be inserted between time-slots for TDMA systems to avoid interference. Most of the second generation (digital) cellular networks are TDMA-based. A well-known example is the Global System for Mobile (GSM) developed in Europe. In GSM, the available frequencies within a cell is divided into channels of 200 KHz wide, each of which is then used to accommodate eight full-rate users using eight time-slots, each of $576.9\mu sec$ duration [47]. Another example is the US-TDMA (IS-54 and IS-136), which uses 30 KHz wide frequency channel to serve three full-rate users, with each user assigned a time-slot of $6.667ms$ [14].

In contrast to FDMA and TDMA, in a DS-CDMA system, all users in the cell spread their signal over the entire available spectrum and transmit at the same time. What differentiates one user from another, as mentioned before, is the user-specific spreading code. DS-CDMA is the core technology used in IS-95, a popular second generation (digital) cellular standard that is mainly developed by Qualcomm and deployed in North America and parts of Asia including South Korea and China. In IS-95, the transmitted signal of all users spread over the same 1.25 MHz wide spectrum in a cell, and the typical spreading gain is 64 [65]. A typical chip rate used in IS-95 is 1.2288 mega-chips per second (Mcps), which corresponds to a chip

duration of approximately 0.8 microseconds. Figure 1-3 illustrates the differences between FDMA, TDMA and DS-CDMA.

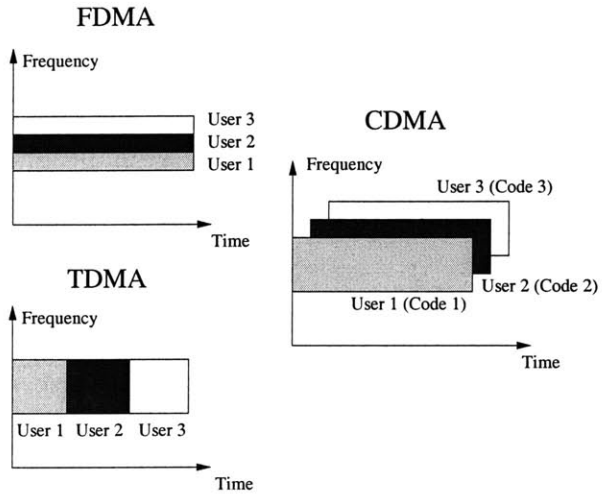

Figure 1-3: Multiple access technologies in cellular network

Within each cell, given the same amount of spectrum, it can be shown that in theory, the total number of available dimensions is the same for FDMA, TDMA, and DS-CDMA [10]. So what is the advantage of using DS-CDMA over the other two? To answer that, we have to first look beyond single-cell setting and consider frequency planning for a large cellular network. In this aspect, both FDMA and TDMA systems have a frequency reuse factor that is greater than one. This means that neighboring cells in these systems cannot use the same frequency. A typical frequency reuse factor for analog FDMA system is 7, while for TDMA system, the reuse factor is normally between 4 and 7, and at best 3 [21]. The need for frequency reuse adds significant trouble to frequency planning. For example, if we need to build a new base station within an existing cell to accommodate the booming subscriber population, frequency allocation for all near-by cells in this case will have to be re-calculated and re-assigned. For DS-CDMA, however, the same spectrum can be reused in every cell, as long as the neighboring cells employ different sets of spreading codes. Hence, the frequency reuse factor in a DS-CDMA system is 1. The feature of universal frequency reuse offered by CDMA network significantly simplifies the task of cellular planning, and

this is in fact one of the main reasons why DS-CDMA is chosen as the dominant technology for the coming third generation (3G) cellular systems, such as wide-band CDMA (WCDMA) (chip rate 4.096 Mcps) and CDMA2000 (chip rate 3.6864 Mcps) [2].

In addition to universal frequency reuse, DS-CDMA also has a soft-capacity, which FDMA and TDMA systems do not have. In both FDMA and TDMA, the maximum number of users allowed in each cell is hard-limited by the number of available frequency or time slots, respectively. In DS-CDMA, however, the capacity is "soft" in a sense that the total number of users in the system is only interference-limited. Users can be admitted into the system as long as the bit-error rate of all in-cell users are within their performance target. Consequently, any reduction in interferences immediately gives room to new users. Thus, practical DS-CDMA systems often use interference reduction schemes, such as sectorization and voice activity detection, to increase the capacity. For instance, in IS-95 CDMA, each cell is divided into three 120 degree sectors using directional antennas, which, ideally, reduces the user-to-user interference by a factor of three. In reality, the gain is slightly less due to spillage between the sectors. In addition, IS-95 uses variable rate voice encoding together with data-burst puncturing technique such that whenever a user is silent during a conversation, the silence is detected and nothing is transmitted. In this way, the low duty cycle of human speech further reduces the user-to-user interferences. It has been suggested in [21] that with sectorization, voice activity detector, and universal frequency reuse, a DS-CDMA network is capable of offering a much higher capacity than FDMA or TDMA based networks.

Radio propagation perspective

In addition to its attractive features in cellular networks, a DS-CDMA system also exhibits robust performance in a general mobile radio propagation environment at relatively low cost. Unlike wire-line channels that are usually stationary and predictable, radio channels are extremely random. The signal path between the transmitter and the receiver in a wireless channel can vary from simple line-of-sight to one that is

severely obstructed by buildings, hills and trees. In addition, speed of the user terminal also affects quality of the received signals. Generally, propagation models have been made to describe the average received signal strength at a given distance from the transmitter, as well as the variability of the signal strength in close proximity to a particular location. Propagation models that predict the mean signal strength for an arbitrary transmitter-receiver separation distance are called *large-scale propagation model*, since they characterize signal strength over a large distance (on the order of tens of kilometers). On the other hand, propagation models that characterize the rapid fluctuations of the received signal strength over short travel distances or short time durations are called *small-scale* or *fading model* [58, 83]. Communication link between a mobile subscriber with its designated near-by base station can be typically described using small-scale fading model, which we briefly describe next.

The small-scale fading effects are mainly created by the existence of time-varying multiple signal paths between the transmitter and the receiver, or in short, multipath propagations. In succinct terms, multipath propagation introduces two types of distortions into the received signal. First, if the bandwidth of the transmitted signal is larger than the coherent bandwidth [55, 83] of the channel (i.e. the portion of channel frequency response that is approximately flat), or equivalently, if the symbol interval is smaller than the delay spread of the channel, the received signal is going to suffer from inter-symbol interferences (ISI), as multipath components of the the current symbol may get into other symbol intervals and therefore cause signal smearing. In such cases, an equalizer is needed to suppress the ISI. Second, due to movements of the user terminal and the surrounding objects, the multipath components in general vary with time. These randomly time-varying phases and amplitudes of the different multipath components cause fluctuations in received signal strength and thereby introduces *fading*. If there is no ISI, then we have frequency-non-selective or flat fading, in which there is one signal path with time-varying amplitude. This signal path is in fact the sum of many weak paths that arrive at the receiver in a very short time interval [83]. If the time offsets between the paths are large enough to cause ISI, then we have multipath or frequency-selective fading, in which the amplitude of

each path varies with time. The amplitude of each faded path is in general modeled as a Rayleigh random variable [55]. Without proper processing, fading significantly degrades the quality of the received signal. For example, in a flat fading channel, the error probability of a single user system only falls off with $1/SNR$ (where SNR is the signal-to-noise ratio (SNR)), whereas in an ideal additive white Gaussian noise (AWGN) channel, the error probability decreases exponentially with increasing SNR [55].

Many wireless systems need to use equalization techniques to suppress multipath interferences (ISI). For example, in a TDMA system, equalization is necessary since the bandwidth of the transmitted signal normally exceeds the coherent bandwidth of the channel. There are many equalization techniques available, such as maximal likelihood detection, zero-forcing, MMSE, precoding, and decision feedback [23, 36]. While equalizations can be quite effective, they also add significant complexity at the receiver. In addition, equalization does not improve the system performance as far as fading is concerned. To combat fading, diversity techniques are typically employed. The underlying principle of diversity is to transmit the same information via different links or channels to the receiver. The motivation is that the more transmission links we use, the more likely that signal strength on one or more of the links will be strong. Typical diversity techniques include frequency-diversity, time-diversity, path-diversity, polarization diversity, and spatial diversity [55]. With diversity, the error probability in single-user channel now falls off with the Lth power of $1/SNR$, where L is the order of diversity, i.e. the number of transmission links used [55].

In DS-CDMA, the chip rate used for DSSS modulation is typically much higher than the coherent bandwidth of the channel. Whereas conventional modulation techniques require an equalizer to suppress ISI, the CDMA spreading codes are designed to provide low correlation (the larger the spreading gain, the lower the correlations) between successive symbols. Thus multipath propagation in this case merely provides multiple versions of the transmitted signal at the receiver. Furthermore, if the multipath components are delayed by more than one chip duration, they can be resolved and combined using a RAKE receiver, which provides diversity gain to combat fading.

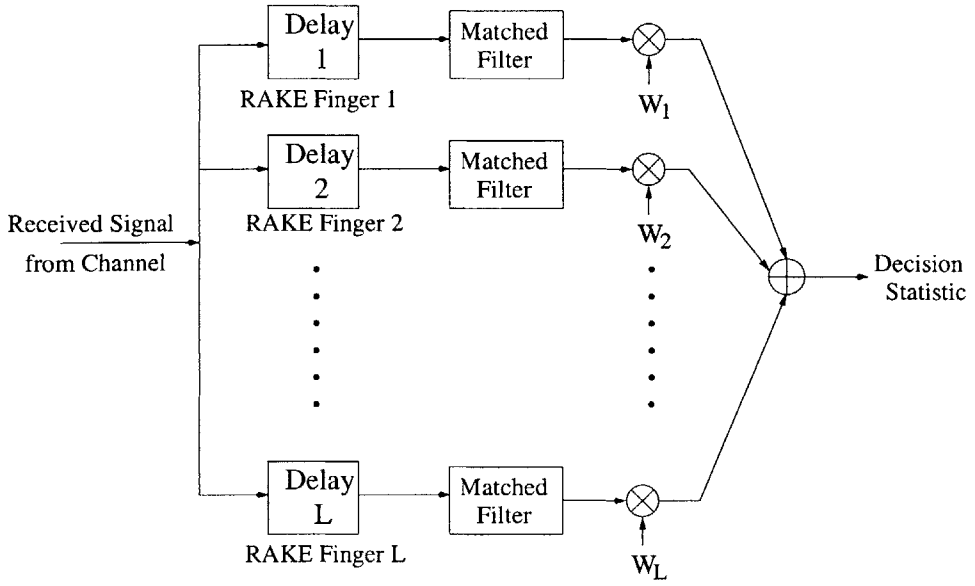

Figure 1-4: RAKE receiver for DS-CDMA systems

The RAKE receiver, as shown in figure 1-4, is essentially a diversity receiver designed specifically for DSSS modulated system, where the diversity is provided by the observation that with large spreading gain, the multipath components are approximately uncorrelated from one another when their relative propagation delays exceed one chip interval [7]. The responsibility of the RAKE receiver is to combine time-delayed versions of the original signal transmission (i.e. caused by multipath) in order to improve the signal-to-noise ratio and obtain diversity gain at the receiver. It accomplishes this task by first using a separate correlation (matched-filter) receiver (a RAKE finger) for each of the resolvable multipath signals and then combining the components from all RAKE fingers using a weighting scheme. Typical weighting schemes used in practice include equal-gain combining (EGC) and maximal ratio combining (MRC). In EGC, decisions from all fingers are assigned equal weights, whereas in MRC, the weight assigned to each finger is proportional to its output SNR, which can be easily measured at the matched-filter output. Subsequently, if M correlators (i.e. M RAKE fingers) are used to capture the M strongest multipath components, the order of diversity gain is approximately M. In the current IS-95 standard, the receiver in the downlink uses three RAKE fingers followed by MRC,

while the uplink receiver uses four RAKE fingers followed by MRC. With RAKE receiver, we essentially turn the originally undesirable multipath propagation into diversity gain to combat fading. Yet, the complexity of RAKE receiver is much less than most of the equalization techniques. Thus, DSSS is preferable over many other modulation techniques from the radio propagation perspective because the use of spreading and RAKE receiver together can lead to robust performance in multipath fading channels.

1.1.3 DS-CDMA transceiver design for up- and downlink

We now examine and compare the transceiver block diagram for a typical DS-CDMA user in the downlink (figure 1-5) and the uplink (figure 1-6). In both links, at the transmitter, the information bits from the source coder (i.e. vocoder or data compressor) of each user first go through channel encoder and interleaver, which offer protections against random and bursty errors introduced by the channel, respectively. The coded and interleaved symbols are phase modulated and spread by the user-specific spreading code via DSSS modulation. The output after the spreading is pulse-shaped and processed by the radio-frequency (RF) front-end before being transmitted to the channel. In the downlink, signals from all users are transmitted by the base station at the same time, while in the uplink, the user signals are transmitted by the individual mobile terminals independently and undergo different transmission delays and channel effects. In both cases, the channel contains signals from all in-cell users distorted by the channel plus additive background noise that can be modeled as zero-mean wide-sense stationary Gaussian process. At the receiver, for both up- and downlink, a conventional DS-CDMA system employs single-user (i.e. matched-filter) detection followed by RAKE combiner for each user. The detected data symbols are further processed by the deinterleaver and the channel decoder to recover the original information bits.

The design considerations for DS-CDMA system are different for the uplink and the downlink. In the downlink, signals of all in-cell users are transmitted synchronously by the base-station transmitter. This enables us to assign orthogonal

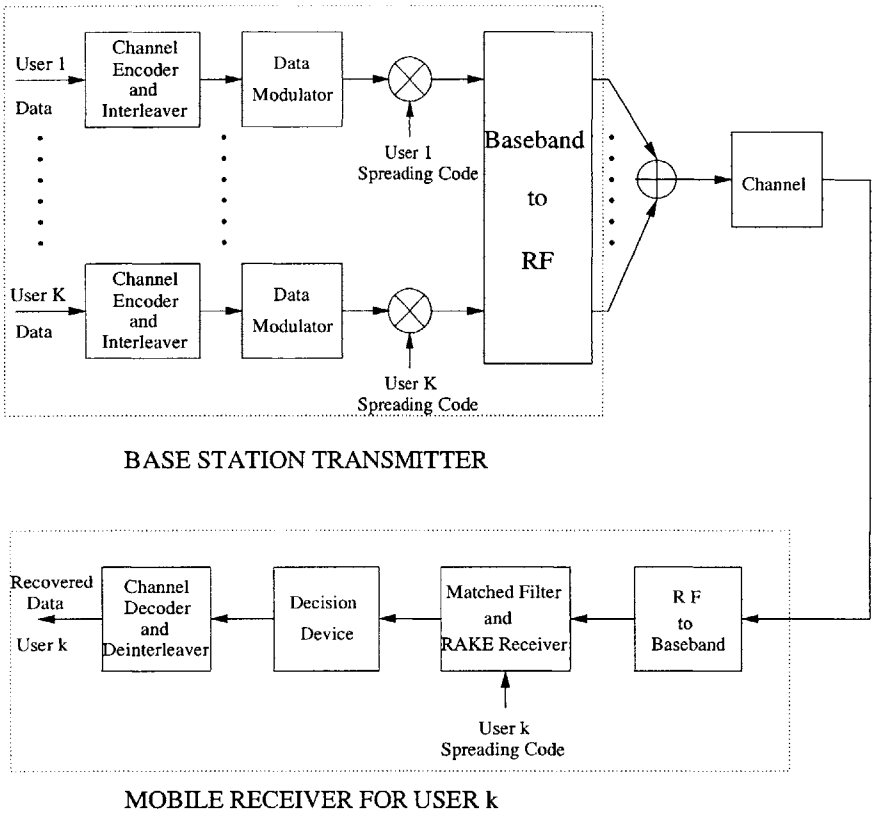

Figure 1-5: Standard DS-CDMA transceivers in the downlink

spreading codes to the subscribers to eliminate user-to-user interferences within each signal path. For example, in IS-95, orthogonal Walsh-Hadamard codes are used for spreading in the downlink. However, multipath creates problems for this system. First, many orthogonal codes, such as Walsh-Hadamard, have poor autocorrelation properties that makes the user vulnerable to multipath interferences from its own signal. To alleviate this problem, the spread data of each user is also scrambled by a long pseudo-random (PN) code with good autocorrelation property before transmission [18]. In practical cellular systems, these PN codes are cell-specific and is hence the same for all users in a given cell. The downlink transmitter of a standard DS-CDMA user is shown in figure 1-7. Second, even though orthogonal codes are used, data of different subscribers may still interfere with each other since the user signals in different paths may not be orthogonal. To solve this problem, since the (base-station) transmitter can tolerate significantly more complexity than the mo-

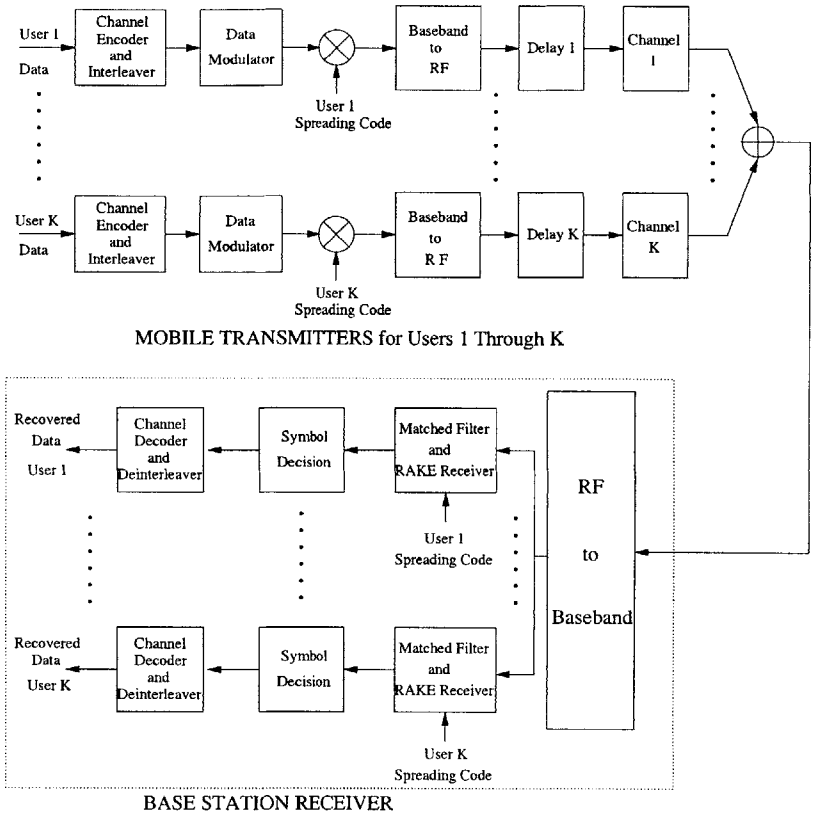

Figure 1-6: Standard DS-CDMA transceivers in the uplink

bile receiver, transmitter precoding and adaptation techniques have been proposed to tune out the user-to-user interferences, which has been addressed in a number of literatures [29, 79, 82]. The basic approach here is that, assuming a slowly time-varying channel, the transmitter learns the channel first using pilot sequences and then assigns subscribers the appropriate spreading codes that lead to minimal user-to-user interferences for the given channel.

In the uplink, which is the focus of this thesis, the interference conditions and design considerations are very different from that in the downlink. Here, since all user terminals transmit asynchronously to the base station, it is very difficult to find enough spreading codes that yield low cross-correlations for all users at all possible time-shifts. In fact, in practical systems such as IS-95, only long PN codes are used for spreading. Therefore, with only matched-filter detection, the user signals interfere with each other even in the same signal path. This leads to the well-known near-

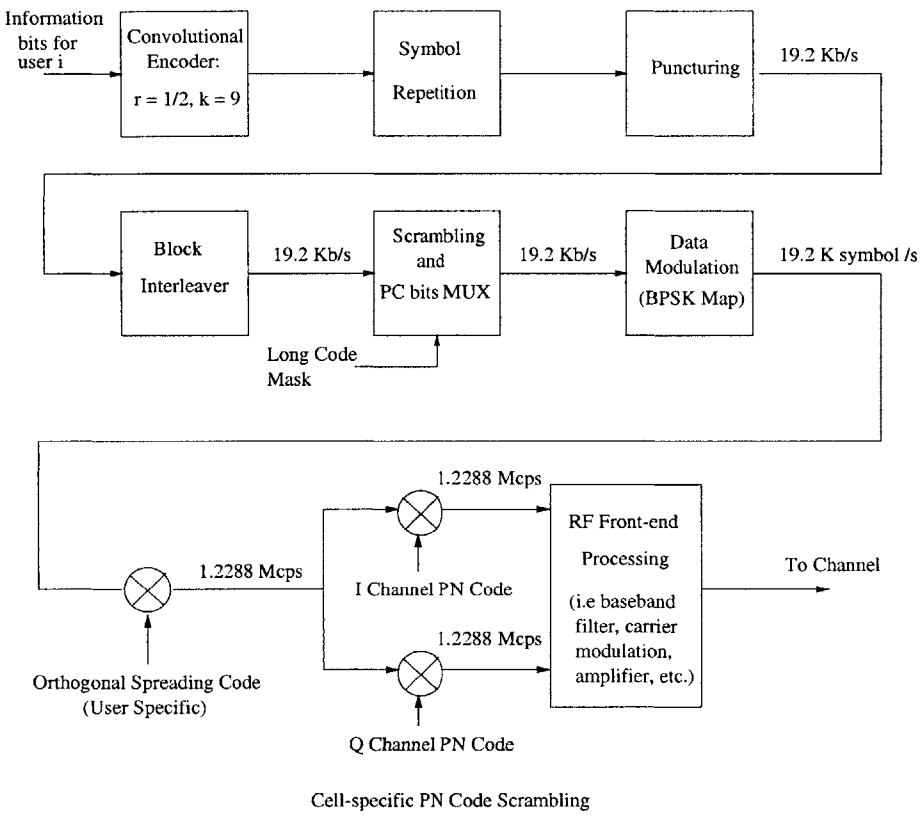

Figure 1-7: The downlink transmitter of a typical DS-CDMA user

far problem in CDMA, in which the transmitted signal of a user very close to the base-station receiver can completely overpower the signal of a far-away user. The user-to-user interference in the uplink, or the so-called multiple-access interference (MAI), significantly limits the capacity of a DS-CDMA network.

There are several ways to alleviate MAI in the uplink. The first method is to make the signal of each user look like white Gaussian noise to the others [21, 73, 78]. Hence, the MAI in this case can be treated as white Gaussian noise, which can be effectively mitigated using powerful low-rate error-correction codes as in single-user communication systems. This is in fact the philosophy used in the IS-95 uplink, which assigns PN spreading codes of long period ($2^{41} - 1$ chips) for each user and employs rate 1/3 convolutional code with constraint-length 9 to combat interferences. Similar approach is used in the uplink of several 3G standards such as wideband CDMA (WCDMA) and CDMA2000 [2]. The main complexity of this approach resides in the

link layer, where stringent power-control mechanism has to be designed and applied to ensure that the received signal of all users have equal power, since otherwise the distribution of MAI may no longer look Gaussian.

The second method is to employ strict timing and synchronization control for the uplink transmission so that the signal of all users arrive at the base station at approximately the same time. In this way, orthogonal or low-correlation spreading codes can be employed to alleviate MAI. This technique is proposed in one of the 3G standards called time-division synchronous code-division multiple access (TD-SCDMA) jointly developed by the Chinese Science Academy and Siemens [66]. In TD-SCDMA, the maximum time-offset between the received signals of different users does not exceed 1/4th of a chip interval. Uplink time control is also used in another potential 3G technology called large area synchronous CDMA (LAS-CDMA) [41], in which transmission of all users in the uplink are coordinated. The most interesting aspect about LAS-CDMA is a very special class of spreading codes that is assigned to the users. This set of codes, originally proposed in [64] and [16], exhibits ideal auto- and cross-correlation for small time offsets, while the tradeoff is that the number of codes that show such desirable correlation behavior is limited. The drawback of this type of solutions in general is that synchronization in the uplink adds significant amount of overhead and complexity to link layer and network operation.

The third solution is multiuser joint detection, which introduces additional signal processing after the matched filter to improve the quality of decision statistics. The justification here is that since the (base-station) receiver can tolerate more complexity than the mobile transmitter, we can apply signal processing algorithms with moderate computational complexity to jointly process the received signals of all users after matched filtering. Unlike single-user (matched-filter) detectors that treat interferences from other users as background noise, these joint detectors exploit the structure of correlations between different users and incorporate this additional knowledge into the detection process. The role of joint detection in a DS-CDMA base-station receiver is shown in figure 1-8, where the joint detector follows immediately after the bank of matched filters. The use of multiuser joint detector has many benefits compared

to single-user detection. First, it has been shown that systems with joint detectors typically have a much larger capacity than one with only matched-filter detection [54, 71, 75, 76, 84]. Second, joint detection relaxes the need for stringent power and timing control, which takes some processing complexity out of the link and network layer. The tradeoff here is, however, that effective joint detection algorithms often introduce significant complexity and cost in the physical layer, which limits its value in practical implementation. A key contribution of this thesis is to design joint detection detection techniques that exhibit good performance-complexity tradeoff.

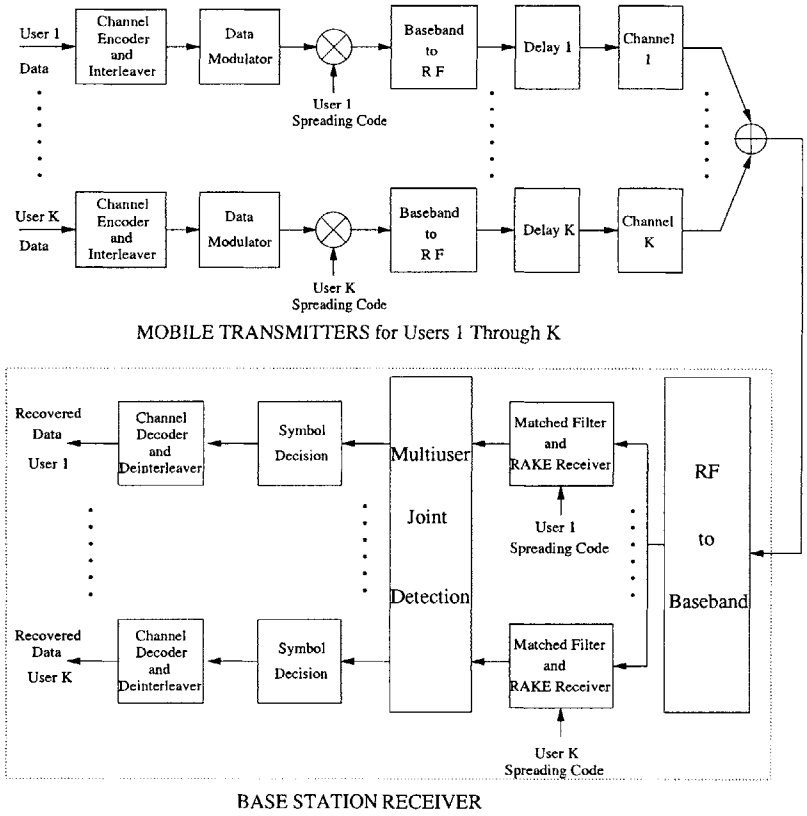

Figure 1-8: Standard DS-CDMA transceivers with joint detection

1.2 Summary of thesis contributions

In this thesis, we investigate efficient modulation and detection schemes for the uplink of a DS-CDMA system. The first part of the thesis focuses exclusively on modulation

and spreading modules at the mobile transmitter. In particular, we evaluate and compare the spectral-efficiency of two promising variable data (symbol) rate DSSS modulation techniques, multicode (MCD) and variable-spreading-gain (VSG) CDMA, under the presence of MAI and multipath interferences. In the second part of the thesis, we focus on joint detection techniques at the base-station receiver. Specifically, we introduce two multiuser detectors with good performance-complexity tradeoff. The first technique is a class of weighted parallel multistage interference cancellation algorithms based on minimum mean-squared error (MMSE) optimization. The second technique is a low-complexity dual-mode multiuser detector that dynamically switches its detection mode between the simple matched-filter receiver and a computationally intensive linear joint detector. In this section, we describe these topics in more specific terms and summarize the main contributions of this thesis.

1.2.1 Analysis of variable rate DS-CDMA transmission techniques

Problem

Early DS-CDMA systems are primarily designed for voice applications, in which all users transmit at the same data rate. Recently, due to the surge of mobile internet and multimedia applications, the network needs to deliver different types of data to different users at different symbol rates, which cannot be accomplished using traditional single-rate systems. This motivates the design of variable data (symbol) rate DS-CDMA systems.

To minimize the cost at RF front-end, it is desirable to vary the symbol rate while keeping the chip rate (and thus the spectrum occupation of the transmitted signal) fixed. For a constant chip-rate DS-CDMA system, there are two promising variable data-rate transmission techniques. The first technique is called multicode (MCD) CDMA, in which each user employs more than one spreading codes (code channels) to transmit in parallel. The second scheme is called variable spreading-gain (VSG) CDMA, in which each user uses a single spreading code but varies the

symbol duration, or equivalently, the spreading gain according to the desired data rate. Figure 1-9 illustrates the idea of MCD and VSG for a simple DS-CDMA system with two users of different rates, in which the symbol rate of the high-rate user is twice that of a low-rate user. In MCD-CDMA, the data symbols of the high-rate user is first split into parallel low-rate symbol streams, and the symbols in each low-rate stream, namely a code channel, is spread by a channelization code. Sum of the signals from all parallel code channels is then transmitted. The channelization codes are chosen to be orthogonal to minimize interferences between the parallel code channels. Since the symbol rate in each parallel code channel is the same as that of a low-rate user, each symbol in MCD is spread with the maximum processing gain. In VSG-CDMA, the transmitter structure is relatively simpler. The high-rate user increases the data rate by shortening its symbol interval. Since the chip rate is fixed, shorter symbol interval leads to reduction in spreading gain. To maintain the same symbol energy for all transmission rates (so that it is the same as that of a low-rate user or a MCD user), the transmit power of a VSG high-rate user has to be increased proportionally with the reduction in spreading gain. Figure 1-10 shows the role of the variable rate modulation and spreading in the uplink transmitter.

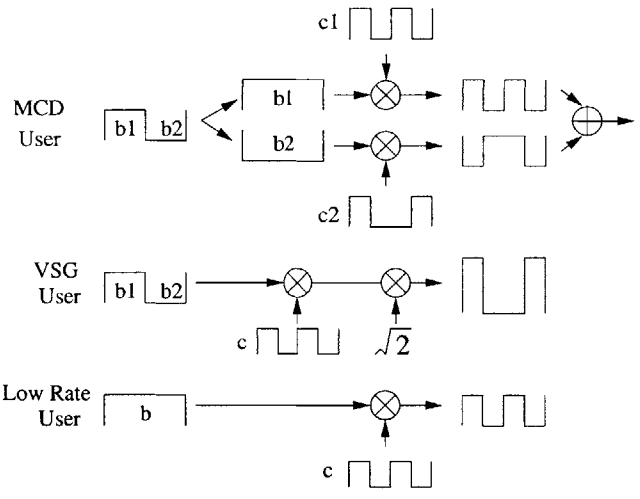

Figure 1-9: Variable symbol rate transmission in DS-CDMA: Dual-rate

The key question that we are going to answer in this thesis is, for a dual-rate

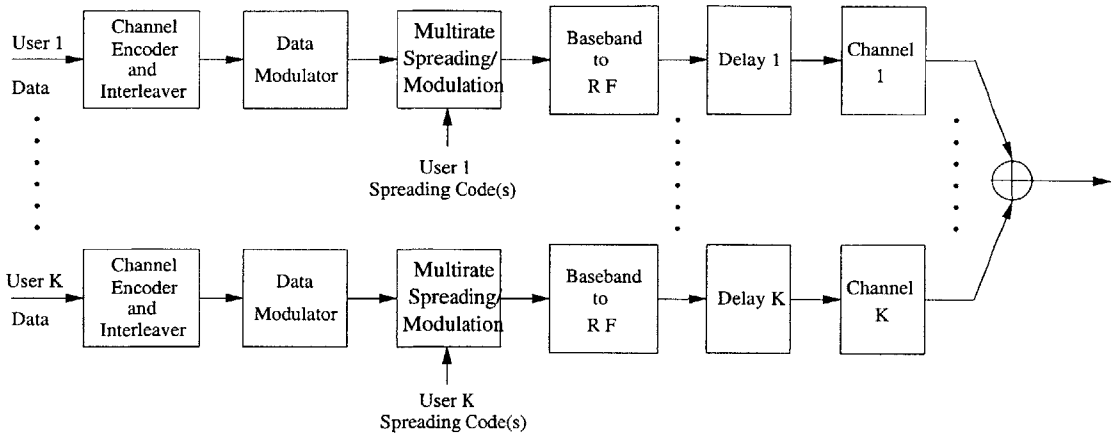

Figure 1-10: DS-CDMA mobile transmitter for variable rate transmission

system, given the same error-rate target, which of the two schemes, MCD or VSG, could lead to a higher capacity in the uplink, or from another perspective, given the same operating environment, which scheme would yield a lower bit-error rate. In essence, there are two main issues to be considered. First, since the transmitted signal of the MCD high-rate user is the summation of the spread signals from all parallel code channels, it has a much larger peak-to-average power ratio than the signal of VSG high rate user. It is possible that the high-rate user signal may cause the low-rate users in MCD-CDMA to have a worse error probability than those in VSG-CDMA. Second, it has been hypothesized that the error performance of the VSG high-rate user may be inferior to that of a MCD user due to the loss of spreading gain. Even though both users have the same symbol energy, it is unsure whether we can trade transmission power for spreading gain on a one-to-one basis.

The error performance of low-rate users has actually been studied in [25], which showed through rigorous analysis that low-rate users in both systems exhibit the same error performance. The error probability of the high-rate users has also been addressed by a number of literatures [3, 49, 39, 68, 88], but the outcomes are debatable due to overly ideal assumptions in the system models. The most questionable assumption made in majority of these studies is the standard Gaussian approxima-

tion, which models all interferences in the system as zero-mean Gaussian random variables. This approximation may give misleading results for realistic systems, as will be seen in chapter 2 of the thesis. Another over-simplification often made is that, in a multipath fading channel, the outputs from different RAKE fingers are assumed to be independent of each other. In realistic systems, however, unless the spreading codes have ideal autocorrelation, the RAKE finger outputs are always going to be correlated, and sometimes the correlation carry a large weight in the final symbol decision, as will be seen in chapter 2. Therefore, a thorough error-rate analysis for the high rate user under more reasonable setting is necessary.

Thesis contribution: error-rate analysis for multirate DS-CDMA transmission

In the first part of this thesis, we analyze the uplink error performance for high-rate users in VSG and MCD systems from a perspective that is different from most of the previous studies. We assume the use of random user-specific spreading codes at the transmitter and the use of matched-filter detection followed by RAKE combining at the receiver. Instead of making Gaussian approximations in error-rate calculation as have been done in the past, our error analysis shows how both power and distributions of the interference together affect the quality of the received symbols of the high-rate user in VSG and MCD system. The outcome of the study not only enhances fundamental understanding on the performance of MCD- and VSG-CDMA but also allows us to recommend the "optimal" modulation technique for different channels and interference environments.

Specifically, assuming both MCD and VSG users have the same operating environment and the same symbol energy, we present two sets of results. First, we show that if the uplink can be modeled as an ideal additive white Gaussian noise (AWGN) channel, the VSG high-rate user has a better error performance than the MCD high rate user if the number of low-rate interferers in the system is small. This gap in error probability is completely contributed by the differences in the distribution of MAI seen by VSG and MCD user. The underlying reason, intuitively, is that when the

number of interferers is small, it is more effective to combat MAI using high transmission power in VSG than spreading in MCD. The same result, however, does not carry over to flat-fading channel, in which case the error performance of MCD and VSG users turn out to be identical. This is because the presence of fading smoothes the distributions of MAI suffered by the VSG user to make it look more like that in MCD-CDMA.

Our second set of results apply to the case when the uplink is a multipath fading channel for all users. We show that in this case, if the time offsets between the different paths are smaller than a fraction of the VSG user's symbol interval (i.e. if the delay spread of the channel is small), then the MCD high-rate user has a larger SIR than the VSG user. On the other hand, if the time offsets are larger, then the VSG user would in general have a better SIR than the MCD user. The difference in the SIR is due to the correlations between the RAKE finger outputs. A higher SIR, however, does not necessarily imply a better error probability. While the multipath interferences are symmetrically distributed for a two-path channel (typical for cellular communication in rural and suburb areas), in which the SIR gives correct inference about the error probability, we show that in channels with more than two paths (such as in urban and indoor environment), the multipath interferences after RAKE combining is not only non-Gaussian but also asymmetric, in which case a higher interference power may actually help the corresponding user to achieve a better error rate.

1.2.2 Multiuser joint-detection

Problem

The goal of multiuser joint detectors is to suppress the multiple-access interferences (MAI), which is particularly serious in the uplink of the DS-CDMA system due to asynchronous transmission. A joint detector can be viewed as an additional signal processing block after the matched-filter receiver to enhance the quality of decision statistics at the input of the symbol-decision device, as shown in figure 1-8. The optimal joint detector that achieves single-user performance (i.e. the case with no

MAI at all) was proposed in [74] using the approach of maximum likelihood sequence search. Its drawback is that the complexity requirement grows exponentially with the product of number of in-cell users and the number of symbols per processing frame, which is too costly to be implemented using today's technology.

Consequently, most of recent researches on joint detection look for suboptimal algorithms that exhibit good performance-complexity tradeoff. These suboptimal techniques can be grossly divided into two categories: linear and non-linear joint detectors. Linear joint detection algorithms, illustrated in figure 1-11, typically perform a linear transformation on the matched-filter output of all users to tune out MAI [46]. One example is the decorrelator, which attempts to completely eliminate the MAI through linear transformation. It is analogous to the zero-forcing equalizer for ISI cancellation in single-user communication. This detector is much simpler than the optimal maximum likelihood (ML) detector and yet significantly outperforms the matched-filter receiver at high signal-to-noise ratio. The drawback of this detector, however, is that the decorrelating linear transformation enhances the background noise. As a result, when background noise dominates over MAI, i.e. at low signal-to-noise ratios, its performance can become poorer than the matched filter. Another linear joint detector is the linear MMSE detector (with similar complexity as the decorrelator), which is obtained by finding the matrix that minimizes the mean-squared-error between the transformation output and the original transmitted symbols. The linear MMSE receiver offers a balance between MAI and background noise suppression and has a better performance than the decorrelator [54]. The drawback of this scheme is that it needs accurate estimate for the received amplitudes of all users' signals as well as the background noise power.

While linear joint detectors are much simpler than the optimal ML detector, their complexity is still significantly higher than the matched filter due to the necessity for matrix inversion when calculating the transformation matrix. This gives a complexity on the order of cubic of the product of number of in-cell users and the number of data symbols per frame, which is quite large for practical implementation. Even though MMSE detection can be implemented using linear adaptive filters, such algorithms

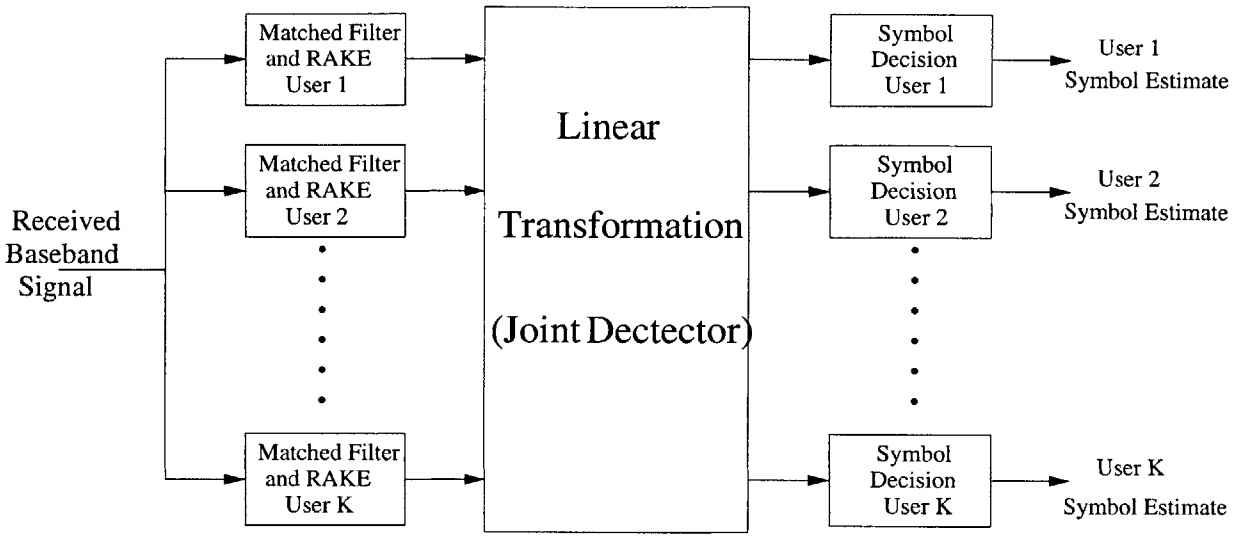

Figure 1-11: Linear joint detector at DS-CDMA base-station receiver

usually diverge for spreading codes with period that spans over many symbols [75]. Yet, the performance of these detectors are no better than the matched filter in low SNR environment. The need for better performance-complexity tradeoff here prompts us to propose a dual-mode linear multiuser receiver that is capable of achieving the performance of decorrelator but with significant reduction in the overall processing power.

In contrast to linear joint detectors, a general class of non-linear detectors try to suppress MAI via decision-feedback interference cancellation. The MAI cancellation can be performed successively or in parallel. In successive interference cancellation (SIC), as illustrated in figure 1-12, the received user signals are first ranked according to the received power. The user signal with the highest power is detected first using matched filter. Its decision is then used to reconstruct its original signal, which is then subtracted from the total received signal. The second strongest user is then detected in the same manner. This process continues until all users in the system are detected. It has been shown [10, 51] that, if the users' received powers are very different, then the performance of SIC can approach single-user performance bound. In most practical systems, however, the use of power control make the received power

of all users to be roughly the same. In this case, the average error performance of SIC is quite poor, not to mention that it also gives rise to extremely unequal performance among users in terms of error rate and latency.

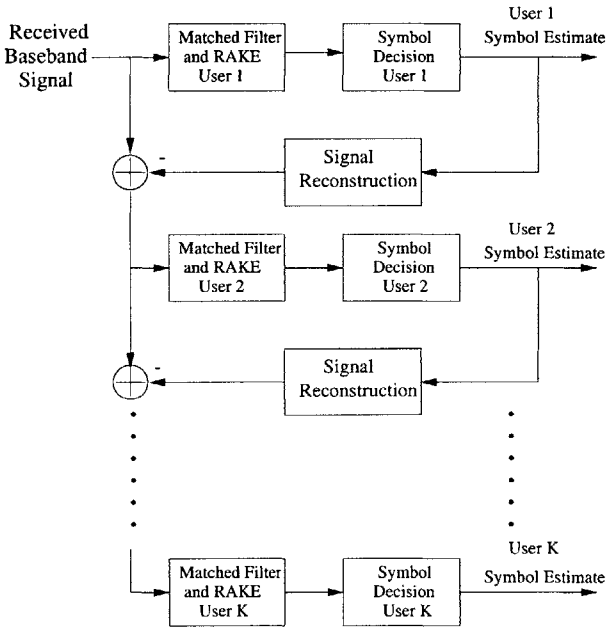

Figure 1-12: Successive interference canceller (SIC) at DS-CDMA base-station receiver

In the presence of power control, as done in practical systems, another type of nonlinear algorithm – the parallel multistage interference canceller (PIC), has been shown to perform better than SIC [46]. The conventional PIC, illustrated in figure 1-13, operates in a stage-by-stage manner, with the matched filter being the first stage [70]. In subsequent stages, the receiver first uses symbol estimates of the previous stage to reconstruct MAI suffered by all users in the system. These MAI estimates are canceled from the matched-filter output of all users in parallel. This receiver performs better much than the matched filter if the user population is not too large, and unlike in SIC, all users under PIC have the same latency. The drawback with this type of algorithm, however, is that at every stage, the receiver assumes the symbol estimates from the previous stage to be completely accurate and hence performs full MAI cancellation based on these estimates, even though they can be quite poor in

reality. If a wrong symbol estimate is used to reconstruct and cancel MAI, the error will propagation through later stages. This error propagation severely limits the performance of conventional PIC such that its error rate may not decrease beyond two stages [75]. In this thesis, we propose a class of parallel multistage interference cancellation algorithms that alleviates the effect of error propagation and achieves significantly better performance than the conventional PIC.

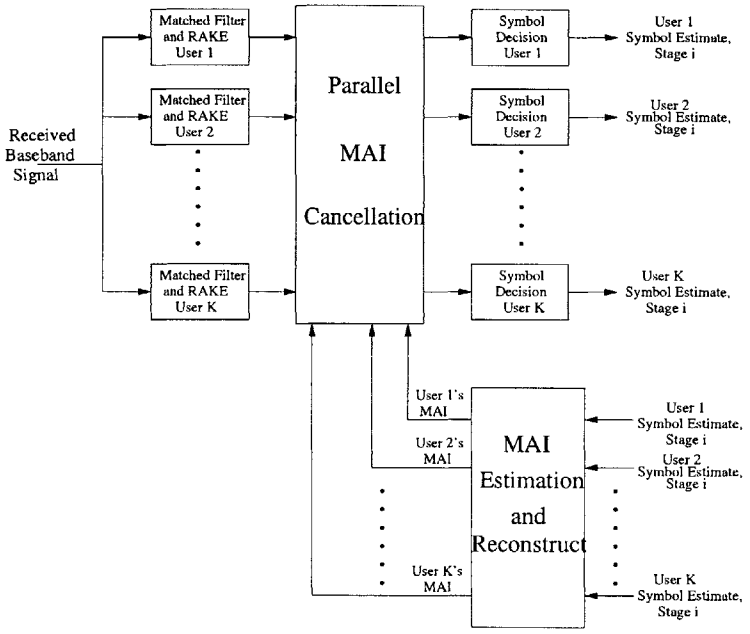

Figure 1-13: Multistage parallel interference cancellation (PIC) at DS-CDMA base-station receiver

Thesis contribution in non-linear joint detection: MMSE-based multistage parallel interference canceller

Another key contribution of this thesis is the design of effective parallel multistage interference cancellation algorithms for DS-CDMA base-station receiver. The design objective here is to maximize the spectral and energy efficiency of the system under a set of given complexity constraints. We show that, by exploiting the reliability of previous symbol estimates used in MAI reconstruction, the proposed receiver significantly outperforms existing joint detectors that are on the same order of complexity.

Specifically, we introduce two algorithms that are differentiated by their computational complexity constraints. The first algorithm is relatively simple, and its complexity is on the same order of that for conventional PIC. This detector is derived by finding the optimal MAI reconstruction and cancellation process that minimizes the mean-squared cancellation error (MSE) at each stage. We show that this MMSE solution can be viewed as a conventional PIC scaled by a weighting matrix. The exact expression of the weighting matrix is derived for M-ary phase-shift-keying (M-PSK) modulated data symbols (typically $M = 2$ for BPSK and $M = 4$ for QPSK). We show that the parameters of the weighting matrix depend mainly on the error probabilities of the symbol estimates in the previous stage, which can be readily obtained via pilot sequences or signal-to-interference ratio (SIR) approximation using today's technology. The proposed receiver demonstrates drastically better error performance over the conventional PIC, particularly for a large system, i.e. a system where the ratio of the number of users to the spreading gain is large.

Compared to the first method, our second algorithm has a higher complexity, which is on the order of that for linear joint detection, as it requires one matrix inversion for each stage. In this detector, we suppress the MAI not only via the feedback MAI reconstruction and cancellation unit but also introduces a preprocessing (feedforward) unit that performs a linear transformation to the matched-filter outputs to tune out part of the MAI even before the feedback cancellation. This leads to the standard framework of decision-feedback multiuser detector with feedforward processing [75], as shown in figure 1-14. In this thesis, we find the optimal feedforward and feedback unit that jointly minimizes the MSE of symbol decisions at each stage. The key element here is again the use of a weighting matrix that is derived in the first algorithm to measure the reliability of symbol estimates in the previous stage. We show that while the complexity of this receiver is on the order of that for linear joint detectors, its error performance is not only superior to linear detectors but is also capable of approaching the optimal (single-user) performance bound in just a few iterations. In simulation, it also shows essential immunity to MAI for multiuser DS-CDMA system employing random spreading codes as long as the load is less than

100%.

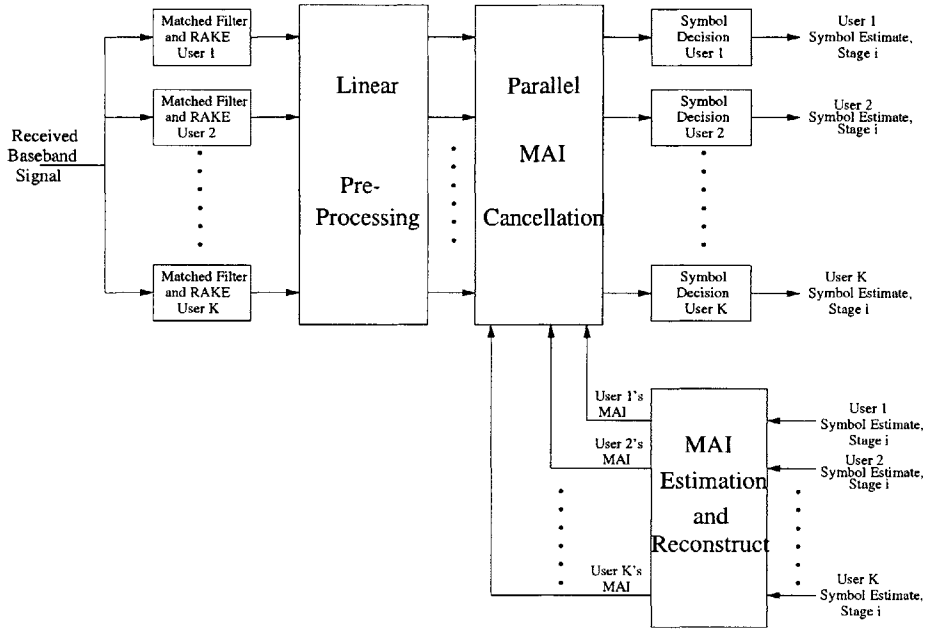

Figure 1-14: Multistage interference cancellation with feedforward and feedback MAI cancellation

Thesis contribution in linear joint detection: A dual-mode linear multiuser detector

In the third part of the thesis, we study linear joint detection techniques for DS-CDMA receiver. The design objective here is to minimize the complexity and processing power while meeting the performance target (such as bit-error-rate target) for each user. By exploring the differences in signal-to-interference ration (SIR) for the decorrelator and the matched filter, we derive a dual-mode detector that is capable of achieving the spectral-efficiency of the decorrelator detector with significantly less processing power and complexity.

The architecture of the dual-mode detector is quite simple: the receiver dynamically switches its mode between decorrelator and matched-filter detection. The basic philosophy of this detector is that since decorrelator outperforms the simple matched-filter detection only in the case when MAI dominates over background interferences,

and yet it yields a much higher computational complexity, the decorrelating operation should be performed only when the background interference is weak relative to MAI. In practical cellular communications, the background interference includes not only thermal noise but also interferences from users in neighboring cells, which can be quite strong sometimes. Consequently, in a system where this dual-mode detection algorithm is implemented in firmware, such as on a DSP chip, skipping the decorrelator operation when necessary is capable of leading to significant savings in processing power, which allows more effective and dynamic resource sharing at the base-station receiver.

The key to this dual-mode detector is the decision criterion as when decorrelator detection should be performed. We derive this decision module based on our analysis and assessment of the amount of noise enhancement introduced by the decorrelator transformation. If our noise-enhancement measure is higher than the MAI suffered by most users, then the decorrelator operation will not be performed. The performance of this dual-mode detector is verified via simulation, in which we show that, while the decorrelating operation is performed less than half of the time, the bit-error rate of this receiver is very close of that of the full decorrelator.

1.2.3 Thesis organization

The rest of the thesis is organized as follows. Chapter 2 presents the bit-error-rate analysis for multicode and variable spreading-gain DS-CDMA modulation techniques. Chapter 3 introduces the two aforementioned multistage interference cancellation techniques that aim to optimize the spectral efficiency of the system while satisfying the complexity constraints. Chapter 4 introduces the dual-mode multiuser receiver that saves processing power while achieving the desired BER target. Concluding remarks and future research directions are given in chapter 5.

Chapter 2

Error-rate Analysis of Multirate DS-CDMA Transmission Schemes

In this chapter, we analyze and compare the error performance of a dual-rate DS-CDMA system using multicode (MCD) and variable-spreading gain (VSG) modulation in the uplink. The uniqueness of our study is that in bit-error-rate evaluation, instead of approximating the interferences as Gaussian noise (which has been done in most of the previous studies), we incorporate both power and distribution of interferences into consideration. Specifically, we present two sets of results. First, we show that in an ideal AWGN channel, the error rate of the VSG high-rate user is better than that of the MCD high rate user if the number of low rate interferers is smaller than a specific threshold. Otherwise, both systems achieve similar error performance. Second, we show that for RAKE reception in a multipath fading channel, the VSG user suffers from a larger interference power than the MCD user if the channel delay spread is small. The reverse is true for a large delay spread. Furthermore, we show that having a larger interference power in this case may lead a better error performance due to the asymmetric distribution of multipath interferences.

2.1 Background and motivation

Early mobile communication networks are primarily designed to provide voice-based services, in which all users transmit at the same data rate. Recently, with the surge of demand for internet applications, a mobile user also desires to communicate using other types of information such as short message, video and multimedia contents. Consequently, traditional modulation method in which all users operate at the same data rate no longer suffices. In order to deliver different quality-of-services (QoS) for the individual customers, efficient variable data-rate transmission techniques are necessary.

In this chapter, we study the performance of variable data-rate modulation techniques in the uplink of DS-CDMA system. Due to wide spectrum occupation of the CDMA signal, it is desirable for a DS-CDMA system to vary data (symbol) rate while fixing the chip rate so that spectrum occupation of the transmitted signal is constant. Under this constraint, there are two promising variable data-rate DS-CDMA modulation techniques. In the first method, the user changes the symbol rate by varying the spreading gain (and thus the symbol interval). The transmit power is changed proportionally at the same time so that the user maintains the same symbol energy for all possible data rates. This is known as variable-spreading gain CDMA (VSG-CDMA) [28] (since spreading gain and transmit power vary with data rate). Under the second technique, a user maintains the maximum spreading gain at all times and increases its data rate by using more than one parallel code channels for simultaneous transmission. In such a system, a high-rate data stream is split into a number of parallel low-rate streams, each operating at the lowest (basic) symbol rate. Data streams in different parallel channels are spread using different orthogonal spreading (channelization) codes to avoid excessive self-interferences. The spread signal from all parallel channels are summed and scrambled by a user-specific signature code before transmission. This scheme is known as multicode CDMA (MCD-CDMA) [27]. The transmitter structure for MCD- and VSG-CDMA systems are shown in figures 2-1 and 2-2, respectively.

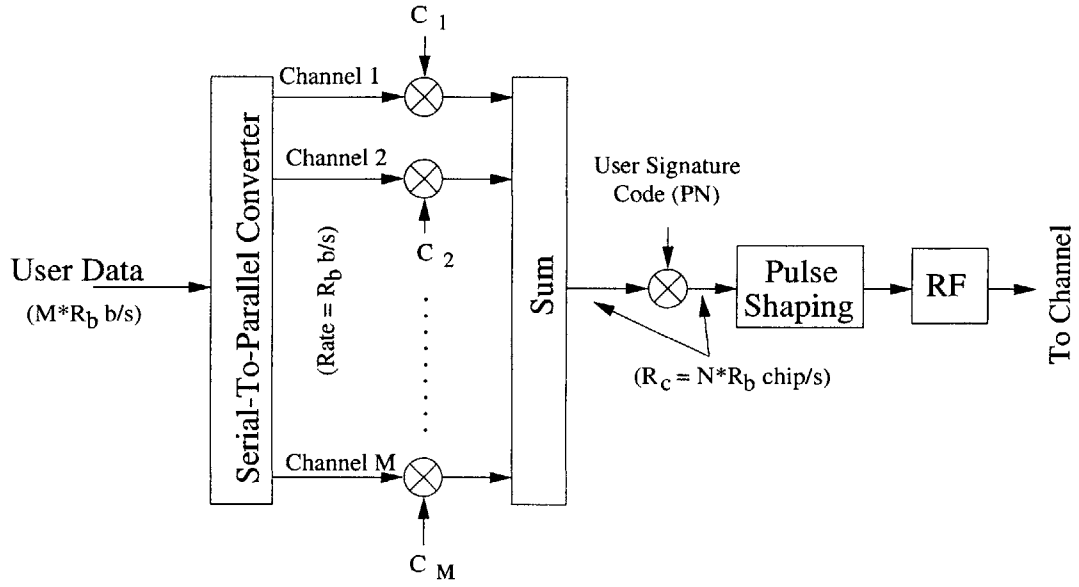

Figure 2-1: Transmitter of multicode CDMA user

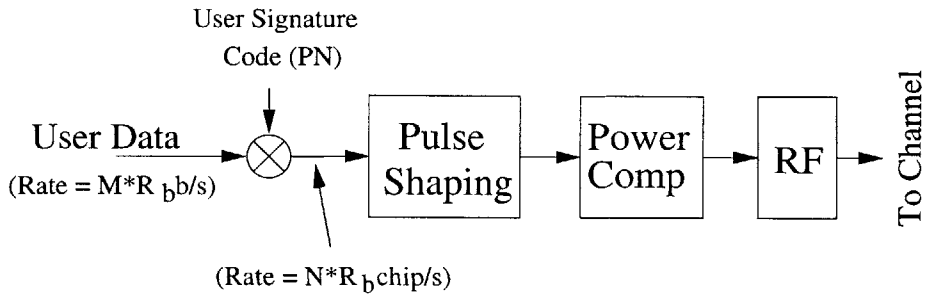

Figure 2-2: Transmitter of variable spreading-gain CDMA user

An important question to ask is which of the two schemes is more suitable for practical systems. The answer depends on a wide range of considerations. In terms of data-rate flexibility, MCD offers more choices of transmission rates than VSG does. While MCD can offer rates that are integer multiples of the basic (minimum) rate, VSG can only employ spreading gains that are integer divisors of the maximum spreading gain [48]. In terms of link-layer complexity, VSG requires more intensive processing than MCD due to a problem known as code blocking in the downlink [45]. On the other hand, from the physical-layer perspective, VSG shows a significant edge over MCD in terms of implementation and operating cost. While the physical

layer of a VSG system does not vary significantly from that of a single-rate DS-CDMA system, a MCD system requires noticeably more expensive hardware because its receiver architecture is non-scalable (the number of RAKE receivers must be equal to the maximum number of code channels available at the transmitter [48]). Also, the transmitted signal from MCD-CDMA has a multi-level envelope because it is the summation over all parallel code channels. This leads to very high peak-to-average power ratio and requires the use of power-inefficient linear amplifier [11, 80].

Aside from the aforementioned practical tradeoffs, the key performance measure of our interest is the spectral efficiency, which determines the capacity (i.e. aggregate data rate of all users) that the system can support at a pre-determined target error rate. Or equivalently, we would like to compare the bit-error rate of the two systems under the same operating conditions. We focus on the uplink, i.e. the transmission link from mobile subscribers to the base-station, where the user-to-user interference, or the so-called multiple-access interference (MAI) in this case is more severe than that in the down-link.

We consider a standard dual-rate system, in which there is one high-rate (HR) user and multiple low-rate (LR) users. For this system, there are two issues to be considered. First, it would be interesting to study the impact of the HR user on LR users, since it has been hypothesized that LR users in MCD-CDMA may have a worse error performance than those in VSG-CDMA because the transmitted signal of a MCD HR user has a much larger peak amplitude than that of the VSG user [25]. Second, we would like to compare the error performance of VSG and MCD HR users. A number of literatures [5, 35, 39] raised concern that the VSG HR user may have a worse performance than the MCD user due to the loss of spreading gain. Even though the VSG user increases its transmission power proportionally with the reduction in spreading gain, it is unsure whether we can trade spreading gain with transmission power on an equal basis. In this chapter, we focus only on the error performance of the HR user and treat LR users as interferers, since the reverse scenario where LR users are the target and HR user is the interferer has been clearly addressed in [25] (which showed that LR users have identical error performance under both VSG and

MCD HR users).

Specifically, we address two fundamental issues. First, we consider a frequency non-selective channel, in which the MAI from LR users is the dominant interference. The key question here is whether it is more effective to combat MAI using a larger spreading gain (as in MCD) or higher transmission power (as in VSG), as it is unsure whether we can trade spreading gain for transmission power on a one-to-one basis. Early work in [49] claimed that MCD and VSG HR users achieve the same error performance in this case. This result, however, is based on an analytical model that approximates the MAI as additive white Gaussian noise, which clearly does not apply to many practical cases [40]. The results from [3] and [68], on the other hand, favored VSG over MCD. They approximated MAI as Gaussian noise as well and in addition assumed the parallel code channels of the MCD user to be non-orthogonal, in which case the VSG user actually has a larger signal-to-interference ratio (SIR) than the MCD user.

Here, instead of employing the classical Gaussian approximation as have been done in previous studies, we incorporate not only power but also distribution of the interferences into error performance evaluation. We show that in an ideal additive white Gaussian noise (AWGN) channel, the VSG HR user achieves a significantly lower error probability than the MCD HR user if the number of LR interferers in the system is small, even though both have the same SIR. This gap in error probability is completely due to differences in the distribution of MAI seen by the VSG and MCD HR user. The same result, however, does not carry over to flat-fading channel, in which case the error performances of MCD and VSG users turn out to be identical. This is because the presence of fading smoothes the distributions of MAIs suffered by both VSG and MCD user to make them look more alike.

The second issue that we address applies to transmission over multipath fading channels, in which RAKE receivers are used as a diversity technique to combat fading [69]. Analyses for conventional CDMA users (i.e. LR users) usually ignore the multipath interferences (MPI) at the RAKE finger outputs because they are typically small when the spreading gain is large [55][9]. Here, however, both MCD and VSG

HR users may experience strong MPI for different reasons. For the MCD user, the MPI is a sum of interferences contributed by cross-correlation among its parallel code channels, while for the VSG user, the MPI is contributed by the partial autocorrelation of its signature code [56], which normally increases with the amount of reduction in spreading gain. The key question here is which type of interferences has a worse impact under the use of RAKE receivers. This topic has been investigated by a number of literatures [49][88][39][35]. It has been claimed in [49] that both types of interferences have the same effect, under the assumption that interferences from different RAKE fingers are mutually independent. Recent work in [88], however, questioned the validity of this assumption and suggested that the RAKE finger outputs of a VSG HR user are strongly correlated, which leads to a much higher error probability than that of the MCD HR user. Both studies model MPIs as a Gaussian random variables conditioned on path delays, amplitudes, and phase offsets.

We investigate this issue by incorporating both power and distribution of MPI into consideration. In terms of interference power, we show that if all pair-wise path time-offsets are smaller than a fraction of the VSG user's symbol interval (i.e. if the delay spread of the channel is small), the MCD HR user has a larger SIR than the VSG user. On the other hand, if the time offsets are larger, then the VSG user would in general have a better SIR than the MCD user. The difference in the SIR is due to correlations between the RAKE finger outputs. A higher SIR, however, does not necessarily imply a lower error probability. We show an example for channels with more than two paths (such as in urban and indoor environment), in which the multipath interferences after RAKE combining is not only non-Gaussian but also asymmetric. In this case, a higher interference power may actually help the corresponding user to achieve a lower error rate.

The rest of the chapter is developed as follows. In section 2, we develop a basic model to analyze MCD- and VSG-CDMA systems. We examine the error performance of both systems in AWGN channel and flat fading channel in sections 3 and 4, respectively. In section 5, we present analytical results for multipath fading channels. Chapter summary is given in section 6.

2.2 System model

We assume a dual-rate system with one high-rate (HR) user and K low-rate (LR) users, where the data symbol of all users are binary phase-shift-keying (BPSK) modulated. We also assume that users transmit asynchronously and that signature codes of all users are independently and randomly generated, with each chip being 1 or -1 with equal probability. All LR users operate at the basic rate, while the HR user transmits at M times the rate of LR users. Mathematically, the baseband signal transmitted by the MCD HR user can be expressed as

$$s^{MCD}(t) = \sum_{m=1}^{M} \sqrt{P} b_m^{(h)}(t) c_m^{(h)}(t), \tag{2.1}$$

where

$$\begin{aligned} b_m^{(h)}(t) &= \sum_{i=-\infty}^{\infty} b_m^{(h)}(i) rect_b(t - iT_b), \\ c_m^{(h)}(t) &= \sum_{i=-\infty}^{\infty} \sum_{j=1}^{N} d_m^{(h)}(j) p^{(h)}(iN + j) \psi(t - iT_b - jT_c), \end{aligned}$$

where P is the transmit power per code channel; $b_m^{(h)}(i) \in \{1, -1\}$ is the ith data symbol in the mth parallel channel; $d_m^{(h)}(j) \in \{1, -1\}$ is the jth chip of the orthogonal spreading code for the mth channel; $p^{(h)}(j) \in \{1, -1\}$ is the jth chip of the HR user's signature code; T_b and T_c are the symbol and chip interval, respectively, where $T_b = NT_c$ with N being the maximum spreading gain; $rect_b(t)$ is a unit-amplitude rectangular pulse from $t = 0$ to $t = T_b$; $\psi(t)$ is the normalized time-limited chip waveform such that $\int_{t=0}^{T_c} |\psi(t)|^2 dt = \frac{1}{N}$ (and $\int_{t=0}^{T_b} |c_m^{(h)}(t)|^2 = 1$ for all m).

Similarly, the transmitted signal of the VSG-CDMA HR user can be expressed as

$$s^{VSG}(t) = \sqrt{MP} b^{(h)}(t) c^{(h)}(t), \tag{2.2}$$

where

$$b^{(h)}(t) = \sum_{i=-\infty}^{\infty} b^{(h)}(i)\widetilde{rect}(t - i\frac{T_b}{M}), \quad c^{(h)}(t) = \sum_{j=-\infty}^{\infty} p^{(h)}(j)\psi(t - jT_c),$$

where $b^{(h)}(i)$ is the ith data symbol of the VSG user; $\widetilde{rect}(t)$ is a unit-amplitude rectangular pulse from $t = 0$ to $t = \frac{T_b}{M}$; p's and $\psi(t)$ are the same as those specified for the MCD user. Note that the symbol interval of the VSG user is shortened by a factor of M compared to the MCD and the LR user. Its transmission power is increased by M times to compensate for the loss of spreading gain so that $\int_{t=0}^{\frac{T_b}{M}} M|c^{(h)}(t)|^2 dt = 1$.

As a side note, the signal of the kth LR user ($k \in [1, K]$) can be expressed as

$$s_k^{(l)}(t) = \sqrt{P} b_k^{(l)}(t) c_k^{(l)}(t) \cos \omega_c t, \tag{2.3}$$

where

$$b_k^{(l)}(t) = \sum_{i=-\infty}^{\infty} b_k^{(l)}(i) rect_b(t - iT_b), \quad c_k^{(l)}(t) = \sum_{j=-\infty}^{\infty} p_{k,j}^{(l)} \psi(t - jT_c),$$

where $b_k^{(l)}(i) \in \{-1, 1\}$ and $p_k^{(l)}(j) \in \{-1, 1\}$ are the ith data symbol and the jth chip of the signature code for the kth LR user, respectively.

Assuming the channel is wide-sense-stationary (WSS) and perturbed by additive white Gaussian noise (AWGN), the composite received signal at baseband is

$$r(t) = \sum_{k=0}^{K} \sum_{q=1}^{Q(k)} A_{k,q} e^{j\phi_{k,q}} s_k(t - \tau_{k,q}) + n(t) \tag{2.4}$$

where $n(t)$ is the background interference and can be modeled as a white Gaussian process with one-sided spectral density of N_0; $A_{k,q}$'s, $\phi_{k,q}$'s, $\tau_{k,q}$'s and $Q(k)$ are the received amplitude, phase, and propagation delay of the qth signal path and the number of resolvable paths for the kth user, respectively; The path gains and delays vary according to the channel model. For notational convenience, we denote user 0 as the HR user.

We assume a receiver that employs matched-filter detection followed by coherent RAKE combining. The decision statistic for the ith bit in the mth code channel of a MCD HR user can then be expressed as

$$y_m^{(h)}(i) = Re\{\sum_{q=1}^{Q(0)} w_q y_{m,q}^{(h)}(i)\}, \tag{2.5}$$

where w_q is the weight for the qth signal path in RAKE combining; For equal-gain combining, signal from all paths are weighed equally, i.e. $w_q = 1$, while in maximal ratio combining, the weights for each path is proportional to its received signal strength, i.e. $w_q = |A_q|$; $y_{m,q}^{(h)}(i)$ is the matched filter output at the qth RAKE finger such that

$$y_{m,q}^{(h)}(i) = \int_{iT_b+\tau_{0,q}}^{(i+1)T_b+\tau_{0,q}} r(t) c_m^{(h)}(t-\tau_{0,q}) e^{-j\phi_{0,q}} dt, \tag{2.6}$$

Similarly, the decision statistic for the ith bit of the VSG user can be found as

$$y^{(h)}(i) = Re\{\sum_{q=1}^{Q(0)} w_q y_q^{(h)}(i)\}, \tag{2.7}$$

where $y_q^{(h)}(i)$ is the matched-filter output from its qth RAKE finger such that

$$y_q^{(h)}(i) = \int_{i\frac{T_b}{M}+\tau_{0,q}}^{(i+1)\frac{T_b}{M}+\tau_{0,q}} r(t) c^{(h)}(t-\tau_{0,q}) e^{-j\phi_{0,q}} dt. \tag{2.8}$$

2.3 Error-rate analysis in AWGN channel

We first analyze the error performance of the HR user in a stationary AWGN channel. The composite received signal in this case can be simplified to

$$r(t) = \sum_{k=0}^{K} s_k(t-\tau_k) e^{j\phi_k} + n(t). \tag{2.9}$$

Without loss of generality, we make the following assumptions to simplify the analysis:

1. Transmission delay and phase offset of the HR user is the point of reference, i.e. $\tau_0 = 0$ and $\phi_0 = 0$.

2. Signals of all LR users arrive after the HR user, i.e. $\tau_k > 0$ for $k = 1, 2, ... K$; Phase offsets of the LR users, i.e the ϕ_k's, are independent and identically distributed (i.i.d.) random variables uniformly distributed between $-\pi$ and π.

3. The system is symbol-asynchronous but chip-synchronous. This means that transmission delays of LR users are integer multiples of chip intervals, i.e. $\tau_k = \delta_k * T_c$, where $\delta_k \in \mathbb{Z}^+$.

The matched-filter output for the ith symbol in the mth code channel of the MCD HR user can then be expressed as

$$\begin{aligned} y_m^{(h)}(i) =& \sqrt{P} b_m^{(h)}(i) + \sqrt{P} \sum_{k=1}^{K} \cos\phi_k (b_k(i)\rho_{m,k}^{(0)}(i) \\ &+ b_k(i-1)\rho_{m,k}^{(-1)}(i)) + n_i \\ =& \sqrt{P}(b_m^{(h)}(i) + \sum_{k=1}^{K} X_{m,k}(j)\cos\phi_k + \frac{n_i}{\sqrt{P}}) \end{aligned} \tag{2.10}$$

where n_i is the background noise term modeled as a zero-mean Gaussian random variable with variance $\frac{N_0}{2}$; The summation term contains MAI from all LR users due to cross-correlation of the spreading (signature) sequences. The correlation terms in the MAI for $k \neq 0$ are defined as

$$\rho_{m,k}^{(0)}(i) = \int_{(i-1)T_b+\tau_k}^{iT_b} c_m^{(h)}(t) c_k(t-\tau_k) dt \tag{2.11}$$

$$\rho_{m,k}^{(-1)}(i) = \int_{(i-1)T_b}^{(i-1)T_b+\tau_k} c_m^{(h)}(t) c_k(t-\tau_k) dt \tag{2.12}$$

Due to chip synchronism, we can further express the correlation terms as

$$\rho_{m,k}^{(0)}(i) = \frac{b_k^{(l)}(i)}{N} \sum_{j=1}^{N-\delta_k} d^{(h)}(j) p^{(h)}(iN+j) p_k^{(l)}(iN+j+\delta_k) \tag{2.13}$$

$$\rho_{m,k}^{(-1)}(i) = \frac{b_k^{(l)}(i-1)}{N} \sum_{j=N-\delta_k}^{N} d^{(h)}(j) p^{(h)}(iN+j) p_k^{(l)}(iN+j+\delta_k) \tag{2.14}$$

where $\frac{1}{N}$ is the energy of each chip, i.e. $\int_{T_c} |\psi(t)|^2 dt = \frac{1}{N}$. Since the signature code of each user, i.e. the p's, are random, independently and equally likely to be 1 or -1, we can model the sum of the correlation terms as a "symmetric binomial" random variable such that

$$X_{m,k}(i) = \rho_{m,k}^{(0)}(i) + \rho_{m,k}^{(-1)}(i) = \sum_{j=1}^{N} \tilde{X}_{k,m}(j) \tag{2.15}$$

where $\tilde{X}_{m,k}(j)$'s are independent and identically distributed (i.i.d.) random variables with the following "symmetric Bernoulli" distribution:

$$p_{\tilde{X}_{m,k}(j)}(x) = \begin{cases} 0.5 & \text{if } x = -\frac{1}{N} \\ 0.5 & \text{if } x = \frac{1}{N} \\ 0 & \text{Otherwise.} \end{cases} \tag{2.16}$$

$X_{m,k}(i)$'s are therefore i.i.d. random variables with "symmetric-binomial" distribution as follows:

$$P_{X_{m,k}(i)}(x) = B(1,x) \tag{2.17}$$

where $B(r,x)$ is the "symmetric binomial function" denoted as

$$B(r,x) = \begin{cases} \begin{pmatrix} Nr \\ \frac{Nx+Nr}{2} \end{pmatrix} (\frac{1}{2})^{Nr} & \text{if } x \in \{-r, \frac{1}{N}-r, \frac{2}{N}-r, \ldots\ldots, r-\frac{1}{N}, r\} \\ 0 & \text{Otherwise.} \end{cases} \tag{2.18}$$

Similarly, the matched-filter output for the ith symbol of the VSG user can be expressed as

$$y^{(h)}(i) = \sqrt{P}(\frac{1}{\sqrt{M}}b^{(h)}(i) + \sum_{k=1}^{K} V_k(i)\cos\phi_k) + n_i^{VSG} \tag{2.19}$$

where the factor $\frac{1}{\sqrt{M}}$ results from shortened symbol interval and power compensation, i.e. the amplitude of the signal component of matched-filter output is

$$\begin{aligned}\int_{\frac{T_b}{M}}^{\sqrt{M}} |c^{(h)}(t)|^2 =& \sqrt{M}\sum_{j=1}^{\frac{N}{M}}\int_{T_c}|\psi(t)|^2 \\ =& \sum_{j=1}^{\frac{N}{M}}\frac{\sqrt{M}}{N} = \frac{1}{\sqrt{M}}.\end{aligned} \tag{2.20}$$

For similar reason, the noise term n_i^{VSG} is now a zero-mean Gaussian random variable with variance $\frac{N_0}{2M}$. $V_k(i)\cos\phi_k$ is the MAI from the kth LR user such that

$$V_k(i) = \int_{(i-1)\frac{T_b}{M}}^{i\frac{T_b}{M}} c^{(h)}(t)c_k^{(l)}(t-\tau_k)dt. \tag{2.21}$$

Due to random spreading, using similar approach as in MCD analysis, we can model $V_k(i)$ as

$$V_k(i) = \sum_{j=1}^{N/M} \tilde{X}_{k,0}(j) \tag{2.22}$$

where $\tilde{X}_{k,0}(j)$'s are i.i.d. symmetric Bernoulli random variable with the same distribution as $\tilde{X}_{m,k}(j)$. Note that due to the shortened symbol interval, the number of terms in the summation is a factor of M less than in the case of MCD. Consequently, the distribution of $V_k(i)$ can be found as:

$$P_{V_k(i)}(v) = B(\frac{1}{M}, v) \tag{2.23}$$

2.3.1 Results based on Gaussian approximation

The simplest method to obtain the error probability is via the standard Gaussian approximation (GA) [17, 49], which assumes the sum of all interferences experienced by the desired user to be a Gaussian random variable. In this case, the error probability of the MCD HR user is

$$Pe^{MCD} = Q(\sqrt{SIR^{MCD}}). \tag{2.24}$$

where $Q(x)$ equals to one minus the cumulative distribution function of a zero-mean, unit-variance Gaussian random variable such that [17]

$$Q(x) = \int_x^{\infty} e^{-\frac{t^2}{2}} dt \tag{2.25}$$

Note that the error probability here is a function of only the MCD user's signal-to-interference ratio (SIR^{MCD}), which can be found as

$$\begin{aligned} SIR^{MCD} &= \frac{P}{PVar(\sum_{k=1}^{K} X_{m,k}(i)\cos\phi_k) + \frac{N_0}{2}} \\ &= \frac{1}{\sum_{k=1}^{K} E[X_{m,k}^2(i)\cos^2\phi_k] + \frac{N_0}{2P}} \\ &= \frac{1}{\sum_{k=1}^{K} E[X_{m,k}^2(i)]E[\cos^2\phi_k] + \frac{N_0}{2P}} \\ &= \frac{1}{\frac{K}{2N} + \frac{N_0}{2P}} \end{aligned} \tag{2.26}$$

where the last step is obtained from

$$E[X_{m,k}^2] = \sum_{j=1}^{N} E[\tilde{X}_{k,m}^2(j)] = \frac{1}{N} \tag{2.27}$$

$$E[\cos^2\phi_k] = \int_{-\pi}^{\pi} \frac{1}{2\pi}\cos^2\phi d\phi = \frac{1}{2}. \tag{2.28}$$

A more accurate method to evaluate the error probability is the improved Gaussian approximation (IGA) [40], the basis of which is that if the phase, delay and amplitude

of all users are fixed, then the MAI can be safely approximated as Gaussian random variable using the central-limit-theorem (CLT). In our case, the amplitude of all users are fixed, and due to random signature codes, chip-synchronism and BPSK modulation, the transmission delay does not affect the distribution of the MAI from each LR user. Therefore, in using IGA to calculate error probability, we just need to average over the phase offsets as follows:

$$\begin{aligned} Pe^{MCD} &= \int \dots \int_{-\pi}^{\pi} Q\left(\sqrt{\frac{1}{\sum_{k=1}^{K} E[X_{m,k}^2]\cos^2\phi_k + \frac{N_0}{2P}}}\right)\left(\frac{1}{2\pi}\right)^K d\phi_1 \dots d\phi_K \\ &= \int \dots \int_{-\pi}^{\pi} Q\left(\sqrt{\frac{1}{\sum_{k=1}^{K} \frac{\cos^2\phi_k}{N} + \frac{N_0}{2P}}}\right)\left(\frac{1}{2\pi}\right)^K d\phi_1 \dots d\phi_K \end{aligned} \tag{2.29}$$

Now we evaluate the error probability of the VSG user using standard GA. The SIR at the matched-filter output for the VSG user can be expressed as

$$\begin{aligned} SIR^{VSG} &= \frac{\frac{P}{M}}{P\sum_{k=1}^{K} Var(V_k\cos\phi_k) + \frac{N_0}{2M}} \\ &= \frac{\frac{P}{M}}{P\sum_{k=1}^{K} E[V_k^2]E[\cos^2\phi_k] + \frac{N_0}{2M}} \\ &= \frac{\frac{P}{M}}{P\frac{K}{2MN} + \frac{N_0}{2M}} \\ &= \frac{1}{\frac{K}{2N} + \frac{N_0}{2P}} \\ &= SIR^{MCD}. \end{aligned} \tag{2.30}$$

which means that under GA, the VSG HR user has the same error probability as that of the MCD HR user.

Now, we calculate the error rate of VSG user using the IGA. In this case, we again just need to average over the phase offsets of all interferers and find the error

probability as

$$
\begin{aligned}
Pe^{VSG} &= \int \dots \int_{-\pi}^{\pi} Q\left(\sqrt{\frac{\frac{P}{M}}{P\sum_{k=1}^{K} Var(V_k)\cos^2\phi_k + \frac{N_0}{2M}}}\right)\left(\frac{1}{2\pi}\right)^K d\phi_1 \dots d\phi_K \\
&= \int \dots \int_{-\pi}^{\pi} Q\left(\sqrt{\frac{\frac{P}{M}}{\sum_{k=1}^{K} \frac{P}{NM}\cos^2\phi_k + \frac{N_0}{2M}}}\right)\left(\frac{1}{2\pi}\right)^K d\phi_1 \dots d\phi_K \\
&= \int \dots \int_{-\pi}^{\pi} Q\left(\sqrt{\frac{1}{\sum_{k=1}^{K} \frac{1}{N}\cos^2\phi_k + \frac{N_0}{2P}}}\right)\left(\frac{1}{2\pi}\right)^K d\phi_1 \dots d\phi_K
\end{aligned}
\tag{2.31}
$$

which again equals to the error probability of the MCD HR user obtained via the IGA. Thus, we see that the use of GA and IGA (with random signature codes and BPSK modulation) tell us that we can trade spreading gain for transmission power on a one-to-one basis.

2.3.2 Exact error-rate analysis

Note that in both GA and IGA, the symmetric binomial correlation components in MAI, i.e $X_{k,m}$'s and V_k's, are assumed to have a Gaussian distribution. For system with random signature codes, perfect power control, large spreading factor and large number of users, the central-limit theorem [17] indeed applies here and validates the Gaussian assumption. However, if these cases do not hold, the Gaussian approximation may give misleading results. In such situations, the exact error probability must be computed to accurately evaluate the error rate of MCD- and VSG-CDMA users.

We first calculate the exact error probability for the case where $\cos\phi_i = 1$ for all i, which constitutes the worst case of MAI [78]. The output of the matched filter for the MCD user now yields

$$
\begin{aligned}
y_m^{(h)}(i) =& \sqrt{P} b_m^{(h)}(i) + \sqrt{P}\sum_{k=1}^{K} X_k + n_i \\
=& \sqrt{P} b_m^{(h)}(i) + \sqrt{P} X + n_i \\
=& \sqrt{P}\left(b_m^{(h)}(i) + X + \frac{n_i}{\sqrt{P}}\right) \\
=& \sqrt{P}\left(b_m^{(h)}(i) + Z\right)
\end{aligned}
\tag{2.32}
$$

where the MAI component $X = \sum_{k=1}^{K} X_k$ has distribution

$$p_X(x) = B(K, x) \tag{2.33}$$

The probability density function (PDF) of $Z = X + \frac{n_i}{\sqrt{P}}$ is the convolution of the PDF of a zero-mean Gaussian random variable with variance $\frac{N_0}{2P}$ and the discrete density function of X, which leads to the following expression

$$f_Z(z) = \sum_{x=-NK}^{NK} B(K, \frac{x}{N})(\frac{1}{\sqrt{2\pi}\sigma} e^{-\frac{(z-\frac{x}{N})^2}{2\sigma^2}}) \tag{2.34}$$

where $\sigma = \sqrt{\frac{N_0}{2P}}$.

Consequently, the exact error probability for the MCD user in this case can be found as

$$\begin{aligned} Pe^{MCD} =& \frac{1}{2}(Prob(Z > 1 | b_m^{(h)}(i) = -1) + Prob(Z < -1 | b_m^{(h)}(i) = 1)) \\ =& Prob(Z > 1) \\ =& \int_1^{\infty} f_Z(z) dz \\ =& \sum_{x=-NK}^{NK} \begin{pmatrix} NK \\ \frac{Nx+NK}{2} \end{pmatrix} (\frac{1}{2})^{NK} Q(\frac{1 - \frac{x}{N}}{\sqrt{\frac{N_0}{2P}}}). \end{aligned} \tag{2.35}$$

In the case of very high SNR, i.e. $\frac{N_0}{2P} \to 0$, the effect of background Gaussian noise gradually vanishes, in which case the error probability of the MCD user converges to

$$\begin{aligned} Pe^{MCD} \to& Prob(\sum_{k=1}^{K} X_k > 1) \\ =& \sum_{x=N}^{NK} B(K, \frac{x}{N}) \end{aligned} \tag{2.36}$$

Note from the expression of $B(K, \frac{x}{N})$ that as long as there is a single LR user, the error probability of the MCD user is nonzero even in this hypothetical absence of the background noise.

We next calculate the exact error rate for the VSG HR user for the same setting. The matched-filter output for the VSG user can be expressed as

$$\begin{aligned} y^{(h)}(i) =& \sqrt{\frac{P}{M}} b^{(h)}(i) + \sqrt{P} \sum_{k=1}^{K} V_k + n_i^{VSG} \\ =& \sqrt{\frac{P}{M}} (b^{(h)}(i) + \sqrt{M} (\sum_{k=1}^{K} V_k + \frac{n_i^{VSG}}{\sqrt{P}})) \\ =& \sqrt{\frac{P}{M}} (b^{(h)}(i) + V + \sqrt{\frac{M}{P}} n_i^{VSG}) \\ =& \sqrt{\frac{P}{M}} (b^{(h)}(i) + W) \end{aligned} \tag{2.37}$$

where the MAI component V has the following distribution:

$$p_V(v) = B(\frac{K}{M}, \frac{v}{\sqrt{M}}) \tag{2.38}$$

and the density of the total interference W can be found in manners analogous to that of Z in the MCD case as

$$f_W(w) = \sum_{v=-\frac{KN}{M}}^{\frac{KN}{M}} B(\frac{K}{M}, \frac{v}{N}) (\frac{1}{\sqrt{2\pi}\sigma} e^{-\frac{(w-\frac{v\sqrt{M}}{N})^2}{2\sigma^2}}). \tag{2.39}$$

The error probability for the VSG HR user can subsequently be found as

$$\begin{aligned} Pe^{VSG} =& (1/2) Prob(W > 1 | b_m^{(h)}(i) = -1) + (1/2) Prob(W < -1 | b_m^{(h)}(i) = 1) \\ =& Prob(W > 1) \\ =& \int_1^{\infty} f_W(w) dw \\ =& \sum_{v=-\frac{NK}{M}}^{\frac{NK}{M}} B(\frac{K}{M}, \frac{v}{N}) Q(\frac{1 - \frac{v\sqrt{M}}{N}}{\sqrt{\frac{N_0}{2P}}}). \end{aligned} \tag{2.40}$$

In the case of high SNR, i.e. $\frac{N_0}{2P} \to 0$, the error probability of the VSG user can

be approximated as

$$\begin{aligned} Pe^{VSG} &\rightarrow Prob(\sum_{k=1}^{K} \sqrt{M} V_k > 1) \\ &= \sum_{v=\lceil \frac{N}{\sqrt{M}} \rceil}^{\frac{NK}{M}} B(\frac{K}{M}, \frac{v}{N}) \end{aligned} \tag{2.41}$$

Note that if $K < \sqrt{M}$, i.e. the number of the LR interferers is less than the square root of the rate factor M, the VSG user can be demodulated error-free in the absence of the background Gaussian noise. This happens for the VSG but not the MCD user because the MAI seen by the MCD user has a wide and smooth distribution, while the distribution of MAI experienced by the VSG user is narrow and dense. Distribution of MAI suffered by the VSG and MCD HR user (i.e. $P_X(x)$ and $P_V(v)$) for a system with $N = 64$, $M = 16$, and $K = 2$ are shown in figures 2-3 and 2-4, respectively, for the case where the phase offsets and delay of all users are fixed. In the plot, the MAI distribution in MCD is nonzero in $[-2, 2]$, while the the probability mass function of MAI for VSG is nonzero only in $[-0.5, 0.5]$. Even though these distribution plots are obtained by fixing the phase and delay offset of all users, variations in phase and time offsets are unlikely going to alter the range of MAI distributions.

The exact error rate for the case of worst MAI as a function of the number of users is plotted in figure 2-5 for $N = 64$ and $M = 32$. The bit-error rates (BER) of the VSG and MCD users with time-varying phase uniformly distributed between $[-\pi, \pi]$ are obtained from numerical simulation (each point averaging from 1000 trials) and shown in figure 2-6 for $N = 128$ and $M = 32$. We observe that both figures show the same behavior for the error rate of the HR users. For small K (i.e. small number of LR users), we see that $P_e^{VSG} < P_e^{MCD}$, and as K increases, the error rates eventually converge. Intuitively, the difference between the error performance of the two systems is completely due to the difference in the range of MAI distribution. As the number of users increases, the range of MAI for both users grow large enough such that the central-limit theorem can be applied, in which case the error rate of both MCD and

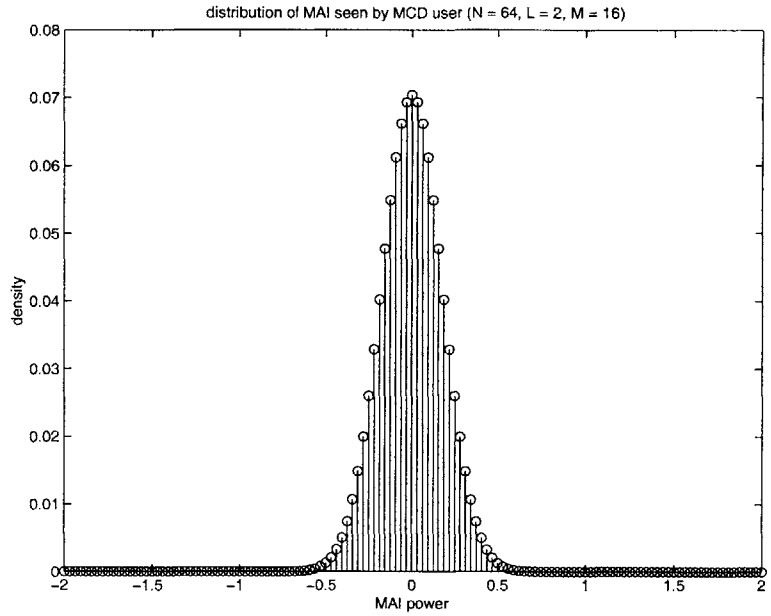

Figure 2-3: Distribution of MAI seen by the MCD-CDMA HR user in AWGN channel (N = 64, M = 16, K = 2)

VSG users become equal since they have the same SIR. Note that these figures are plotted for a moderately high signal-to-noise ratio (SNR) with $\frac{E_b}{N_0} = 12dB$. As $\frac{E_b}{N_0}$ becomes smaller, the difference between the BER of VSG and MCD HR user will be less obvious, as the effect of background Gaussian noise will gradually dominate over that of the MAI.

2.4 Error-rate analysis in flat-fading channel

We now consider a frequency-nonselective Rayleigh fading channel with slow fading such that the received amplitude for each user is constant over T_b. For the MCD HR

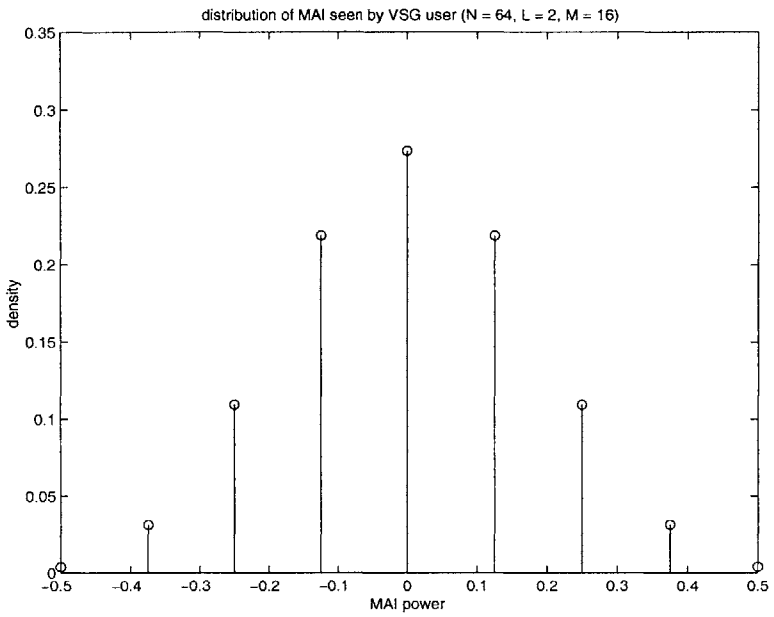

Figure 2-4: Distribution of MAI seen by the VSG-CDMA HR user in AWGN channel (N = 64, M = 16, K = 2)

user, the matched-filter output of the ith symbol in the mth code channel is

$$\begin{aligned} y_m^{(h)}(i) =& \sqrt{P}(A_0 b_m^{(h)}(i) + \sum_{i=1}^{K} A_k X_{m,k} \cos\phi_k + \frac{n_i}{\sqrt{P}}) \\ =& \sqrt{P}(A_0 b_m^{(h)}(i) + \sum_{i=1}^{K} \bar{X}_k + \frac{n_i}{\sqrt{P}}) \\ =& \sqrt{P}(A_0 b_m^{(h)}(i) + \tilde{X} + \frac{n_i}{\sqrt{P}}) \end{aligned} \tag{2.42}$$

where the A's are i.i.d. with Rayleigh distribution as follows:

$$f_A(a) = \frac{2a}{\sigma^2} e^{-\frac{a^2}{\sigma^2}}, a \geq 0. \tag{2.43}$$

Conditioned on A's and ϕ's, $\bar{X}_k$ (the MAI term from the kth LR user) has the following probability distribution

$$p_{\bar{X}_k|A_k,\phi_k}(x) = B(1, \frac{x}{A_k \cos\phi_k}) \tag{2.44}$$

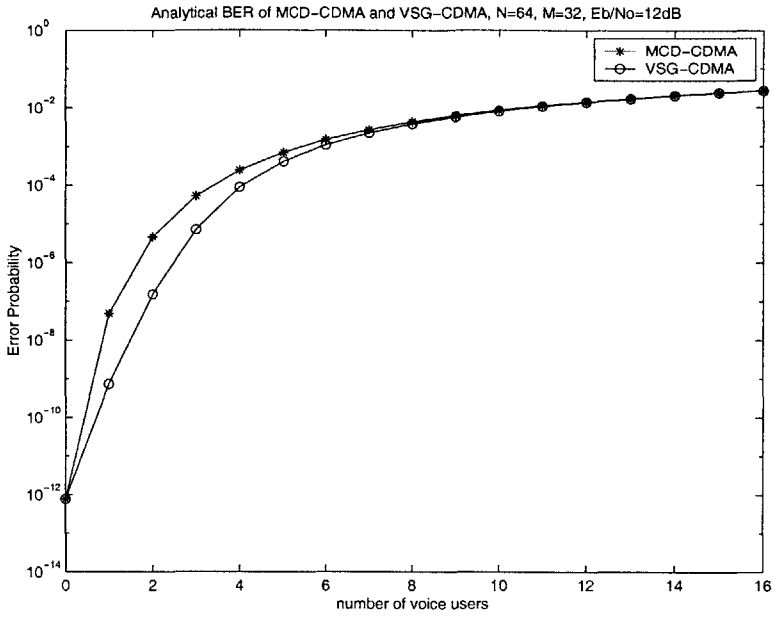

Figure 2-5: The exact error probability of MCD and VSG CDMA users with fixed phase in AWGN channel as a function of the number of LR users with $N = 64$, $M = 32$ and $E_b/N_0 = 12dB$

The density of each of the X_k's can be evaluated as

$$f_{\bar{X}_k}(x) = \int_0^{\infty} \int_{-\pi}^{\pi} \frac{1}{2\pi} B(1, \frac{x}{a\cos\phi}) f_A(a) d\phi da \tag{2.45}$$

Subsequently, we can find the probability density function of the sum of MAI from all LR users, i.e. $\tilde{X} = \sum_{i=1}^{K} \bar{X}_k$ as

$$f_{\tilde{X}}(x) = f_{\bar{X}_1}(x) * f_{\bar{X}_2}(x) * \ ... \ * f_{\bar{X}_k}(x) \tag{2.46}$$

where "*" denotes convolution.

To calculate the exact error probability, we see that if we fix $\tilde{X}$ and A_0, then $y^{(h)}(i)$ has a Gaussian distribution, from which the error probability can be evaluated as

$$P^{MCD}(\text{error}|\tilde{X}, A_0) = Q(\frac{A_0 + \tilde{X}}{\sqrt{\frac{N_0}{2P}}}) \tag{2.47}$$

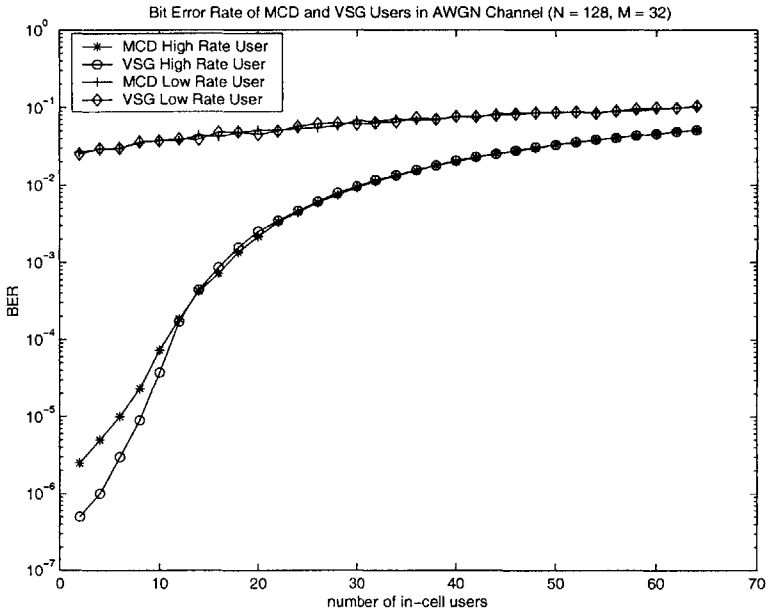

Figure 2-6: BER of MCD and VSG CDMA users in AWGN channel as a function of the number of LR users with $N = 128$, $M = 32$ and $E_b/N_0 = 12dB$

The exact error rate can then be found as

$$\begin{aligned} P_e^{MCD} &= E_{A_0,\tilde{X}}[Q(\frac{A_0+\tilde{X}}{\sqrt{\frac{N_0}{2P}}})] \\ &= \int_{-\infty}^{\infty}\int_{0}^{\infty} Q(\frac{a+x}{\sqrt{\frac{N_0}{2P}}}) f_{\tilde{X}}(x) f_A(a) da dx, \end{aligned} \tag{2.48}$$

The numerical value of the error probability can be evaluated using analytical software or approximated by averaging P_e^{MCD} from a large number of independent trials over the distribution of $\tilde{X}$'s and A's.

Using similar method, we now evaluate the error probability of VSG HR user in flat fading channel. The matched-filter output for the ith symbol of the VSG HR

user in this case can be described as

$$\begin{aligned} y^{(h)}(i) =& \sqrt{P}(\frac{1}{\sqrt{M}} A_0 b^{(h)}(i) + \sum_{k=1}^{K} A_k^{(l)} \cos\phi_k V_k + \frac{\tilde{n}_i}{\sqrt{P}}) \\ =& \sqrt{P}(\frac{1}{M} A_0 b^{(h)}(i) + \sum_{k=1}^{K} \bar{V}_k + \frac{\tilde{n}_i}{P}) \\ =& \sqrt{P}(\frac{1}{M} A_0 b^{(h)}(i) + \tilde{V} + \frac{\tilde{n}}{P}) \end{aligned} \tag{2.49}$$

Conditioned on all A's and ϕ's, $\bar{V}_k$, the MAI term from the kth LR user, has the following probability distribution

$$p_{\bar{V}_k|A_k,\phi_k}(v) = B(\frac{1}{M}, \frac{x}{A_k \cos\phi_k}) \tag{2.50}$$

The density of each V_k's can then be evaluated as

$$f_{\bar{V}_k}(v) = \int_0^{\infty} \int_{-\pi}^{\pi} \frac{1}{2\pi} B(\frac{1}{M}, \frac{x}{a\cos\phi}) f_A(a) d\phi da \tag{2.51}$$

Subsequently, we can find the probability density function of the sum of MAI from all LR users, i.e. $\tilde{X} = \sum_{i=1}^{K} \bar{X}_k$ as

$$f_{\tilde{V}}(v) = f_{\bar{V}_1}(v) * f_{\bar{V}_2}(v) * \ ... \ * f_{\bar{V}_k}(v). \tag{2.52}$$

To calculate the exact error probability, we see that conditioned on $\tilde{V}$ and A_0, $y^{(h)}(i)$ has a Gaussian distribution, from which the error probability can be evaluated as

$$P^{VSG}(\text{error}|\tilde{V}, A_0) = Q(\frac{A_0 + \sqrt{M}\tilde{V}}{\sqrt{\frac{N_0}{2P}}}) \tag{2.53}$$

The exact error rate can then be found as

$$\begin{aligned} P_e^{VSG} &= E_{A_0,\tilde{V}}[Q(\frac{A_0+\sqrt{M}\tilde{V}}{\sqrt{\frac{N_0}{2P}}})] \\ &= \int_{-\infty}^{\infty}\int_{0}^{\infty} Q(\frac{a+\sqrt{M}v}{\sqrt{\frac{N_0}{2P}}}) f_{\tilde{V}}(v) f_A(a) da dv. \end{aligned} \tag{2.54}$$

The numerical values of the error probability expression can then be evaluated using analytical software (such as Mathematica) or approximated by averaging P_e^{VSG} over a large number of independent trials over the distribution of A's and V's.

The error probability of the VSG and MCD user in frequency-non-selective Rayleigh fading channel (obtained by averaging the error probability over a large number of trials with independent fading and MAI statistics) is plotted in figure 2-7 for $N = 128$, $M = 32$, and $\frac{E_b}{N_0} = 12dB$. We observe that the error rate of the two systems are practically the same, even when the number of users is very small. The BER gap that is evident in analysis for the AWGN channel is closed here because averaging over the fading statistics widens and smoothes the distribution of the MAI seen by the VSG user. In this case, we predict that the HR user in both systems would have identical error performance. Simulation results also show the same behavior.

2.5 Results in multipath fading channel

We now compare the error performance of MCD and VSG HR users in a frequency-selective (multipath) Rayleigh fading channel. We assume the absence of LR users to emphasize the effect of multipath interference caused by the HR user's own signal. This assumption is justified since the interference caused by LR users from multiple paths are essentially MAI, the effect of which has been addressed in the previous sections.

Under our assumptions, the received signal from a Q-path channel with only the

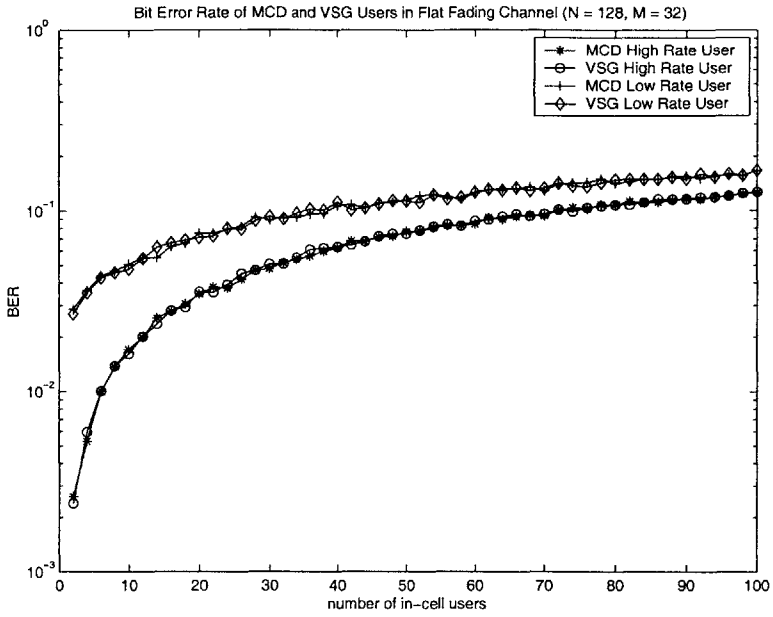

Figure 2-7: BER of MCD and VSG CDMA users in Frequency non-selective Rayleigh fading channel

HR user can be expressed as

$$r(t) = \sum_{q=1}^{Q} A_q e^{j\phi_q} s_0(t - \tau_q) + n(t) \tag{2.55}$$

where A_q, ϕ_q, τ_q are the amplitude, phase, and delay of the received signal from the qth path, respectively. Using matched-filter detection followed by coherent RAKE combining, the soft decision for the ith symbol in the mth code channel of the MCD user can be expressed as

$$y_m^{MCD}(i) = Re\{\sum_{q=1}^{Q} w_q e^{-j\phi_q} y_{m,q}^{MCD}(i)\} \tag{2.56}$$

where $w_q \geq 0$ is the weighting factor for the qth signal path during the combining process; For example, $w_q = A_q$ for maximal ratio combining (MRC), and $w_q = 1$ for equal gain combining (EGC)) [55]; $y_{m,q}(i)$ is the output from the matched filter

receiver at the RAKE finger corresponding to the qth signal path such that

$$\begin{aligned} y_{m,q}^{MCD}(i) &= \int_{(i-1)T_b-\tau_{q,r}}^{iT_b-\tau_{q,r}} r(t)c_m^{(h)}(t-\tau_{q,r})dt \\ &= A_q\sqrt{P}e^{j\phi_q}b_m^{(h)}(i) + \sum_{r=1,r\neq q}^{Q} A_r\sqrt{P}e^{j\phi_r}\sum_{l=1}^{M}(b_l^{(h)}(i)\rho_{m,l}^{(0)}(\tau_{q,r}) \\ &\quad + b_l^{(h)}(i+1)\rho_{m,l}^{(1)}(\tau_{r,q})u(\tau_{r,q}) + b_l^{(h)}(i-1)\rho_{m,l}^{(-1)}(\tau_{q,r})u(\tau_{q,r})) + n_{m,q} \end{aligned} \tag{2.57}$$

where $n_{m,q}$ is the background Gaussian noise term with zero-mean and variance $\frac{N_0}{2}$; $u(t)$ is the step function, $\tau_{q,r} = \tau_r - \tau_q$, which gives $\tau_{q,r} = -\tau_{r,q}$; the ρ's are correlation terms such that

$$\begin{aligned} \rho_{m,l}^{(0)}(\tau_{q,r}) = &\int_{(i-1)T_b+\tau_{q,r}}^{iT_b} c_m^{(h)}(t)c_l^{(h)}(t-\tau_{q,r})u(\tau_{q,r})dt \\ &+ \int_{(i-1)T_b}^{iT_b-\tau_{r,q}} c_m^{(h)}(t)c_l^{(h)}(t+\tau_{r,q})u(\tau_{r,q})dt \end{aligned} \tag{2.58}$$

$$\rho_{m,l}^{(-1)}(\tau_{q,r}) = \int_{(i-1)T_b}^{(i-1)T_b+\tau_{q,r}} c_m^{(h)}(t)c_l^{(h)}(t-\tau_{q,r})dt \tag{2.59}$$

$$\rho_{m,l}^{(1)}(\tau_{r,q}) = \int_{iT_b-\tau_{r,q}}^{iT_b} c_m^{(h)}(t)c_l^{(h)}(t+\tau_{r,q})dt \tag{2.60}$$

Note that $\rho_{m,l}^{(0)}(\tau_{q,r}) = \rho_{l,m}^{(0)}(\tau_{r,q})$. For analytical convenience, we assume that the receiver can only resolve paths that are separated by integer multiples of chip intervals. In this case, we have $\tau_{q,r} = \delta_{q,r}T_c$, where $\delta_{q,r} \in \mathbb{Z}$. Since the user signature codes ($p^{(h)}(j) \in \{-1,1\}$'s) are random, $\rho_{m,l}^{(0)}(\tau_{q,r})$, $\rho_{m,l}^{(1)}(\tau_{r,q})$, and $\rho_{m,l}^{(-1)}(\tau_{q,r})$ are zero-mean "symmetric binomial" random variables with the following variances:

$$var(\rho_{m,l}^{(0)}(\tau_{q,r})) = \frac{N-|\delta_{q,r}|}{N^2} \tag{2.61}$$

$$var(\rho_{m,l}^{(1)}(\tau_{r,q})) = var(\rho_{m,l}^{(-1)}(\tau_{q,r})) = \frac{|\delta_{q,r}|}{N^2} \tag{2.62}$$

where $\delta_{q,r} = \delta_r - \delta_q$.

Similarly, for the VSG user, the soft decision for the ith symbol after RAKE

combining can be expressed as

$$y^{VSG}(i) = Re\{\sum_{l=1}^{L} w_q e^{-\phi_q} y_q^{VSG}(i)\} \tag{2.63}$$

where $y_q(i)$, the matched-filter output for the finger corresponding to the qth signal path, can be expressed as

$$\begin{aligned} y_q^{VSG}(i) =& \int_{(i-1)T_b-\tau_q}^{iT_b+\tau_q} r(t)c^{(h)}(t-\tau_q)dt \\ =& A_q\sqrt{\frac{P}{L}}e^{j\phi_q}b^{(h)}(i) + \sum_{r=1,r\neq q}^{Q} A_r\sqrt{LP}e^{j\phi_r}(b^{(h)}(i)\tilde{\rho}^{(0)}(\tau_{q,r}) \\ &+ b^{(h)}(i+1)\tilde{\rho}^{(1)}(\tau_{q,r})u(\tau_{r,q}) + b^{(h)}(i-1)\tilde{\rho}^{(-1)}(\tau_{q,r})u(\tau_{q,r})) + n_q \end{aligned} \tag{2.64}$$

where n_q is the background Gaussian noise with zero-mean and variance $\frac{N_0}{2M}$, and

$$\begin{aligned} \tilde{\rho}^{(0)}(\tau_{q,r}) =& \int_{(i-1)T_b+\tau_{q,r}}^{iT_b} c^{(h)}(t)c^{(h)}(t-\tau_{q,r})u(\tau_{q,r})dt \\ &+ \int_{(i-1)T_b}^{iT_b-\tau_{r,q}} c^{(h)}(t)c^{(h)}(t+\tau_{r,q})u(\tau_{r,q})dt \end{aligned} \tag{2.65}$$

$$\tilde{\rho}^{(-1)}(\tau_{q,r}) = \int_{(i-1)T_b}^{(i-1)T_b+\tau_{q,r}} c^{(h)}(t)c^{(h)}(t-\tau_{q,r})dt \tag{2.66}$$

$$\tilde{\rho}^{(1)}(\tau_{q,r}) = \int_{iT_b-\tau_{r,q}}^{iT_b} c^{(h)}(t)c^{(h)}(t+\tau_{r,q})dt. \tag{2.67}$$

Since the user spreading codes are random, the $\tilde{\rho}$'s are zero-mean symmetric binomial random variables with the following variances:

$$var(\tilde{\rho}^{(0)}(\tau_{q,r})) = \frac{\frac{N}{M} - |\delta_{q,r}|}{N^2} \tag{2.68}$$

$$var(\tilde{\rho}^{(-1)}(\tau_{q,r})) = var(\tilde{\rho}^{(1)}(\tau_{q,r})) = \frac{|\delta_{q,r}|}{N^2} \tag{2.69}$$

To evaluate the error performance, we first consider a simple 2-path channel, i.e. $l \in \{1,2\}$. We assume that $\tau_1 = \phi_1 = 0$ and that $\tau_2 = \delta_2 T_c$, where $\delta_2 \in [1, \frac{N}{M}]$.

We first analyze the MCD user, for which the RAKE finger outputs in this case are simplified to

$$\begin{aligned} y_{m,1}^{MCD}(i) =& A_1\sqrt{P}b_m(i) + \sum_{j=1}^{M} A_2\sqrt{P}e^{j\phi_2}(b_l^{(h)}(i)\rho_{m,l}^{(0)}(\tau_2) \\ &+ b_l^{(h)}(i-1)\rho_{m,l}^{(-1)}(\tau_2)) + n_{m,1} \end{aligned} \tag{2.70}$$

$$\begin{aligned} y_{m,2}^{MCD}(i) =& A_2\sqrt{P}e^{j\phi_2}b_m(i) + \sum_{j=1}^{M} \sqrt{P}A_1(b_l^{(h)}(i)\rho_{m,l}^{(0)}(-\tau_2) \\ &+ b_l^{(h)}(i+1)\rho_{m,j}^{(1)}(-\tau_2)) + n_{m,2}. \end{aligned} \tag{2.71}$$

The soft decision after RAKE combining is then

$$\begin{aligned} y_m^{MCD}(i) =& Re\{\sum_{q=1}^{2} w_q e^{-j\phi_q} y_{m,l}^{MCD}(i)\} \\ =& (w_1A_1 + w_2A_2)\sqrt{P}b_m(i) + (w_1A_1 + w_2A_2)\sqrt{P}\cos\phi_2 b_m^{(h)}(i)\rho_{m,m}^{(0)}(\tau_2) \\ &+ \cos\phi_2\sqrt{P}(\sum_{l=1,l\neq m}^{M}(A_2w_1b_l^{(h)}(i)\rho_{m,l}^{(0)}(\tau_2) \\ &+ A_1w_2b_l^{(h)}(i)\rho_{m,l}^{(0)}(-\tau_2)) + \sum_{j=1}^{M}(A_2b_l^{(h)}(i+1)w_1\rho_{m,l}^{(-1)}(\tau_2) \\ &+ A_1w_2b_l^{(h)}(i-1)\rho_{m,l}^{(1)}(-\tau_2))) + w_1n_{m,1} + w2n_{m,2}\cos\phi_2 \end{aligned} \tag{2.72}$$

where, since the data symbols are transmitted as 1 or -1 with equal probability, $b_l^{(h)}(i)\rho_{m,l}^{(0)}(\tau_2)$, $b_l^{(h)}(i)\rho_{m,l}^{(0)}(-\tau_2)$, $b_l^{(h)}(i-1)\rho_{m,l}^{(-1)}(\tau_2)$, and $b_l^{(h)}(i+1)\rho_{m,l}^{(1)}(-\tau_2)$ are independent, zero-mean symmetric binomial random variables with the following variances:

$$\begin{aligned} var(b_l^{(h)}(i)\rho_{m,l}^{(0)}(\tau_2)) &= \frac{N-\delta_2}{N^2},\ var(b_l^{(h)}(i)\rho_{m,l}^{(0)}(-\tau_2)) = \frac{N-\delta_2}{N^2}, \\ var(b_l^{(h)}(i-1)\rho_{m,l}^{(-1)}(\tau_2)) &= \frac{\delta_2}{N^2},\ var(b_l^{(h)}(i+1)\rho_{m,l}^{(1)}(-\tau_2)) = \frac{\delta_2}{N^2}. \end{aligned}$$

Also, note from eq. 2.72 that the term $b_m^{(h)}(i)\rho_{m,m}^{(0)}(\tau_2)$ appears in both RAKE fingers.

This is the correlated multipath interference (CMPI) component, as it introduces correlation between the output of RAKE fingers 1 and 2. All other ρ's contribute to the uncorrelated MPI (UCMPI) [9].

Subsequently, the SIR of the MCD user conditioned on A_q, ϕ_q, and τ_q can be expressed as

$$SIR^{MCD} = \frac{(w_1 A_1 + w_2 A_2)^2}{I^{MCD} + \frac{N_0}{2P}(w_1^2 + w_2^2 \cos^2 \phi_2)} \tag{2.73}$$

where $I^{MCD} = I^{MCD}_{CMPI} + I^{MCD}_{UCMPI}$ is the overall multipath interference power normalized by the transmit power, where I^{MCD}_{CMPI} and I^{MCD}_{UCMPI} are the normalized power of correlated and uncorrelated MPI, respectively, which can be expressed as

$$I^{MCD}_{CMPI} = (w_1 A_2 + w_2 A_1)^2 \cos^2 \phi_2 \frac{N - \delta}{N^2} \tag{2.74}$$

$$I^{MCD}_{UCMPI} = (A_2^2 w_1^2 + A_1^2 w_2^2) \cos^2 \phi_2 \frac{M\delta + (M-1)(N-\delta)}{N^2} \tag{2.75}$$

Note that the weight on CMPI, i.e. $(w_1 A_2 + w_2 A_1)^2$ is larger than that on each of the UCMPI, i.e. $(A_2^2 w_1^2 + A_1^2 w_2^2)$. However, also note that for large M, the total MPI suffered by the MCD user is always dominated by the UCMPI.

We now analyze the received SIR for the VSG HR user in the same two-path channel. The output from each of the RAKE fingers of the VSG HR user can be expressed as

$$\begin{aligned} y_1^{VSG}(i) =& A_1 \sqrt{\frac{P}{M}} b(i) + \sqrt{MP} A_2 e^{j\phi_2} (b(i)\tilde{\rho}^{(0)}(\tau_2) \\ &+ b(i-1)\tilde{\rho}^{(-1)}(\tau_2)) + \tilde{n}_1 \end{aligned} \tag{2.76}$$

$$\begin{aligned} y_2^{VSG}(i) =& A_2 \sqrt{\frac{P}{M}} e^{j\phi_2} b(i) + A_1 \sqrt{MP} (b(i)\tilde{\rho}^{(0)}(\tau_2) \\ &+ b(i+1)\tilde{\rho}^{(1)}(-\tau_2)) + \tilde{n}_2 \end{aligned} \tag{2.77}$$

The soft decision after coherent RAKE combining is then

$$\begin{aligned} y^{VSG}(i) =& Re\{\sum_{q=1}^{2} w_q e^{-\phi_q} y_l^{VSG}(i)\} \\ =& (w_1 A_1 + w_2 A_2)\sqrt{\frac{P}{M}} b(i) \\ &+ (A_1 w_2 + A_2 w_1)\cos\phi_2 \sqrt{PM}\tilde{\rho}^{(0)}(\tau_2) \\ &+ A_2 w_1 \sqrt{PM}\cos\phi_2 \tilde{\rho}^{(-1)}(\tau_2) + A_1 w_2 \cos\phi_2 \sqrt{PM}\tilde{\rho}^{(1)}(-\tau_2) \\ &+ w1\tilde{n}_1 + w_2 \tilde{n}_2 \cos\phi_2 \end{aligned} \tag{2.78}$$

With random spreading codes and BPSK modulated symbols, $b(i)\tilde{\rho}^{(0)}(\tau)$, $b(i-1)\tilde{\rho}^{(-1)}(\tau)$, and $b(i+1)\tilde{\rho}^{(1)}(-\tau)$ are mutually independent, zero-mean symmetric binomial random variables with the following variances:

$$Var(\tilde{\rho}^{(0)}(\tau)) = \frac{\frac{N}{M} - \delta_2}{N^2} \tag{2.79}$$

$$Var(\tilde{\rho}^{(-1)}(\tau)) = \frac{\delta_2}{N^2} \tag{2.80}$$

$$Var(\tilde{\rho}^{(1)}(-\tau)) = \frac{\delta_2}{N^2} \tag{2.81}$$

We also observe from eq. 2.76 that the term $\sqrt{PM}\tilde{\rho}^{(0)}(\tau_2)$ appears in both RAKE fingers and is hence the CMPI.

The SIR of the VSG user can subsequently be found as

$$SIR^{VSG} = \frac{(w_1 A_1 + w_2 A_2)^2}{I^{VSG} + \frac{N_0}{2P}(w_1^2 + w_2^2 \cos\phi_2{}^2)} \tag{2.82}$$

where $I^{VSG} = I_{CMPI}^{VSG} + I_{UCMPI}^{VSG}$ is the total multipath interference power suffered by the VSG HR user normalized by its transmit power; I_{CMPI}^{VSG} and I_{UCMPI}^{VSG} are the normalized correlated and uncorrelated MPI power, respectively, and can be expressed

as

$$I_{CMPI}^{VSG} = M^2(A_1w_2 + A_2w_1)^2\cos^2\phi_2\frac{\frac{N}{M} - \delta_2}{N^2} \tag{2.83}$$

$$I_{UCMPI}^{VSG} = M^2\cos^2\phi_2\frac{\delta_2}{N^2}(A_2^2w_1^2 + A_1^2w_2^2) \tag{2.84}$$

Note that if δ_2 is much smaller than $\frac{N}{M}$, the correlated MPI will have a much larger power than the uncorrelated MPI for large M.

We now compare the SIR of the MCD and VSG HR user in the two-path channel. Since contributions from symbol energy and background noise in both cases are the same as shown in eq. (2.73) and (2.82), the comparison of SIR can be reduced to finding the differences in the power of multipath interferences (MPI). The MPI experienced by the MCD HR user can be expressed as:

$$\begin{aligned} I^{MCD} =& (w_1A_2 + w_2A_1)^2\cos^2\phi_2\frac{N - \delta_2}{N^2} \\ &+ (A_2^2w_1^2 + A_1^2w_2^2)\cos^2\phi_2\frac{M\delta_2 + (M-1)(N-\delta_2)}{N^2} \\ =& \cos^2\phi_2((w_1A_2 + w_2A_1)^2\frac{N - \delta_2}{N^2} \\ &+ (A_1^2w_2^2 + A_2^2w_1^2)(\frac{(M-1)N + \delta_2}{N^2})) \\ =& \cos^2\phi_2(2w_1w_2A_1A_2\frac{N - \delta_2}{N^2} + (w_1^2A_2^2 + w_2^2A_1^2)\frac{M}{N}) \end{aligned} \tag{2.85}$$

while the MPI suffered by the VSG user can be rearranged as

$$\begin{aligned} I^{VSG} =& M^2(A_1w_2 + A_2w_1)^2\cos^2\phi_2\frac{\frac{N}{M} - \delta_2}{N^2} \\ &+ M^2\cos^2\phi_2\frac{\delta_2}{N^2}(A_2^2w_1^2 + A_1^2w_2^2) \\ =& \cos^2\phi_2((A_1^2w_2^2 + A_2^2w_1^2)\frac{M(N-\delta_2) - M(M-1)\delta_2 + M^2\delta_2}{N^2} \\ &+ 2A_1A_2w_1w_2\frac{M(N - M\delta_2)}{N^2}) \\ =& \cos^2\phi_2(2w_1w_2A_1A_2\frac{M(N - M\delta_2)}{N^2} + (w_1^2A_2^2 + w_2^2A_1^2)\frac{M}{N}). \end{aligned} \tag{2.86}$$

The difference in their MPI power is then:

$$\begin{aligned} I_{diff} =& I^{VSG} - I^{MCD} \\ =& \cos^2\phi_2 2w_1w_2A_1A_2(\frac{MN - M^2\delta_2}{N^2} - \frac{N-\delta_2}{N^2}) \\ =& \cos^2\phi_2 2w_1w_2A_1A_2\frac{(M-1)N - (M^2-1)\delta_2}{N^2} \\ =& \cos^2\phi_2 2w_1w_2A_1A_2\frac{(M-1)(N-(M+1)\delta_2)}{N^2} \end{aligned} \tag{2.87}$$

The above equation gives several important insights:

1. As long as w_1, w_2, A_1, A_2 are all positive (i.e. as long as we combine the output of the paths), and $M > 1$ (i.e. HR transmission), the VSG user suffers from a larger MPI power than the MCD user if $\delta_2 < \frac{N}{M+1}$ (i.e. $\tau_2 < \frac{T_b}{M+1}$). If $\frac{T_b}{M+1} < \tau_2 < \frac{T_b}{M}$, then the MCD user suffers a larger MPI power than the VSG user.

2. The SIR of MCD and VSG users from just a single RAKE finger should be exactly the same, as this corresponds to the case of selection combining where either w_1 or w_2 is zero but not both.

The intuitive explanation for the statements made above is that when time offset between the two paths is small compared to the symbol interval of the VSG user, the VSG user suffers a great deal of CMPI, while the interferences seen by the MCD user is always dominated by UCMPI contributed by other parallel code channels. As the time offset grows, the CMPI suffered by the VSG user quickly decreases, while the MCD user still has some CMPI component from the code channel where the desired symbol lies. Note that the threshold at which the SIR of MCD and VSG are equal is independent of the amplitude and the weighting factor used for each path.

Furthermore, if we let τ_2 grows beyond $\frac{T_b}{M}$ but less than T_b, i.e. by letting $\frac{T_b}{M} < \delta_2 < T_b$, while the SIR expression for the MCD user are not affected, the VSG user

will not have CMPI anymore. In this case, the MPI suffered by the VSG becomes

$$\begin{aligned} I^{VSG} =& M^2(A_1^2w_2^2 + A_2^2w_1^2)\cos^2\phi_2\frac{\frac{N}{M}-\delta_2}{N^2} \\ &+ M^2\cos^2\phi_2\frac{\delta_2}{N^2}(A_2^2w_1^2 + A_1^2w_2^2) \\ =& (A_1^2w_2^2 + A_2^2w_1^2)\cos^2\phi_2\frac{M}{N^2} \end{aligned} \tag{2.88}$$

In this case, we see that

$$I^{VSG} - I^{MCD} = -2w_1w_2A_1A_2\cos^2\phi_2\frac{N-\delta_2}{N^2} < 0 \tag{2.89}$$

where the difference is contributed by the CMPI suffered by the MCD user. In this case, VSG user will always have a higher SIR than the MCD user.

If we let τ_2 grow even further such that it is larger than T_b (which makes $\delta_2 > N$) then neither VSG or MCD user will suffer from any CMPI. In this case, the MPI suffered by both users can be expressed as

$$I^{VSG} = I^{MCD} = (A_1^2w_2^2 + A_2^2w_1^2)\cos^2\phi_2\frac{M}{N^2} \tag{2.90}$$

which means that MCD and VSG users have identical SIR.

We now extend the analysis to a general Q-path channel, where $Q \geq 2$. We rank the path i.d. according to the delay offsets, i.e. $\tau_1 \geq \tau_2 \geq \ldots \geq \tau_Q$ and assume that $\tau_Q - \tau_1 < \frac{T_b}{M}$, i.e. the delay spread of the channel is less than the symbol interval of a VSG HR user. In this case, the soft decision of the MCD user after RAKE combining can be expressed as

$$\begin{aligned} y_m^{MCD}(i) =& \sqrt{P}(\sum_{q=1}^{Q} w_qA_qb_m(i) + \sum_{q=1}^{Q-1}\sum_{r=q+1}^{Q}\cos\phi_{q,r}(U_{CMPI}(\tau_{q,r}) \\ &+ U_{UCMPI}(\tau_{q,r})) + \sum_{q=1}^{Q} w_q\frac{n_{q,m}}{\sqrt{P}}\cos\phi_q) \end{aligned} \tag{2.91}$$

where $U_{CMPI}(\tau_{q,r})$ and $U_{UCMPI}(\tau_{q,r})$ are the normalized correlated and uncorrelated

MPI components, respectively, between paths q and r, which can be expressed as

$$U_{CMPI}(\tau_{q,r}) = \ (w_q A_r + w_r A_q) b_m(i) \rho^{(0)}_{m,m}(\tau_{q,r}) \tag{2.92}$$

$$\begin{aligned} U_{UCMPI}(\tau_{q,r}) =& w_q A_r \Big(\sum_{l=1, l\neq m}^{M} (b_l(i)\rho^{(0)}_{m,l}(\tau_{q,r}) + b_l(i-1)\rho^{(-1)}_{m,l}(\tau_{q,r}) \\ &+ b_m(i-1)\rho^{(-1)}_{m,m}(\tau_{q,r})) + w_r A_q \Big(\sum_{l=1, l\neq m}^{M} (b_l(i)\rho^{(0)}_{m,l}(\tau_{r,q}) \\ &+ b_l(i+1) rho^{(1)}_{m,l}(\tau_{r,q})) + b_m(i+1)\rho^{(1)}_{m,m}(\tau_{r,q})). \end{aligned} \tag{2.93}$$

Due to the random spreading and BPSK modulated transmitted symbols, we observe that

1. $E[U_{CMPI}(\tau_{q,r})] = E[U_{UCMPI}(\tau_{q,r})] = 0$,
2. $U_{CMPI}(\tau_{q,r})$ and $U_{UCMPI}(\tau_{q,r})$ are uncorrelated for all $1 \leq q \leq Q-1$ and $q+1 \leq r \leq Q$.
3. Both $U_{CMPI}(\tau_{q,r})$ and $U_{UCMPI}(\tau_{q,r})$ are i.i.d. for all pairs of q and r, where $1 \leq q \leq Q-1$ and $q+1 \leq r \leq Q$.

With these observations, we first see that the variance of the MPI components, found in the same way as that in the two-path case, can be expressed as

$$\begin{aligned} var(U_{CMPI}(\tau_{q,r})) =& E[U^2_{CMPI}(\tau_{q,r})] \\ =& (w_q A_r + w_r A_q)^2 \frac{N - |\delta_{q,r}|}{N^2} \end{aligned} \tag{2.94}$$

$$\begin{aligned} var(U_{UCMPI}(\tau_{q,r})) =& E[U^2_{UCMPI}(\tau_{q,r})] \\ =& (w_q^2 A_r^2 + w_r^2 A_q^2)((M-1)\frac{N - |\delta_{q,r}|}{N^2} + M\frac{|\delta_{q,r}|}{N^2}) \end{aligned} \tag{2.95}$$

and that given A's and ϕ's, the overall power of multipath interferences can be ex-

pressed as

$$\begin{aligned} I^{MCD} =& var(\sum_{q=1}^{Q-1}\sum_{r=q+1}^{Q}\cos\phi_{q,r}(U_{CMPI}(\tau_{q,r})+U_{UCMPI}(\tau_{q,r}))) \\ =& E[(\sum_{q=1}^{Q-1}\sum_{r=q+1}^{Q}\cos\phi_{q,r}(U_{CMPI}(\tau_{q,r})+U_{UCMPI}(\tau_{q,r})))^2] \\ =& \sum_{q=1}^{Q-1}\sum_{r=q+1}^{Q}\cos^2\phi_{q,r}(E[U^2_{CMPI}(\tau_{q,r})]+E[U^2_{UCMPI}(\tau_{q,r})]) \\ =& \sum_{q=1}^{Q-1}\sum_{r=q+1}^{Q}\cos^2\phi_{q,r}((w_qA_r+w_rA_q)^2\frac{N-|\delta_{q,r}|}{N^2} \\ &+(w_q^2A_r^2+w_r^2A_q^2)((M-1)\frac{N-|\delta_{q,r}|}{N^2}+M\frac{|\delta_{q,r}|}{N^2})) \end{aligned} \tag{2.96}$$

Subsequently, conditioned on A's and ϕ's, the SIR of the MCD user can be expressed as

$$SIR^{MCD} = \frac{(\sum_{q=1}^{Q}A_qw_q)^2}{I^{MCD}+\sum_{q=1}^{Q}w_q^2\cos^2\phi_q\frac{N_0}{2P}} \tag{2.97}$$

We now evaluate the SIR of the VSG HR user using the same approach. The soft decision for the VSG user after coherent RAKE combining in a Q-path channel can be expressed as

$$\begin{aligned} y^{VSG}(i) =& \frac{P}{\sqrt{M}}(\sum_{q=1}^{Q}w_qA_qb(i) \\ &+\sum_{q=1}^{Q-1}\sum_{r=q+1}^{Q}\cos\phi_{q,r}(\tilde{U}_{CMPI}(\tau_{q,r})+\tilde{U}_{UCMPI}(\tau_{q,r})) \\ &+\sum_{q=1}^{Q}w_q\frac{\tilde{n}_q\sqrt{M}}{\sqrt{P}}\cos\phi_q) \end{aligned} \tag{2.98}$$

where $\tilde{U}_{CMPI}(\tau_{q,r})$ and $\tilde{U}_{UCMPI}(\tau_{q,r})$ are the normalized correlated and uncorrelated MPI components, respectively, between path q and r, which can be expressed as

$$\tilde{U}_{CMPI}(\tau_{q,r}) = (w_qA_r+w_rA_q)Mb(i)\tilde{\rho}^{(0)}(\tau_{q,r}) \tag{2.99}$$

$$\begin{aligned}\tilde{U}_{UCMPI}(\tau_{q,r}) =& w_q A_r Mb(i-1)\tilde{\rho}^{(-1)}(\tau_{q,r})) \\ &+ w_r A_q \sqrt{M} b(i+1)\tilde{\rho}^{(1)}(\tau_{r,q})).\end{aligned} \tag{2.100}$$

where the $\tilde{U}$'s possess the same statistical properties that are specified for the U's earlier (such as pairwise independence, i.i.d., etc.). The variance of each of the MPI components, found in the same way as that in the two-path case, can be expressed as

$$\begin{aligned}var(\tilde{U}_{CMPI}(\tau_{q,r})) =& E[\tilde{U}^2_{CMPI}(\tau_{q,r})] \\ =& (w_q A_r + w_r A_q)^2 \frac{M(N-|\delta_{q,r}|)}{N^2}\end{aligned} \tag{2.101}$$

$$\begin{aligned}var(\tilde{U}_{UCMPI}(\tau_{q,r})) =& E[\tilde{U}^2_{UCMPI}(\tau_{q,r})] \\ =& (w_q^2 A_r^2 + w_r^2 A_q^2) M \frac{|\delta_{q,r}|}{N^2}\end{aligned} \tag{2.102}$$

Conditioned on A's and ϕ's, the overall power of multipath interference can be expressed as

$$\begin{aligned}I^{VSG} =& var(\sum_{q=1}^{Q-1}\sum_{r=q+1}^{Q} \cos\phi_{q,r}(\tilde{U}_{CMPI}(\tau_{q,r}) + \tilde{U}_{UCMPI}(\tau_{q,r}))) \\ =& \sum_{q=1}^{Q-1}\sum_{r=q+1}^{Q} \cos^2\phi_{q,r}(E[U^2_{CMPI}(\tau_{q,r})] + E[U^2_{UCMPI}(\tau_{q,r})]) \\ =& \sum_{q=1}^{Q-1}\sum_{r=q+1}^{Q} \cos^2\phi_{q,r}((w_q A_r + w_r A_q)^2 \frac{M(N-|\delta_{q,r}|)}{N^2} \\ &+ (w_q^2 A_r^2 + w_r^2 A_q^2)\frac{M|\delta_{q,r}|}{N^2})\end{aligned} \tag{2.103}$$

Subsequently, the SIR of the VSG user can be expressed as

$$SIR^{VSG} = \frac{(\sum_{q=1}^{Q} A_q w_q)^2}{I^{VSG} + \sum_{q=1}^{Q} w_q^2 \cos^2\phi_q \frac{N_0}{2P}} \tag{2.104}$$

As before, the difference between the SIR of MCD and VSG user depends on the

difference of their MPI power, which can be found as

$$\begin{aligned} I_{diff} =& I^{VSG} - I^{MCD} \\ =& \sum_{q=1}^{Q-1} \sum_{r=q+1}^{Q} \cos^2 \phi_{q,r} (w_q A_r + w_r A_q)^2 \frac{M(N - |\delta_{q,r}|)}{N^2} \\ &+ (w_q^2 A_r^2 + w_r^2 A_q^2) \frac{M|\delta_{q,r}|}{N^2} - (w_q A_r + w_r A_q)^2 \frac{N - |\delta_{q,r}|}{N^2} \\ &- (w_q^2 A_r^2 + w_r^2 A_q^2)((M-1)\frac{N - |\delta_{q,r}|}{N^2} - M\frac{|\delta_{q,r}|}{N^2}) \\ =& \sum_{q=1}^{Q-1} \sum_{r=q+1}^{Q} \cos^2 \phi_{q,r} 2 w_q A_r w_r A_q \frac{(M-1)(N - (M+1)|\delta_{q,r}|)}{N^2} \end{aligned} \tag{2.105}$$

In this case, we see that if time offsets between all possible pairs of paths are small, i.e. if $\delta_{q,r} < \frac{N}{M+1}$ or equivalently $\tau_{q,r} < \frac{T_b}{M+1}$ for $1 \leq q \leq Q-1$ and $q+1 \leq r \leq Q$ (such as indoor or densely populated urban area), the VSG user will suffer from a larger MPI power than the MCD user. On the opposite, if $\frac{T_b}{M+1} < \tau_{q,r} \leq \frac{T_b}{M}$ for all possible q's and r's (such as in less populated urban and suburban areas), the SIR of the MCD user is going to be worse than that of the VSG user.

Similar as the two-path case, if we let all $\tau_{q,r}$'s grow beyond $\frac{T_b}{M}$ but less than T_b, i.e. by letting $\frac{T_b}{M} < \tau_{q,r} < T_b$ for all $1 \leq q \leq Q-1$ and $q+1 \leq r \leq Q$, while the SIR expression for the MCD user is not affected, the VSG user will not have CMPI anymore. In this case, the MPI suffered by the VSG becomes

$$I^{VSG} = \sum_{q=1}^{Q-1} \sum_{r=q+1}^{Q} \cos^2 \phi_{q,r} (A_q^2 w_r^2 + A_r^2 w_q^2) \frac{M}{N^2} \tag{2.106}$$

In this case, we see that

$$I^{VSG} - I^{MCD} = -\sum_{q=1}^{Q-1} \sum_{r=q+1}^{Q} 2 w_r w_q A_r A_q \cos^2 \phi_{q,r} \frac{N - \delta_{q,r}}{N^2} < 0 \tag{2.107}$$

where the difference is contributed by the CMPI suffered by the MCD user. In this case, VSG user will always have a higher SIR than the MCD user.

If we let $\tau_{q,r}$'s exceed T_b, then neither VSG or MCD user will suffer from any

CMPI. In this case, the MPI suffered by both can be expressed as

$$I^{VSG} = I^{MCD} = \sum_{q=1}^{Q-1} \sum_{r=q+1}^{Q} (A_q^2 w_r^2 + A_r^2 w_q^2) \cos^2 \phi_{q,r} \frac{M}{N^2} \tag{2.108}$$

which shows that both MCD and VSG users will have the same SIR.

So far, we have analyzed the SIR of VSG and MCD users in multipath channels. We showed that, conditioned on the path amplitudes and phase offsets, the SIR of the VSG user is likely to be worse than that of the MCD user if the channel has a very small delay spread. On the other hand, for channels with a large delay spread, the VSG user is likely to outperform MCD user in terms of the SIR. So what is the implication of this result in terms of error probability? It has been suggested in [88] that in a channel with very small delay spread, since the MCD user has a better SIR than the VSG user, the error probability of the MCD user will be lower also. The basis for this claim is that the error probability for each user can be calculated by approximating MPI as Gaussian interference, from which the error probability can be computed as follows:

$$P_e = \int \int Q(SIR(\mathbf{a}, \phi)) f_{\mathbf{A}}(\mathbf{a}) f_{\mathbf{\Phi}}(\phi) d\mathbf{a} d\phi \tag{2.109}$$

where $\mathbf{A} = [A_1 \, A_2 \ldots A_Q]^T$ are the i.i.d. Rayleigh distributed path amplitudes and $\mathbf{\Phi} = [\phi_1 \, \phi_2 \ldots \phi_Q]^T$ are the received phase offsets of each path.

For a two-path channel, it can be verified from our equations that the CMPI and UCMPI indeed have a symmetric binomial distribution and thus can be approximated as Gaussian if the number of additive components is large enough. In figure 2-10, we plot the simulated bit-error-rate (BER) for VSG and MCD users with different delay spread in two-path Rayleigh fading channel for $N = 128$ and $M = 32$ averaged over 1000 trials. For small delay spread, the path difference varies between 1 and 2 chips, while for large delay spread, the path difference randomly fluctuates between 5 and 9 chips. It is clear that the BER of VSG user with small delay spread is the worst due to large CMPI. The BER difference between MCD and VSG for large delay spread

may be a bit subtle, since MCD is always dominated by UCMPI, but with careful observation, we do see that the BER of the VSG user slightly outperforms that of the MCD user in this case.

Interestingly, when the number of paths grows beyond two, we do not have a conclusive answer as to which scheme outperforms the other, even though we know how SIRs of the two systems compare. The key observation we have is that in this case the use of Gaussian approximation may lead to serious errors in BER calculation because the MPIs are not only non-Gaussian but may also have an asymmetric distribution. In this case, a user with a larger correlated multipath interference power (and thus smaller SIR) may actually have a better BER.

To see an example, let us consider the case where $N = 64$, $M = 16$, $Q = 3$, and the delays being $\tau_1 = 0$, $\tau_2 = T_c$, and $\tau_3 = 3T_c$. The received signal of the VSG HR user from different paths is shown in figure 2-8.

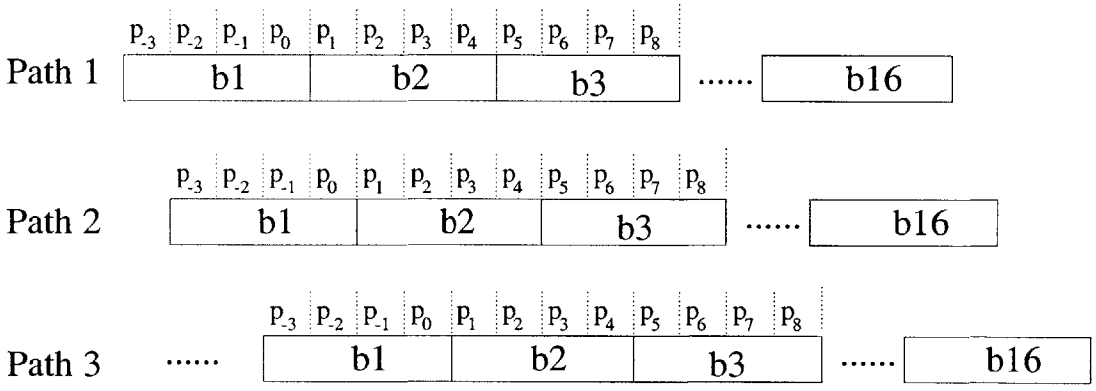

Figure 2-8: VSG Signals in a Multipath Channel

Without loss of generality, let's look at the demodulation of bit 2 assuming equal

gain combining and fixed path amplitudes. The VSG user sees the following MPI:

$$\begin{aligned} I_{MP}^{VSG} =& \frac{4\sqrt{P}}{64}(2b_2(p_1p_2 + p_2p_3 + p_3p_4 + p_1p_4 + p_1p_3 + p_2p_4) \\ &+ b_1(p_0p_1 + p_1p_{-2} + p_2p_{-1} + p_3p_0 + p_1p_{-1} + p_2p_0) \\ &+ b_3(p_4p_5 + p_2p_5 + p_3p_6 + p_4p_7 + p_3p_5 + p_4p_6)) \\ =& \frac{\sqrt{P}}{16}(I_2 + I_1 + I_3) \end{aligned} \tag{2.110}$$

where p_i's are i.i.d. symmetric Bernoulli random variables with probability of 0.5 being 1 and probability of 0.5 of being -1; I_i is the corresponding normalized MPI from the ith bit, for which we see that

$$I_1 = b_1(p_0p_1 + p_1p_{-2} + p_2p_{-1} + p_3p_0 + p_1p_{-1} + p_2p_0) \tag{2.111}$$

$$I_2 = 2b_2(p_1p_2 + p_2p_3 + p_3p_4 + p_1p_4 + p_1p_3 + p_2p_4) \tag{2.112}$$

$$I_3 = b_3(p_4p_5 + p_2p_5 + p_3p_6 + p_4p_7 + p_3p_5 + p_4p_6) \tag{2.113}$$

It is clear that I_2 causes CMPI while I_1 and I_3 causes UCMPI. To compute the error probability, it can be easily verified that the distribution of UCMPI, i.e. $I_1 + I_3$, are symmetric binomial and can therefore be approximated as Gaussian since the number of terms in the sum is sufficiently large. The CMPI, i.e. I_2, on the other hand, has the following distribution shown in figure 2-9, which is clearly neither Gaussian nor symmetric. Since the I's are correlated with each other, the variance of the MPI can be calculated as

$$var(I^{VSG}) = \frac{P}{256}(var(I_1) + var(I_2) + var(I_3)) = \frac{36P}{256} \tag{2.114}$$

and the SIR of the VSG user can be found as

$$SIR_{MP}^{VSG} = \frac{144}{36 + \frac{24N_0}{P}} \tag{2.115}$$

With a given received power, the error probability of the VSG user can be calculated

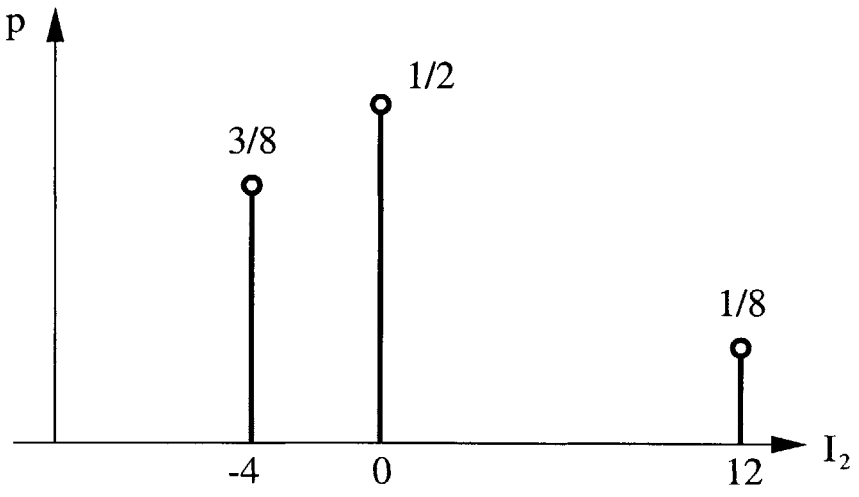

Figure 2-9: An example of the probability mass function for the correlated MPI of VSG user in a three-path channel with short delay spread

as

$$Pe_{MP}^{VSG} \approx \frac{3}{8}Q(\frac{8}{\sqrt{12+\frac{24N_0}{P}}}) + \frac{1}{8}Q(\frac{24}{\sqrt{12+\frac{24N_0}{P}}}) + \frac{1}{2}Q(\frac{12}{\sqrt{12+\frac{24N_0}{P}}}) \quad (2.116)$$

where we assume the UCMPI, i.e. I_1 and I_3 as Gaussian interferences since the sum of the two is a sufficiently large binomial random variable that can be approximated as Gaussian. It can be verified that Pe_{MP}^{VSG} is significantly smaller than $Q(\sqrt{SIR_{MP}^{VSG}})$ for SNR (i.e. $\frac{E_b}{N_0} = \frac{2P}{N_0}$) exceeds 0dB.

Let us now consider demodulation of the bit from the second code channel of the MCD user in this case. Since most of the multipath interferences for the MCD users come from other code channels, the total SIR can be approximated as

$$SIR_{MP}^{MCD} \approx \frac{144}{24+\frac{24N_0}{P}} \quad (2.117)$$

by ignoring the correlated MPI for code channel 2. This SIR is clearly greater than SIR_{MP}^{VSG}. The corresponding error probability for a given received power can then be

approximated as

$$Pe_{MP}^{MCD} \approx Q(SIR_{MP}^{MCD}) \tag{2.118}$$

which is slightly optimistic than the realistic error probability due to the ignorance of the correlated MPI. However, the reader can verify that Pe_{MP}^{MCD} will be greater than Pe_{MP}^{VSG} for $\frac{2P}{N_0}$ exceeds 3dB.

In figure 2-11, we plot the BER performance of MCD and VSG HR user in a three-path Rayleigh fading channel under different types of delay-spread for $N = 128$ and $M = 32$. We see that for small delay spread ($\tau_{1,2} = T_c$ and $\tau_{2,3} = 2T_c$), the VSG user outperforms the MCD user even though it sees a larger MPI power. On the other hand, if the delay spread is large ($\tau_{1,2} = 6T_c$ and $\tau_{2,3} = 8T_c$), the MCD user outperforms the VSG user. The BER behavior in three-path channel is therefore completely opposite of that in the two-path channel because of the asymmetric distribution of MPI.

At this point, the reader may question how would addition of LR users into the system impact the result. We can answer this question by approximating the effect of LR users as additional background noise. From figures 2-10 and 2-11, we see that as the amount of background noise increases and gradually dominates over the MPI, the differences between the BER of MCD and VSG HR user diminishes. We therefore expect the same thing to happen if the number of LR users in the system increases. In such cases, the choice of using MCD or VSG will depend more on tradeoffs between physical layer and higher layer implementation costs since both systems exhibit practically the same error performance.

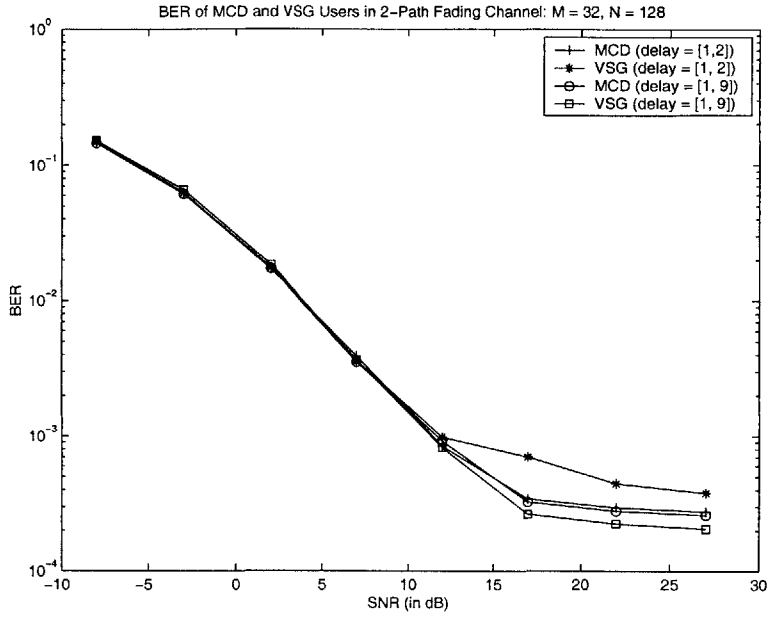

Figure 2-10: BER of MCD and VSG HR users in a two-path Rayleigh fading channel

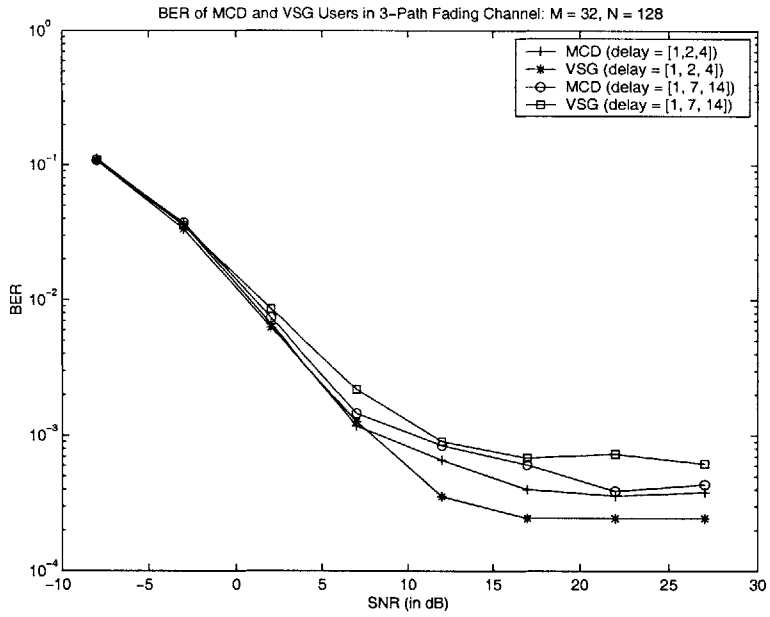

Figure 2-11: BER of MCD and VSG HR users in a three-path Rayleigh fading channel

2.6 Chapter Summary

In this chapter, we compared the error performance of MCD- and VSG-CDMA HR users in AWGN, flat-fading and multipath fading channels. Instead of employing traditional Gaussian approximation that assumes all interferences to be Gaussian random variables, we evaluate the bit-error rate using the true interference distributions. We made three key observations. First, in an ideal AWGN channel, we found that the VSG user outperforms MCD user at moderately high E_b/N_0 if the number of LR interferers in the cell is small. As the population of LR user increases, both users achieve the same error rate. In flat-fading channel, however, both MCD and VSG user seem to have identical bit-error rate, since averaging over fading smoothes the distribution of interferences seen by both users and make them become similar. Second, in multipath fading channels, we found that the VSG user is likely to suffer from a larger interference power than the MCD user if the channel has a small delay spread. The opposite is true for channels with moderately large delay spread. Third, we found that for channels with three or more paths, the SIR does not truly represent the error probability because multipath interferences may have an asymmetric distribution. Therefore, the decision on whether to use VSG or MCD for such channels should be decided on a case-by-case basis rather than rely on theoretical SIR comparison as has been done in the past[48].

Chapter 3

Multistage Interference Cancellation based on MMSE Optimization

In this chapter, we present two effective decision-feedback multistage interference cancellation algorithms that can be used at the DS-CDMA base-station receiver to suppress the user-to-user (multiple-access) interferences (MAI). Both detection algorithms are derived by minimizing the mean-squared error (MSE) of the cancellation output at each stage, and both schemes use a weighting matrix to incorporate the reliability of MAI reconstruction in every stage into the cancellation process. Our first algorithm uses a MMSE optimized feedback matrix to reconstruct and cancel the MAI and has similar computational complexity as that of a conventional multistage parallel interference canceller (PIC). We show that this scheme exhibits significantly better spectral- and energy-efficiency than the conventional PIC. Our second algorithm is more complex than the first one such that it uses a feedforward matrix together with feedback cancellation to suppress MAI. We deduce the jointly optimal (MMSE) feedforward and feedback processing matrices at each stage. We illustrate that, with complexity on the same order as that for linear joint detection, the performance of this receiver not only significantly surpasses that of the linear joint detectors but also approaches the single-user performance bound.

3.1 Background and motivation

The idea of suppressing multiple-access interferences (MAI) in a DS-CDMA system using multistage interference cancellation (IC) was first proposed in [70]. This type of receiver, shown in figure 3-1, operates in a stage-by-stage manner. The initial stage is a matched-filter bank followed by minimum-distance decision devices (i.e. quantizers). In every subsequent stage, the receiver first reconstructs the MAI suffered by each user based on symbol estimates of all in-cell users made at the previous stage and then subtracts these MAI estimates from the users' matched-filter outputs. The results from the cancellation process are sent to quantization devices to determine the symbol estimates for the current stage. This multistage IC is also referred to as the conventional parallel IC (PIC) [46], as it performs MAI cancellation for all users (simultaneously) in parallel.

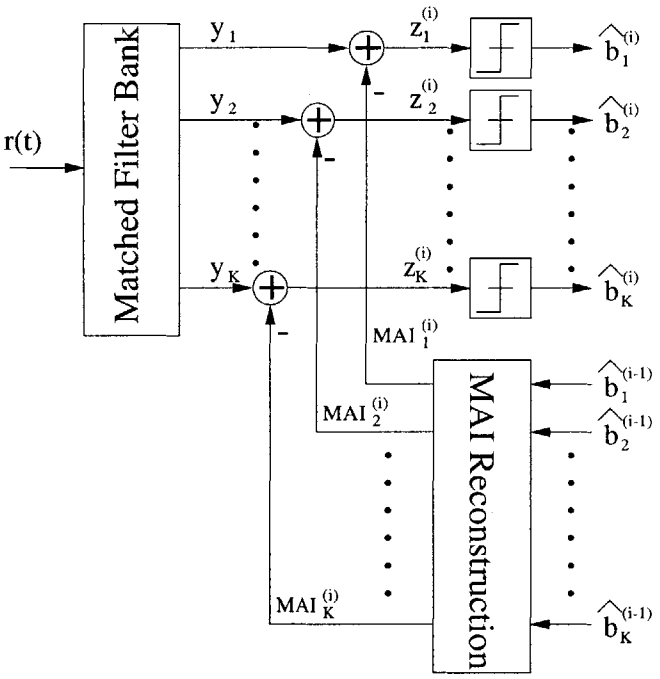

Figure 3-1: A general multi-stage decision-feedback interference canceller

The PIC is attractive for practical implementation because it has a lower complexity than many other joint detectors [46]. A key weakness with the conventional PIC,

however, is that it assumes the symbol estimates made at every stage to be entirely accurate [71, 86]. Hence, complete MAI cancellation based on tentative decisions from the previous stage is always performed. Since the quality of symbol estimates at early stages, particularly the initial stage, can be quite poor due to excessive MAI, the performance of this receiver often suffers from severe error propagation [62]. Consider, for example, in a binary phase-shift-keying (BPSK) modulated system, if a wrong symbol estimate is used to reconstruct the MAI, the power of the corresponding MAI component will be quadrupled after cancellation. Subsequently, the error rate of a PIC often diverges, in which case the probability of symbol error at later stages becomes higher than that at earlier stages [75].

To alleviate the effect of error propagation, [62] proposed the use of partial MAI cancellation. The essential idea is that since the symbol estimates tend to be inaccurate at early stages, only a fraction of MAI based on those estimates should be canceled. As symbol decisions become more reliable in later stages, more substantial MAI cancellation becomes appropriate. To implement this idea, the receiver assigns a small weight to MAI cancellation (to cancel a fraction of MAI) at early stages and a larger cancellation weight at later stages. The performance of this receiver has been shown to significantly outperform the conventional PIC in a system employing perfect power control [62]. Two aspects of this receiver can still be improved, however. First, the cancellation weights are generated in a trial-and-error fashion from computer simulations rather than via a systematic method. It is therefore unclear which set of cancellation weights leads to the optimal performance under a specific design criterion. Second, the receiver assumes uniform error performance among all subscribers and thereby assigns the same weight to cancel the MAI from all users' at a given stage. In reality, however, even with random spreading codes and reasonable power control, the quality of symbol estimates may still differ significantly from one user to another [75]. It is therefore preferable to assign disparate cancellation weights to the MAI caused by different users to further improve the system performance.

An alternative approach to PIC is the well-known successive interference canceller (SIC), which can actually be viewed as a weighted multistage IC that detects one user

per stage [78, 51]. In a typical SIC, users are ranked according to their received signal power. The strongest user is detected first based on its matched-filter output. The MAI from this user is then reconstructed based on its symbol estimate and subtracted from matched-filter output of all other users. The receiver then proceeds to determined the received symbol of the second strongest user, after which it reconstructs and cancels the MAI caused by this user from the matched-filter output of the remaining users. This procedure continues until all users in the system are detected. For a system with K users, SIC can be viewed as a K-stage weighted IC that, at stage k, it assigns a cancellation weight of 1 to the MAI from the first $k-1$ users (with the largest received signal power) and a weight of 0 to the MAI from all other users. Only the kth user is detected at the kth stage. It has been shown that the use of SIC can asymptotically eliminate the effect of MAI and approach the single-user performance bound, provided that the received powers of the users differ in exponential order [51]. In practice, however, it is almost impossible to make the users' received powers to be exponentially distributed, and thus SIC almost never approach such good performance. In fact, in today's DS-CDMA system where good power control is employed, the received powers of all users are approximately the same. In this case, the performance of the SIC, both in terms of bit-error rate (BER) and latency, is often inferior to that of conventional PIC [46].

An alternative solution to weighted or partial interference cancellation is to enhance the quality of symbol estimates at the first stage using linear joint detectors (such as the decorrelator or the linear MMSE detector) instead of the matched filter [75]. Such approaches indeed lead to performance that surpasses the conventional PIC but at the expense of higher complexity. Furthermore, it is known that the error performance of this type of receivers at later stages may be worse than that of the decorrelator or the linear MMSE detector alone [75]. This happens because these receivers make use of the noisy matched-filter output at subsequent stages. To further improve the receiver performance, a feedforward linear processing unit has been introduced to work together with feedback cancellation at every stage. Such proposals lead to several decision feedback joint detectors with feedforward process-

ing [8, 13, 31, 75]. Most of these receivers, however, still assume that the symbol estimates from the previous stage is completely accurate and hence may suffer from severe error propagation when the assumption fails.

Here, we present two types of weighted multistage ICs derived using constrained MMSE optimization at every stage, and the key difference between our algorithms and most of the prior techniques is the use of a weighting matrix that assesses the quality of symbol estimates in the previous stage. The weighting matrix mainly depends on the error probability of the symbol estimates in the previous stage, which can be easily approximated by estimating the SIR of the cancellation output or by using interleaved pilot sequences. These two ICs differentiate from each other in complexity constraints. The first algorithm uses a MMSE-optimized feedback matrix to reconstruct and suppress MAI and has a complexity comparable to that of the partial and conventional PIC. We show that this detector clearly outperforms both the conventional and partial PIC in terms of spectral- and energy-efficiency. However, due to its complexity constraint, this scheme may not perform as well as the linear joint detectors do, and its error performance is far from the single-user bound for a crowded system. Our second technique applies jointly (MMSE) optimized feedforward and feedback matrices to suppress MAI and therefore has a higher complexity than our first method. It exhibits superior error-rate performance, which not only significantly surpasses that of the linear joint detectors but also approaches the single-user performance bound in a few iterations. Yet, the complexity of this receiver is comparable to that of linear joint detectors.

The outline of this chapter is as follows. Section 2 introduces the basic system model for multistage interference cancellation. Our first algorithm that employs MMSE-optimized feedback MAI cancellation is presented in section 3, and its performance is shown in section 4. Our second algorithm that uses feedforward and feedback matrices to suppress MAI is presented in section 5, and its performance is illustrated in section 6. Section 7 summarizes the chapter. Derivations of the weighting matrix is shown in appendix A.

3.2 Existing multistage decision-feedback interference canceller

3.2.1 System model

We consider a DS-CDMA system with K equal-rate users communicating simultaneously over a common frequency-nonselective channel, each using a unique spreading code. The composite baseband signal arriving at the receiver can be expressed as

$$r(t) = \sum_{k=1}^{K} A_k s_k(t - \tau_k) e^{j\phi_k} + n(t) \tag{3.1}$$

where A_k, ϕ_k and τ_k are the received amplitude, phase and delay of the kth user's signal, respectively; $n(t)$ is the additive white Gaussian noise (AWGN) with one-sided spectral density $N_0 = 2\sigma^2$; $s_k(t)$ is the kth user's transmitted signal such that

$$\begin{aligned} s_k(t) &= \sum_{i=-\infty}^{\infty} b_k(i) c_k(t - iT_b) \\ &= \sum_{i=-\infty}^{\infty} b_k(i) \sum_{j=1}^{N} c_k(iN + j) \psi(t - iT_b - jT_c) \end{aligned} \tag{3.2}$$

where $b_k(i)$ is the ith data symbol of user k; $c_k(j) \in \{-1, 1\}$ is the jth chip of user k's spreading code; T_b and T_c are the symbol and chip durations, respectively, where $T_b = NT_c$, with N being the spreading gain; $\psi(t)$ is the time-limited chip modulating waveform such that $\int_{T_c} |\psi(t)|^2 dt = \frac{1}{N}$.

For analytical convenience, we assume that the receiver has perfect timing, phase, and amplitude estimation for all users, which makes coherent detection possible. Without loss of generality, we also assume that each user transmits a frame of L symbols, where $L \geq 1$, and that the maximum difference in reception delay between different users is less than one symbol interval, i.e. $\tau_{max} - \tau_{min} < T_b$, where $\tau_{max} = max_{1 \leq k \leq K}\{\tau_k\}$ and $\tau_{min} = min_{1 \leq k \leq K}\{\tau_k\}$. In this case, the matched-filter output for

the lth symbol transmitted by user k, denoted as $y_k(l)$, can be described as follows:

$$\begin{aligned} y_k(l) = & \int_{lT_b+\tau_k}^{(l+1)T_b+\tau_k} r(t)c_k(t-\tau_k)e^{-j\phi_k} \\ = & A_k(l)b_k(l) + \sum_{m=1,m\neq k}^{K} e^{j(\phi_m-\phi_k)}(A_m(l)b_m(l)\rho_{k,m}^{(0)}(l) \\ & + A_m(l-1)b_m(l-1)\rho_{k,m}^{(-1)}(l)u(\tau_m-\tau_k) \\ & + A_m(l+1)b_m(l+1)\rho_{k,m}^{(1)}(l)u(\tau_k-\tau_m)) + n_k(l) \end{aligned} \tag{3.3}$$

where $n_k(l)$, the background noise term, is a zero-mean Gaussian random variable with variance σ^2; $A_k(l)$ is the amplitude of user k's received signal in its lth symbol interval; $u(t)$ is a unit-step function such that $u(t) = 1$ if $t > 0$ and equals to 0 otherwise. The summation term contains MAI from all other users (on user k) due to cross-correlation of the spreading (signature) sequences. The correlation terms in the MAI for $k \neq m$ are defined as

$$\rho_{k,m}^{(0)}(l) = \begin{cases} \int_{(l-1)T_b+\tau_k+\tau_m}^{lT_b+\tau_k} c_k(t-\tau_k)c_m(t-\tau_m)dt & \text{if } \tau_m \geq \tau_k. \\ \int_{(l-1)T_b+\tau_k}^{lT_b+\tau_k-\tau_m} c_k(t-\tau_k)c_m(t-\tau_m)dt & \text{if } \tau_k > \tau_m. \end{cases} \tag{3.4}$$

$$\rho_{k,m}^{(-1)}(l) = \int_{(l-1)T_b+\tau_k}^{(l-1)T_b+\tau_k+\tau_m} c_k(t-\tau_k)c_m(t-\tau_m)dt \tag{3.5}$$

$$\rho_{k,m}^{(1)}(l) = \int_{lT_b+\tau_k-\tau_m}^{lT_b+\tau_k} c_k(t-\tau_k)c_m(t-\tau_m)dt. \tag{3.6}$$

Note that $\rho_{k,m}^{(-1)}(l) = \rho_{m,k}^{(1)}(l-1)$. The corresponding symbol decision $\hat{b}_k(l)$ can be made based on $y_k(l)$ using the minimum-distance rule [19].

We now develop a vector notation for detection in the case where each user transmits a frame of L symbols, i.e. $l = 1, 2, \ldots L$. We let $\mathbf{y} = [\mathbf{y}(1)\ \mathbf{y}(2)\ \ldots\ \mathbf{y}(L)]^T$, where $\mathbf{y}(l) = [y_1(l)\ y_2(l)\ \ldots\ y_K(l)]^T$. It is straightforward to verify that the vector $\mathbf{y}$ can be

expressed as

$$\mathbf{y} = \mathbf{R_a A b} + \mathbf{n} \tag{3.7}$$

where $\mathbf{n} = [n_1(1)\ n_2(1)\ ...\ n_k(l)\ n_{k+1}(l)\ ...\ n_{K-1}(L)\ n_K(L)]$ is the noise vector; $\mathbf{R_a}$ is the LK-by-LK conjugate-symmetric correlation matrix such that

$$\mathbf{R_a} = \begin{bmatrix} \mathbf{R}^{(0)}(1) & \mathbf{R}^{(1)H}(2) & \mathbf{0} & ... & ... & \mathbf{0} \\ \mathbf{R}^{(1)}(2) & \mathbf{R}^{(0)}(2) & \mathbf{R}^{(1)H}(3) & \mathbf{0} & ... & \mathbf{0} \\ ... & ... & ... & ... & ... & ... \\ \mathbf{0} & \mathbf{0} & \mathbf{0} & ... & \mathbf{R}^{(1)}(L) & \mathbf{R}^{(0)}(L) \end{bmatrix} \tag{3.8}$$

where ^{H} denotes conjugate transpose; $\mathbf{R}^{(0)}(l)$ and $\mathbf{R}^{(1)}(l)$ are K-by-K matrices with entries as follows:

$$R^{(0)}(l)_{k,m} = \begin{cases} e^{j(\phi_m - \phi_k)} \rho^{(0)}_{k,m}(l) & \text{if } k \neq m \\ 1 & \text{if } k = m \end{cases} \tag{3.9}$$

$$R^{(1)}(l)_{k,m} = \begin{cases} e^{j(\phi_m - \phi_k)} \rho^{(-1)}_{k,m}(l) & \text{if } \tau_k < \tau_m \\ 0 & \text{otherwise} \end{cases}. \tag{3.10}$$

$\mathbf{A}$ is the amplitude matrix such that

$$\mathbf{A} = \begin{bmatrix} \mathbf{A}(1) & \mathbf{0} & ... & ... & ... & \mathbf{0} \\ \mathbf{0} & \mathbf{A}(2) & \mathbf{0} & ... & ... & \mathbf{0} \\ \mathbf{0} & \mathbf{0} & \mathbf{A}(3) & \mathbf{0} & ... & \mathbf{0} \\ ... & ... & ... & ... & ... & ... \\ ... & ... & ... & ... & \mathbf{0} & \mathbf{A}(L) \end{bmatrix} \tag{3.11}$$

where $\mathbf{A}(l)$ is a diagonal matrix such that

$$\mathbf{A}(l) = \begin{bmatrix} A_1(l) & 0 & ... & ... & ... \\ 0 & A_2(l) & 0 & ... & ... \\ ... & ... & ... & ... & ... \\ ... & ... & ... & 0 & A_K(l). \end{bmatrix} \tag{3.12}$$

It is clear that the diagonal terms in the product $\mathbf{R_a A}$ are amplitudes of the desired signals and the off-diagonal terms contribute to the MAI.

To complete the vector notation, we denote the transmitted symbol vector $\mathbf{b}$ as

$$\mathbf{b} = [\mathbf{b}(1)^T \ \mathbf{b}(2)^T \ ... \ \mathbf{b}(L)^T]^T \tag{3.13}$$

where $\mathbf{b}(l) = [b_1(l) \ b_2(l) \ ... \ b_k(l)]^T$ with ^{T} denoting transpose.

3.2.2 Existing methods

For a typical multistage (parallel) interference canceller (IC) as shown in figure 3-2, the cancellation output at the ith stage, $\mathbf{z}^{(i)}$, can be expressed as

$$\mathbf{z}^{(i)} = \mathbf{y} - \mathbf{F}^{(i)}\hat{\mathbf{b}}^{(i-1)} \tag{3.14}$$

where $\mathbf{F}^{(i)}$ is the feedback matrix that reconstructs the MAI according to receiver-specific criterion; $\hat{\mathbf{b}}^{(i-1)} = [\hat{b}_1^{(i-1)}(1) \ \hat{b}_2^{(i-1)}(1) \ ... \ \hat{b}_K^{(i-1)}(1) \ \hat{b}_1^{(i-1)}(2) \ ... \ \hat{b}_K^{(i-1)}(L)]^T$ is the vector of symbol estimates for all users made in stage $i-1$ and is generated by passing $\mathbf{z}^{(i-1)}$ through the minimum-distance decision (quantization) device. For instance, if the symbols are BPSK modulated, then $\hat{\mathbf{b}}^{(i)} = sgn(\mathbf{z}^{(i)})$, where $sgn(x) = 1$ if $x > 0$ and -1 otherwise. Note that the matched-filter detection corresponds to the initial stage where $i = 1$, in which case $\hat{\mathbf{b}}^{(0)} = \mathbf{0}$ and $\mathbf{z}^{(1)} = \mathbf{y}$.

Using this model, the conventional PIC is one that defines $\mathbf{F}$ to be [71]

$$\mathbf{F}^{(i)} = (\mathbf{R_a} - \mathbf{I})\mathbf{A} \tag{3.15}$$

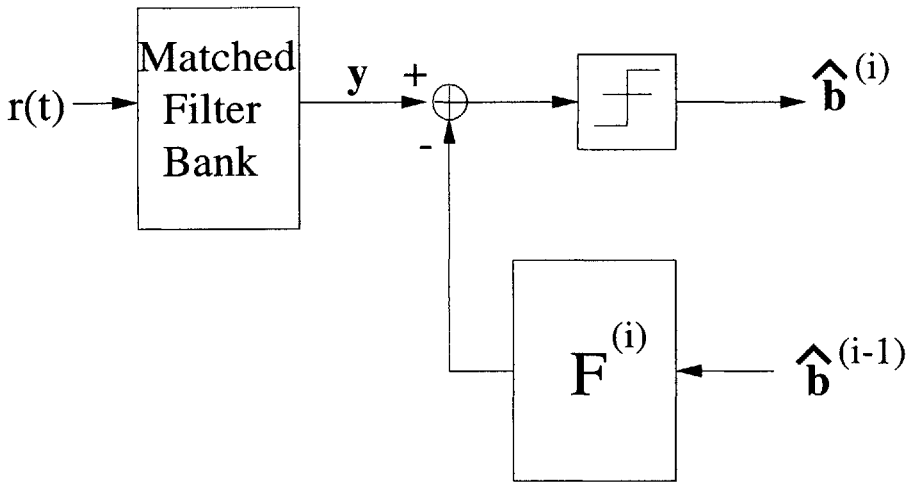

Figure 3-2: Multi-stage decision-feedback interference canceller in vector form

for all stages. Intuitively, this means that at every stage, the receiver attempts to cancel all off-diagonal terms in $\mathbf{R_a A}$ (i.e. complete MAI cancellation). This model was derived assuming that the previous symbol estimates used for MAI reconstruction exactly resembles the original data symbols. In realistic systems, however, the quality of these symbol estimates can be quite poor, particularly at early stages [62, 81]. The error propagation caused by the wrong estimates significantly degrades the error performances of the conventional PIC such that under many circumstances its error rate does not decrease beyond two stages [75].

To improve the performance of conventional PIC, partial PIC is proposed, which defines the feedback matrix as: [62], [81]

$$\mathbf{F}^{(i)} = p^{(i)}(\mathbf{R_a} - \mathbf{I})\mathbf{A} \tag{3.16}$$

where $p^{(i)} \in [0, 1]$ is a weighting constant depending on the stage number i. At early stages (i.e. small i), $p^{(i)}$ is small since the tentative symbol decisions are likely to be unreliable. The value of $p^{(i)}$ increases with i as symbol decisions become more reliable in later stages. While this method offers significant performance improvement over the conventional PIC for a system with perfect power control, two aspects of this mechanism can be further improved. First, the receiver assigns all users the same

cancellation constant and is thus not favorable for systems where the users' error performance clearly deviates from one another. Second, the cancellation weights at each stage were chosen arbitrarily in a trial-and-error fashion. A simple, systematic and robust method needs to be developed to calculate the cancellation weights. Next, we introduce a class of weighted multistage ICs that overcomes these two problems and offers a much improved performance over both conventional PIC and partial PIC.

3.3 MMSE-based multistage decision-feedback interference cancellation

3.3.1 Derivation

In this section, we propose a MMSE-based weighted parallel interference canceller (WPIC) that dynamically adjusts the feedback matrix $\mathbf{F}^{(i)}$ to minimize the mean-squared error (MSE) between the actual transmitted symbols and the symbol estimates in each stage. In specific terms, we would like to find $\mathbf{F}^{(i)}$ that satisfies

$$\mathbf{F}^{(i)} = \mathbf{F}^{(i)*} = \text{argmin}_{\mathbf{F}^{(i)}}\{E[(\mathbf{z}^{(i)} - \mathbf{Ab})^H(\mathbf{z}^{(i)} - \mathbf{Ab})]\} \tag{3.17}$$

For the derivation process, we make three assumptions that are typically used in analyzing the uplink of a DS-CDMA system. First, we assume that data symbols of different users are independent and that the successive symbols from the same user are also independent. Thus, in terms of correlations, we have $E[b_k(l)b_m^H(j)] = \delta[k-m]\delta[i-j]$ for all l, j, k, and m, where $\delta[n]$ is the unit-sample (discrete impulse) function. Second, we assume that $E[\hat{b}_k(l)\hat{b}_m^H(j)] \ll E[\hat{b}_k(l)\hat{b}_k^H(l)] = 1$ for all $l \neq j$ and/or $m \neq k$. This implies that the detected symbol estimates retain the statistical properties of the transmitted symbols. Third, we assume that spreading codes and received amplitudes of all users are known and deterministic rather than random, as in a realistic system with reasonable power control.

Under the given assumptions, we proceed to find $\mathbf{F}^{(i)*}$. Since minimizing the

mean-squared error denoted in eq. 3.17 is equivalent to minimizing the trace of the covariance matrix of $\mathbf{z}^{(i)} - \mathbf{Ab}$, i.e.

$$\mathbf{F}^{(i)} = argmin_{\mathbf{F}^{(i)}}\{tr(cov(\mathbf{z}^{(i)} - \mathbf{Ab}))\} \tag{3.18}$$

where $tr(.)$ denotes the trace operation. We start the derivation process by simplifying the covariance matrix as follows:

$$\begin{aligned}
cov(\mathbf{z}^{(i)} - \mathbf{Ab}) &= cov((\mathbf{R_a} - \mathbf{I})\mathbf{Ab} + \mathbf{n} - \mathbf{F}\hat{\mathbf{b}}^{(\mathbf{i-1})}) \\
&= E[((\mathbf{R_a} - \mathbf{I})\mathbf{Ab} + \mathbf{n} - \mathbf{F}\hat{\mathbf{b}}^{(\mathbf{i-1})})((\mathbf{R_a} - \mathbf{I})\mathbf{Ab} + \mathbf{n} - \mathbf{F}\hat{\mathbf{b}}^{(\mathbf{i-1})})^H] \\
&= (\mathbf{R_a} - \mathbf{I})\mathbf{A}E[\mathbf{bb}^H]\mathbf{A}^H(\mathbf{R_a} - \mathbf{I})^H + \sigma^2\mathbf{R_a} + \mathbf{F}^{(i)}E[\hat{\mathbf{b}}^{(i-1)}\hat{\mathbf{b}}^{(i-1)H}]\mathbf{F}^{(i)H} \\
&\quad -(\mathbf{R_a} - \mathbf{I})\mathbf{A}E[\mathbf{b}\hat{\mathbf{b}}^{(i-1)H}]\mathbf{F}^{(i)H} - \mathbf{F}^{(i)}E[\hat{\mathbf{b}}^{(i-1)}\mathbf{b}^H]\mathbf{A}^H(\mathbf{R_a} - \mathbf{I})^H \\
&= (\mathbf{R_a} - \mathbf{I})\mathbf{A}\mathbf{A}^H(\mathbf{R_a} - \mathbf{I})^H + \mathbf{F}^{(i)}\mathbf{F}^{(i)H} - (\mathbf{R_a} - \mathbf{I})\mathbf{A}E[\mathbf{b}\hat{\mathbf{b}}^{(i-1)H}]\mathbf{F}^{(i)H} \\
&\quad -\mathbf{F}^{(i)}E[\hat{\mathbf{b}}^{(i-1)}\mathbf{b}^H]\mathbf{A}^H(\mathbf{R_a} - \mathbf{I})^H + \sigma^2\mathbf{R_a}
\end{aligned}$$

where simplification in the last step comes from assumptions that $E[\mathbf{bb}^H] = \mathbf{I}$, $E[\mathbf{nb}^H] = E[\mathbf{n}\hat{\mathbf{b}}^H] = 0$, and $E[\hat{\mathbf{b}}^{(i-1)}\hat{\mathbf{b}}^{(i-1)H}] = \mathbf{I}$. Let $E[\mathbf{b}\hat{\mathbf{b}}^{(i-1)H}] = \mathbf{\Lambda_a}^{(i-1)}$, we can rewrite the covariance matrix as

$$\begin{aligned}
cov(\mathbf{z}^{(i)} - \mathbf{Ab}) &= (\mathbf{R_a} - \mathbf{I})\mathbf{A}\mathbf{A}^H(\mathbf{R_a} - \mathbf{I})^H + \mathbf{F}^{(i)}\mathbf{F}^{(i)H} - (\mathbf{R_a} - \mathbf{I})\mathbf{A}\mathbf{\Lambda_a}^{(i-1)}\mathbf{F}^{(i)H} \\
&\quad -\mathbf{F}^{(i)}\mathbf{\Lambda_a}^{(i-1)H}\mathbf{A}^H(\mathbf{R_a} - \mathbf{I})^H + \sigma^2\mathbf{R_a} \\
&= ((\mathbf{R_a} - \mathbf{I})\mathbf{A}\mathbf{\Lambda_a}^{(i-1)} - \mathbf{F}^{(i)})((\mathbf{R_a} - \mathbf{I})\mathbf{A}\mathbf{\Lambda_a}^{(i-1)} - \mathbf{F}^{(i)})^H \\
&\quad +\sigma^2\mathbf{R_a} + (\mathbf{R_a} - \mathbf{I})\mathbf{A}(\mathbf{I} - \mathbf{\Lambda_a}^{(i-1)}\mathbf{\Lambda_a}^{(i-1)H})\mathbf{A}^H(\mathbf{R_a} - \mathbf{I})^H
\end{aligned}$$

Since $((\mathbf{R_a} - \mathbf{I})\mathbf{A}\mathbf{\Lambda_a}^{(i-1)} - \mathbf{F}^{(i)})((\mathbf{R_a} - \mathbf{I})\mathbf{A}\mathbf{\Lambda_a}^{(i-1)} - \mathbf{F}^{(i)})^H$ is positive semi-definite, we see that the choice of $\mathbf{F}^{(i)}$ that minimizes the trace of the covariance matrix (and thus the mean-squared error) at the ith stage is

$$\mathbf{F}^{(i)*} = (\mathbf{R_a} - \mathbf{I})\mathbf{A}\mathbf{\Lambda_a}^{(i-1)} \tag{3.19}$$

where $\mathbf{\Lambda_a}^{(i-1)} = E[\mathbf{b}\hat{\mathbf{b}}^{(i-1)H}]$.

Clearly, the choice of $\mathbf{\Lambda_a}^{(i)}$ determines $\mathbf{F}^{(i)*}$. If we let $\mathbf{\Lambda_a}^{(i)} = \mathbf{I}$ for all i, then we obtain the conventional PIC. Similarly, if we assign $\mathbf{\Lambda_a}^{(i)} = p^{(i)}\mathbf{I}$, we have partial PIC. The $\mathbf{\Lambda_a}^{(i)}$ of our choice, which is derived in appendix A for a M-ary phase-shift-keying modulated (M-PSK) system, is a LK-by-LK matrix such that

$$\mathbf{\Lambda_a}^{(i)} = \begin{bmatrix} \mathbf{\Lambda}^{(i),0}(1) & \mathbf{\Lambda}^{(i),1}(1) & \mathbf{0} & \cdots & \cdots & \mathbf{0} \\ \mathbf{\Lambda}^{(i),-1}(2) & \mathbf{\Lambda}^{(i),0}(2) & \mathbf{\Lambda}^{(i),0}(2) & \mathbf{0} & \cdots & \mathbf{0} \\ \cdots & \cdots & \cdots & \cdots & \cdots & \cdots \\ \mathbf{0} & \cdots & \cdots & \mathbf{0} & \mathbf{\Lambda}^{(i),-1}(L) & \mathbf{\Lambda}^{(i),0}(L) \end{bmatrix} \tag{3.20}$$

where

$$\Lambda^{(i),0}(l)_{m,k} = \begin{cases} 1 - (1 - \cos\frac{2\pi}{M})Pe_k^{(i)} & \text{if } k = m \\ \frac{1}{M}\sum_{m=0}^{M-1} e^{j\frac{2m\pi}{M}}(Q(\sin(\frac{\pi}{M} - \theta_{m,k}(l))\sqrt{\gamma_{m,k}(l)})(e^{-j\frac{2\pi}{M}} - 1) & \\ +Q(\sin(\frac{\pi}{M} + \theta_{m,k}(l))\sqrt{\gamma_{m,k}(l)})(e^{j\frac{2\pi}{M}} - 1)) & \text{if } k \neq m \text{ and } i = 1 \\ 0 & \text{if } k \neq m \text{ and } i > 1 \end{cases}$$

$$\begin{aligned} \Lambda^{(i),1}(l)_{m,k} &= u(\tau_m - \tau_k)u(2-i)\frac{1}{M}\sum_{m=0}^{M-1} e^{j\frac{2m\pi}{M}}(Q(\sin(\frac{\pi}{M} - \tilde{\theta}_{m,k}(l))\sqrt{\tilde{\gamma}_{m,k}(l)})(e^{-j\frac{2\pi}{M}} - 1) \\ &\quad +Q(\sin(\frac{\pi}{M} + \tilde{\theta}_{m,k}(l))\sqrt{\tilde{\gamma}_{m,k}(l)})(e^{j\frac{2\pi}{M}} - 1)) \end{aligned}$$

$$\begin{aligned} \Lambda^{(i),-1}(l)_{m,k} &= u(\tau_k - \tau_m)u(2-i)\frac{1}{M}\sum_{m=0}^{M-1} e^{j\frac{2m\pi}{M}}(Q(\sin(\frac{\pi}{M} - \bar{\theta}_{m,k}(l))\sqrt{\bar{\gamma}_{m,k}(l)})(e^{-j\frac{2\pi}{M}} - 1) \\ &+ Q(\sin(\frac{\pi}{M} + \bar{\theta}_{m,k}(l))\sqrt{\bar{\gamma}_{m,k}(l)})(e^{j\frac{2\pi}{M}} - 1)) \end{aligned}$$

where $Pe_k^{(i)}$ is the symbol error probability of user k in the ith stage, $u(t)$ is unit-step

function, and

$$\theta_{m,k}(l) = \tan^{-1} \frac{A_m(l)\rho_{k,m}^{(0)}(l)\sin(\frac{2m\pi}{M}+\phi_m-\phi_k)}{A_k(l)+A_m(l)\rho_{k,m}^{(0)}(l)\cos(\frac{2m\pi}{M}+\phi_m-\phi_k)}$$

$$\gamma_{m,k} = \frac{A_k(l)^2+A_m(l)^2(\rho_{k,m}^{(0)}(l))^2+2A_k(l)A_m(l)\rho_{k,m}^{(0)}(l)\cos(\frac{2m\pi}{M}+\phi_m-\phi_k)}{MAI_k(l)-A_m^2(l)(\rho_{k,m}^{(0)}(l))^2+\sigma^2}$$

$$\tilde{\theta}_{m,k}(l) = \tan^{-1} \frac{A_m(l)\rho_{k,m}^{(-1)}(l+1)\sin(\frac{2m\pi}{M}+\phi_m-\phi_k)}{A_k(l+1)+A_m(l)\rho_{k,m}^{(-1)}(l+1)\cos(\frac{2m\pi}{M}+\phi_m-\phi_k)}$$

$$\tilde{\gamma}_{m,k}(l) = \frac{A_k(l+1)^2+A_m(l)^2(\rho_{k,m}^{(-1)}(l+1))^2+2A_k(l+1)A_m(l)\rho_{k,m}^{(-1)}(l+1)\cos(\frac{2m\pi}{M}+\phi_m-\phi_k)}{MAI_k(l+1)-A_m^2(l)(\rho_{k,m}^{(-1)}(l+1))^2+\sigma^2}$$

$$\bar{\theta}_{m,k}(l) = \tan^{-1} \frac{A_m(l)\rho_{k,m}^{(1)}(l-1)\sin(\frac{2m\pi}{M}+\phi_m-\phi_k)}{A_k(l-1)+A_m(l)\rho_{k,m}^{(1)}(l-1)\cos(\frac{2m\pi}{M}+\phi_m-\phi_k)}$$

$$\bar{\gamma}_{m,k}(l) = \frac{A_k(l-1)^2+A_m(l)^2(\rho_{k,m}^{(1)}(l-1))^2+2A_k(l-1)A_m(l)\rho_{k,m}^{(1)}(l-1)\cos(\frac{2m\pi}{M}+\phi_m-\phi_k)}{MAI_k(l-1)-A_m^2(l)(\rho_{k,m}^{(1)}(l-1))^2+\sigma^2}$$

where

$$MAI_k(l) = \sum_{m=1,m\neq k}^{K} ((A_m(l)\rho_{k,m}^{(0)}(l))^2+(A_m(l-1)\rho_{k,m}^{(-1)}(l))^2u(\tau_m-\tau_k) + (A_m(l+1)\rho_{k,m}^{(1)}(l))^2u(\tau_k-\tau_m)).$$

is the total MAI power suffered by user k during its lth symbol interval.

Intuitively, $\mathbf{\Lambda_a}^{(i)}$ measures the correlation between the symbol estimates at stage i and the actual transmitted symbols. The mth diagonal term $(\Lambda_a(m,m))$, where $m = K(l-1)+k$, denotes the correlation between the the estimate for the lth symbol or user k in stage i with its original transmitted symbol. Therefore, the diagonal terms measures the reliability of symbol estimates in stage i. Each off-diagonal term, on the other hand, denotes the correlation between a transmitted symbol and the detector output for another different symbol. These correlation terms arise from the effect of MAI.

3.3.2 Asymptotic approximation

The necessity to compute every entry in $\mathbf{\Lambda_a}$ leads to significant amount of computations in addition to conventional PIC (particularly at the first stage), despite the fact that complexities of these receivers are all on the same order. We now show that by examining the asymptotic behavior of $\mathbf{\Lambda_a}^{(i)}$, we can significantly reduce the complexity of our proposed receiver for a large system with reasonable power control.

As the number of users become large, i.e. $K \to \infty$, $\mathbf{\Lambda_a}^{(i)}$ can be approximated as a diagonal matrix (as shown in appendix A) such that

$$\mathbf{\Lambda_a}^{(i)} \approx \begin{bmatrix} \mathbf{W}^{(i)} & \mathbf{0} & \mathbf{0} & \dots & & \dots & \mathbf{0} \\ \mathbf{0} & \mathbf{W}^{(i)} & \mathbf{0} & \mathbf{0} & \dots & \dots & \mathbf{0} \\ \dots & \dots & \dots & \dots & \dots & \dots & \dots \\ \mathbf{0} & \dots & \dots & \dots & \mathbf{0} & \mathbf{0} & \mathbf{W}^{(i)} \end{bmatrix} \tag{3.21}$$

where $\mathbf{W}^{(i)}$ is a K-by-K diagonal matrix that can be evaluated depending on modulation format used in the system. For a M-PSK modulated system, we found (in appendix A) that

$$W_{k,k}^{(i)} \approx 1 - Pe_k^{(i)}(1 - \cos\frac{2\pi}{M}). \tag{3.22}$$

Intuitively, the reason why $\mathbf{\Lambda_a}^{(i)}$ can be approximated as a diagonal matrix for large K is because as number of users in the system increases, the effect of MAI from any particular user becomes negligible when compared to the MAI from all users, and therefore the correlation between transmitted and received symbols of different users approaches zero. Hence, under asymptotic approximation, the cancellation weights in the ith stage solely depend on $W_{k,k}^{(i)}$'s, which measures the reliability of each user's symbol estimates at the ith stage. The larger $W_{k,k}^{(i)}$ is, the more reliable user k's estimate is, and a larger weight will subsequently be applied to cancel the MAI from this user.

The proposed receiver implemented using asymptotic approximation is shown in

figure 3-3. The soft decision output for the lth symbol of the kth user in stage i can now be expressed as

$$\begin{aligned} z_k^{(i)}(l) =& y_k(l) - \sum_{m=1,m\neq k}^{K} e^{j(\phi_m-\phi_k)} W_{m,m}^{(i-1)} (A_m(l)\hat{b}_m^{(i-1)}(l)\rho_{k,m}^{(0)}(l) \\ &+ A_m(l-1)\hat{b}_m^{(i-1)}(l-1)\rho_{k,m}^{(-1)}(l)u(\tau_m - \tau_k) \\ &+ A_m(l+1)\hat{b}_m^{(i-1)}(l+1)\rho_{k,m}^{(1)}(l)u(\tau_k - \tau_m)) + n_k(l) \end{aligned} \tag{3.23}$$

Here, instead of computing all entries of the LK-by-LK matrix $\mathbf{F}$, we only need to compute one cancellation weight for each user and hence achieve significant complexity reduction.

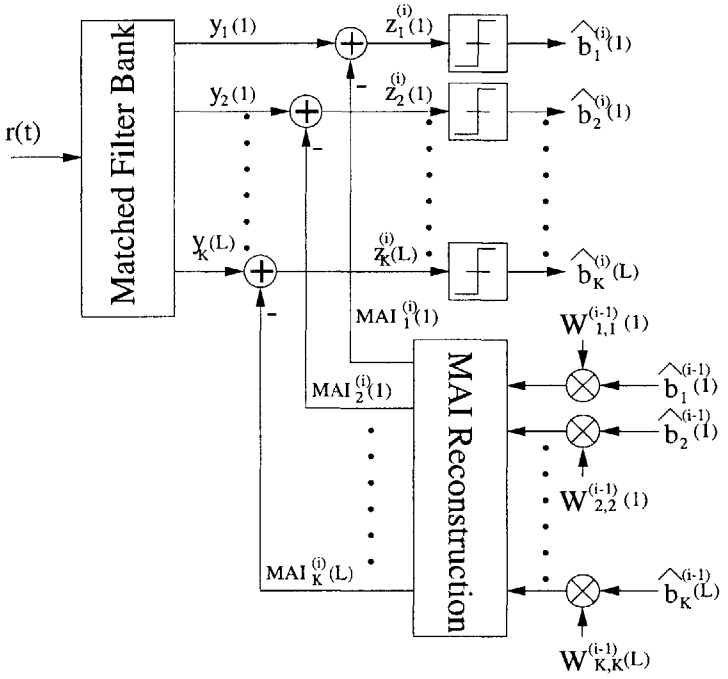

Figure 3-3: Weighted multistage interference canceller

3.3.3 Simplified MMSE-based weighted PIC

So far, the complexity of our proposed receiver can be reduced for a large system such that it just needs to compute one cancellation weight for each individual user at each

stage. To further reduce its complexity so that it is equivalent to that of conventional or partial PIC, we constrain the weighting matrix $\mathbf{\Lambda^{(i)}}$ to be:

$$\mathbf{\Lambda}^{(i)} = w^{(i)}\mathbf{I} \tag{3.24}$$

where $w^{(i)}$ is a cancellation constant applied to all (M-PSK modulated) users in stage i and $\mathbf{I}$ is the identity matrix. In this case, the cancellation output becomes

$$\mathbf{z}^{(i)} = \mathbf{R_a Ab} - w^{(i)}(\mathbf{R_a} - \mathbf{I})\mathbf{A}\hat{\mathbf{b}}^{(i-1)} + \mathbf{n} \tag{3.25}$$

We would again like to find the optimal choice of $w^{(i)}$ such that it minimizes the mean-squared error at stage i under the constraint, i.e.

$$w^{(i),opt} = min_{w^{(i)}}\{E[(\mathbf{z}^{(i)} - \mathbf{Ab})^H(\mathbf{z}^{(i)} - \mathbf{Ab})]\} \tag{3.26}$$

To proceed, we first assume that

$$E[b_k(l)b_m(j)^H] = E[\hat{b}_k(l)\hat{b}_m(j)^H] = \begin{cases} 1 & \text{if } k = m \text{ and } l = j, \\ 0 & \text{otherwise.} \end{cases} \tag{3.27}$$

$$E[b_k(l)\hat{b}_m(j)^{(i)}] = \begin{cases} 1 - Pe_k^{(i)}(1 - \cos\frac{2\pi}{M}) & \text{if } k = m \text{ and } l = j, \\ 0 & \text{otherwise.} \end{cases} \tag{3.28}$$

Now we simplify the mean-squared error as follows:

$$\begin{aligned}
MSE^{(i)} &= E[(\mathbf{z}^{(i)} - \mathbf{Ab})^H(\mathbf{z}^{(i)} - \mathbf{Ab})] \\
&= E[((\mathbf{R_a} - \mathbf{I})\mathbf{A}(\mathbf{b} - w^{(i)}\mathbf{b}) + \mathbf{n})^H(\mathbf{R_a} - \mathbf{I})\mathbf{A}(\mathbf{b} - w^{(i)}\mathbf{b}) + \mathbf{n})] \\
&= E[((\mathbf{R_a} - \mathbf{I})\mathbf{A}(\mathbf{b} - w^{(i)}\mathbf{b}))^H((\mathbf{R_a} - \mathbf{I})\mathbf{A}(\mathbf{b} - w^{(i)}\mathbf{b})) + E[\mathbf{n^H n}] \\
&= E[\mathbf{b}^H\mathbf{A}^H(\mathbf{R_a} - \mathbf{I})^H(\mathbf{R_a} - \mathbf{I})\mathbf{Ab} + w\hat{\mathbf{b}}^H\mathbf{A}^H(\mathbf{R_a} - \mathbf{I})^H(\mathbf{R_a} - \mathbf{I})\mathbf{A}\hat{\mathbf{b}}w \\
&\quad -\mathbf{b}^H\mathbf{A}^H(\mathbf{R_a} - \mathbf{I})^H(\mathbf{R_a} - \mathbf{i})\mathbf{A}\hat{\mathbf{b}}w - w\hat{\mathbf{b}}^H\mathbf{A}^H(\mathbf{R_a} - \mathbf{I})^H(\mathbf{R_a} - \mathbf{I})\mathbf{Ab}] \\
&\quad +E[\mathbf{n^H n}] \\
&= \sum_{l=1}^{L}\sum_{i=1}^{K}(MAI_k(l) + (w^{(i)})^2 MAI_k(l) \\
&\quad -2wMAI_k(l)(1 - Pe_k^{(i-1)}(1 - \cos\frac{2\pi}{M}))) + LK\sigma^2
\end{aligned}$$

where $MAI_k(l)$ is defined in eq. (3.21). To find the $w^{(i)}$ that minimizes $MSE^{(i)}$, we simply take the derivative of $MSE^{(i)}$ with respect to $w^{(i)}$ and obtain

$$\frac{d\{MSE^{(i)}\}}{dw^{(i)}} = 2\sum_{l=1}^{L}\sum_{i=1}^{K}(w^{(i)}MAI_k(l) - MAI_k(l)(1 - Pe_k^{(i-1)}(1 - \cos\frac{2\pi}{M}))) \quad (3.29)$$

The choice of $w^{(i)}$ that satisfies the MMSE criterion under this constraint is thus

$$w^{(i),opt} = \frac{\sum_{l=1}^{L}\sum_{k-1}^{K}(1 - Pe_k^{(i-1)}(1 - \cos\frac{2\pi}{M}))MAI_k(l)}{\sum_{l=1}^{L}\sum_{k=1}^{K}MAI_k(l)} \quad (3.30)$$

In the case of perfect power control and random spreading codes, the amount of MAI experienced by all users in every symbol period is approximately the same. The weighting factor can then be simplified as

$$\begin{aligned}
w^{(i),opt} &\approx \frac{\sum_{k=1}^{K}(1 - Pe_k^{(i-1)}(1 - \cos\frac{2\pi}{M}))MAI_k}{\sum_{k=1}^{K}MAI_k} \\
&\approx \frac{\sum_{k=1}^{K}1 - Pe_k^{(i-1)}(1 - \cos\frac{2\pi}{M})}{K}
\end{aligned} \quad (3.31)$$

Intuitively, $w^{(i)}$ depends on the average error probability of all users at stage i weighted by the MAI suffered by each user at the output of its matched filter. This receiver, which we name as the simplified weighted PIC (SWPIC), is considerably simpler than the our previous solutions because only it only computes one cancellation weight for each stage.

3.3.4 Practical considerations

To implement the proposed receiver in a practical system, we carry out the following procedures in stage i:

1. Estimate the symbol error rate for each user in the previous stage.
2. Compute the weighting matrix $\mathbf{\Lambda_a}^{(i-1)}$ according to eq. 3.20. (For a large system, just compute the corresponding weight for each user (i.e. $W^{(i-1)}(l)_{k,k}$) according to eq. 3.22; For SWPIC, just compute $w^{(i)}$ according to eq. 3.30.)
3. Find $\mathbf{R_a}$ and A using the knowledge of user signature waveform and received amplitude, phase, and delay offsets.
4. Subtract $\mathbf{R_a A \Lambda_a}^{(i-1)}\hat{\mathbf{b}}^{(i-1)}$ from the matched-filter output vector $\mathbf{y}$.
5. For each user, pass its corresponding cancellation output through the quantization device to obtain the updated symbol estimates for the current stage.
6. Repeat procedures 1 through 5 for subsequent stages until the target BER has been reached for all users in the system or as desired.

In practical applications, since the proposed receiver operates on a frame of data symbols each time, the data frame size, i.e. L, needs to be carefully chosen based on the tradeoff consideration between bit-error rate and latency requirement. The larger the frame is, the longer the latency, but the better the performance since interferences at the edge of the frame will be negligible when compared to the frame size.

A remaining question is how to estimate the error probability for each user at a given stage. There are two solutions. First, the error probability of each user

can be approximated by first estimating the signal-to-interference ratios (SIR) of the cancellation outputs (i.e. elements in $\mathbf{z}^{(i)}$) and then applying Gaussian approximation. For a M-PSK modulated system, the error probability can be approximated as $P_e \approx Q(\sqrt{SIR}\sin\frac{\pi}{M})$ [55]. Second, each user can employ interleaved pilot (training) sequences within each data frame. The error probability can then be estimated by observing the error rate of these pilot sequences. Even though the use of these training sequences result in some loss of throughput, we will see in section 3.4 that such loss is negligible comparing to the overall capacity improvement achieved by the proposed receivers over the conventional PIC.

3.4 Performance analysis of MMSE-based weighted multistage decision-feedback IC

3.4.1 Asymptotic error-rate analysis

In this section we analyze the error performance of the proposed receivers (using MMSE feedback cancellation and Λ_a) for a M-PSK modulated DS-CDMA system with K users. Since computation of the exact error probability is burdensome for multistage IC (as illustrated in [71]) and does not yield significant insight, we evaluate the error probability for a large system using classical Gaussian approximation [40]. We assume $K \to \infty$, $N \to \infty$ and $\frac{N}{K} = \beta$, and that the user spreading (signature) codes are random, which is a good model for a practical DS-CDMA system that uses pseudo-random (PN) signature sequences with period much longer than the spreading factor. We also assume a symbol-synchronous system, i.e. $\tau_k = 0$ for all $k \in [1, K]$, which corresponds to the case of strongest MAI [78]. In this case, the correlation terms in the MAI can be simplified such that $\rho_{m,k}^{(1)} = \rho_{m,k}^{(-1)} = 0$ for all m, $k \in \{1,\ 2,\ \ldots\ K$, and $\rho_{m,k}^{(0)} = \rho_{m,k}$.

An important measure of the system performance is the signal-to-interference ratio

(SIR). In our case, the SIR at the matched-filter output for user k can be found as

$$\begin{aligned} SIR_k^{MF} &= \frac{A_k^2}{\sum_{j=1,j\neq k}^{K} A_j^2 E[\rho_{j,k}^2] E[b_j b_j^H] + \frac{N_0}{2}} \\ &= \frac{A_k^2}{\sum_{j=1,j\neq k}^{K} \frac{A_j^2}{N} + \frac{N_0}{2}} \end{aligned} \tag{3.32}$$

where $E[b_j b_j^H] = 1$ for M-PSK modulation with equi-probable selection of constellation points and $E[\rho_{j,k}^2] = \frac{1}{N}$ due to random spreading. Furthermore, in the case of perfect power control, i.e. $A_1 = A_2 = ... = A_K = A$, the SIR of matched-filter detection for all users can be simplified to:

$$SIR^{MF} = \frac{1}{\frac{K-1}{N} + \frac{N_0}{2A^2}} \approx \frac{1}{\beta + \frac{N_0}{2A^2}} \tag{3.33}$$

for a large system.

We proceed to compute the SIR for the conventional PIC. The SIR for the cancellation output of user k at stage i is

$$\begin{aligned} SIR_k^{PIC,(i)} &= \frac{A_k^2}{\sum_{j=1,j\neq k}^{K} A_j^2 E[\rho_{j,k}^2] E[(b_j - \hat{b}_j^{(i-1)})(b_j - \hat{b}_j^{(i-1)})^H] + \frac{N_0}{2}} \\ &= \frac{A_k^2}{\sum_{j=1,j\neq k}^{K} \frac{A_j^2}{N} 2Pe_j^{(i-1)}(1 - \cos\frac{2\pi}{M}) + \frac{N_0}{2}} \end{aligned} \tag{3.34}$$

where the relationship $E[(b_j - \hat{b}_j^{(i-1)})(b_j - \hat{b}_j^{(i-1)})^H] \approx 2Pe_j^{(i-1)}(1 - \cos\frac{2\pi}{M})$ for a large system has been derived in appendix A. Again, this SIR can be simplified in the case of perfect power control as

$$SIR^{PIC,(i)} \approx \frac{1}{2\beta Pe^{(i-1)}(1 - \cos\frac{2\pi}{M}) + \frac{N_0}{2A^2}} \tag{3.35}$$

where $Pe^{(i-1)}$ is the average symbol error rate of all users in stage $i-1$.

Similarly, for our proposed detector, i.e. the weighted PIC (WPIC) with MMSE feedback cancellation, the SIR for the kth user at stage i after weighted MAI cancel-

lation can be found as

$$\begin{aligned} SIR^{WPIC,(i)} &= \frac{A_k^2}{\sum_{j=1,j\neq k}^{K} A_j^2 E[\rho_{j,k}^2] E[(b_j - W_{j,j}^{(i)}\hat{b}_j^{(i-1)})(b_j - W_{j,j}^{(i)}\hat{b}_j^{(i-1)})^H] + \frac{N_0}{2}} \\ &\approx \frac{A_k^2}{\frac{1}{N}\sum_{j=1,j\neq k}^{K} A_j^2 (1 - (W_{j,j}^{(i)})^2) + \frac{N_0}{2}} \\ &= \frac{A_k^2}{\frac{1}{N}\sum_{j=1,j\neq k}^{K} A_j^2 Pe_j^{(i-1)}(1-\cos\frac{2\pi}{M})(2 - (1-\cos\frac{2\pi}{M})Pe_j^{(i-1)}) + \frac{N_0}{2}} \end{aligned}$$

where $W_{j,j}^{(i)} = 1 + (\cos\frac{2\pi}{M} - 1)Pe_j^{(i-1)}$. Simplification at the second step comes from the approximation that $E[(b_j - W_{j,j}^{(i)}\hat{b}_j^{(i-1)})(b_j - W_{j,j}^{(i)}\hat{b}_j^{(i-1)})^H] \approx 1 - (W_{j,j}^{(i)})^2$. Too see this is a valid approximation, we have

$$\begin{aligned} E[||b_j - W_{j,j}^{(i)}\hat{b}_j^{(i-1)}||^2] =& E[(b_j - W_{j,j}^{(i)}\hat{b}_j^{(i-1)})(b_j - W_{j,j}^{(i)}\hat{b}_j^{(i-1)})^H] \\ =& 1 - 2W_{j,j}^{(i)} E[b_j \hat{b}_j^{(i-1)}] + (W_{j,j}^{(i)})^2 \\ \approx& 1 - 2W_{j,j}^{(i)} W_{j,j}^{(i)} - (W_{j,j}^{(i)})^2 \\ =& 1 - (W_{j,j}^{(i)})^2 \end{aligned} \tag{3.36}$$

where the approximation in the last step assumes $E[b_j\hat{b}_j^{(i-1)}] = W_{j,j}^{(i)}$ and $E[\hat{b}_j^{(i-1)}\hat{b}_j^{(i-1)}] = 1$, which has been validated in the last section and appendix A. We see that in this case, the interference power from the jth user is suppressed by a factor of $\frac{2}{2-(1-\cos\frac{2\pi}{M}Pe^{(i-1)})}$. In the case of perfect power control, we can deduce the SIR of all users to be

$$SIR^{WPIC,i} = \frac{1}{\beta Pe^{(i-1)}(1-\cos\frac{2\pi}{M})(2 - (1-\cos\frac{2\pi}{M})Pe^{(i-1)}) + \frac{N_0}{2A^2}}. \tag{3.37}$$

The error probability for all three receivers can be calculated using classical Gaussian approximation [17] as

$$Pe^{(i)} = Q(\sin\frac{\pi}{M}\sqrt{SIR^{(i)}}). \tag{3.38}$$

We are interested in analyzing the convergence behavior of our proposed algorithm

under Gaussian approximation in AWGN channel. Note that since $SIR^{WPIC,(i)}$ is a function of $Pe^{WPIC,(i-1)}$ through the weighting matrix $\mathbf{\Lambda_a}^{(i-1)}$, $Pe^{WPIC,(i)}$ is then also a function of $Pe^{WPIC,(i-1)}$, i.e.

$$Pe^{WPIC,(i)} = H(Pe^{WPIC,(i-1)}). \tag{3.39}$$

To find the error probability at which the receiver reaches convergence, we just need to find when $Pe^{WPIC,(i)} = Pe^{WPIC,(i-1)}$.

Figures 3-4 (a)-(f) show the convergence behavior of WPIC as a function of the number of stages for small, large, and over-loaded systems with BPSK modulation and signal-to-noise ratio (SNR = E_b/N_0) of 7dB. The convergence curve for PIC is also plotted for comparison. We see that, in figures 3-4(a) and 3-4(b), which corresponds to a system with load $\beta = 0.5$ and 0.75, respectively, the error floor for WPIC and PIC are essentially the same, except that it takes WPIC fewer stages to reach convergence. In system with larger load, i.e. $\beta = 1$ and $\beta = 1.25$, which corresponds to figures 3-4(c) and 3-4(d), respectively, we see that the error floors of WPIC becomes better than PIC, while WPIC also takes much fewer iterations to reach convergence. For overloaded system, i.e. figures 3-4(e) and 3-4(f), which corresponds to $\beta = 1.5$ and 2, respectively, we see that both receivers perform poorly, with WPIC being slightly better.

3.4.2 Simulation verification

The performance of (MMSE-based) WPIC is verified via simulation for an asynchronous BPSK modulated and uncoded (i.e. no channel coding) system employing random spreading codes with a spreading gain of $N = 128$. The signal-to-(background)noise ratio (SNR) for each user is 7 dB, which resembles perfect power control. The IC operates on every frame of 800 data symbols, which includes 12 training symbols. For a system with more than 64 users, asymptotic approximation is applied for WPIC. The performance of the WPIC and SWPIC in AWGN channels in one stage, two stages, and five stages are shown in figures 3-5(a), 3-5(b),

and 3-5(c), respectively, where we plot the average BER vs. the number of active users. The corresponding performances in a flat-fading channel are plotted in figures 3-6(a), 3-6(b), and 3-6(c), with the average SNR per user being around 20 dB. The amplitude of each user in this case fades independently from symbol to symbol and is modeled as a Rayleigh random variable. Error performance of the matched filter and conventional PIC are also plotted in each figure for comparison. From these figures, we see that the loss of 1.25 percent in throughput due to the use of training sequence is negligible compared to the amount of capacity gain achieved by WPIC and SWPIC over conventional PIC. For instance, for a two-stage IC in an AWGN channel, if we impose a BER target of 10^{-3}, the use of WPIC can accommodate about 65 users, while the conventional PIC can only accommodate about 45 users. This corresponds to 45 percent increase in the capacity.

Tradeoff between BER and E_b/N_0 for the different receivers after 1, 2, and 5 stages are shown in figures 3-7(a), 3-7(b) and 3-7(c), respectively, for a half loaded system (64 users with a spreading gain of 128). We see that in all stages, the WPIC not only exhibits a better tradeoff than the other algorithms but also yields a much lower error floor and can converge more quickly than the others to reach the target error rate. The SWPIC also exhibits a better tradeoff than the conventional PIC. Its behavior is significantly worse than WPIC in later stages, however, due to the lack of disparate weighting factor for each user, even though the simulations are done for the case of perfect power control and random spreading codes.

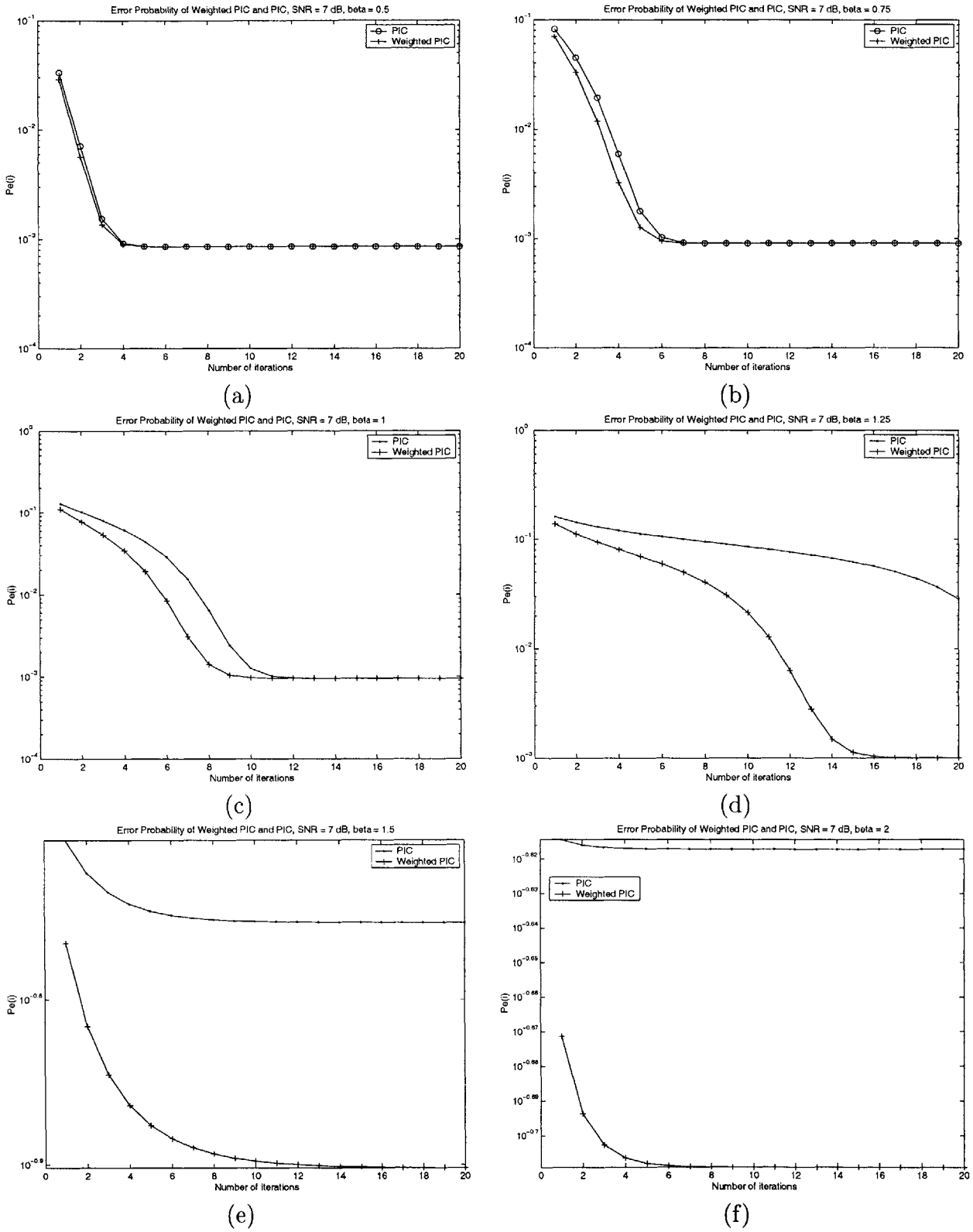

Figure 3-4: Error probability convergence based on Gaussian approximation for WPIC and PIC for system with Loading (a) $\beta = 0.5$, (b) $\beta = 0.75$, (c)$\beta = 1$, (d) $\beta = 1.25$, (e) $\beta = 1.5$, (f) $\beta = 2$.

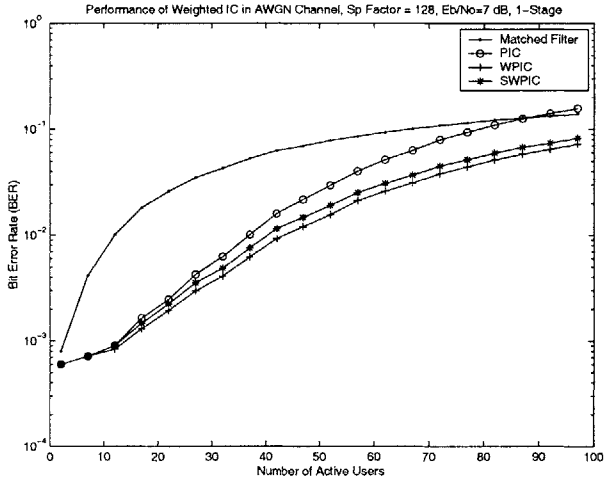

(a)

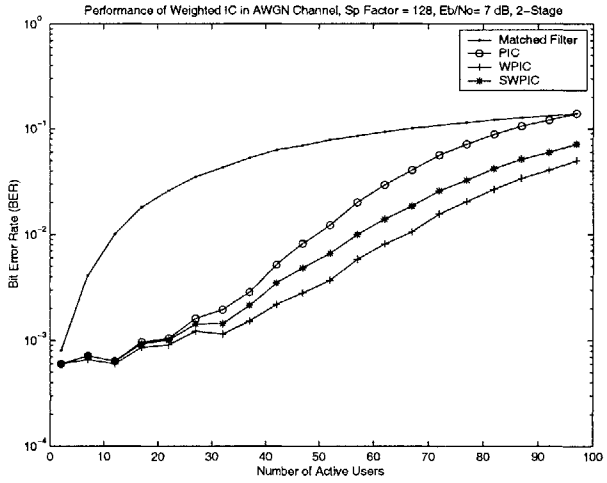

(b)

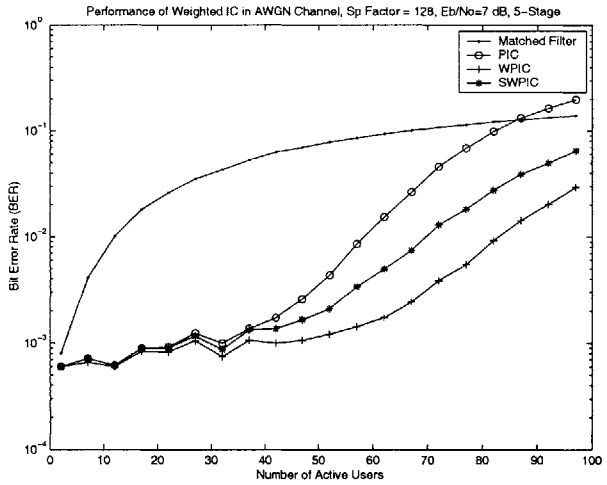

(c)

Figure 3-5: Error probability of weighted PIC vs. the total number of users in AWGN channel, (a) 1 stage, (b) 2 stages, (c) 5 stages

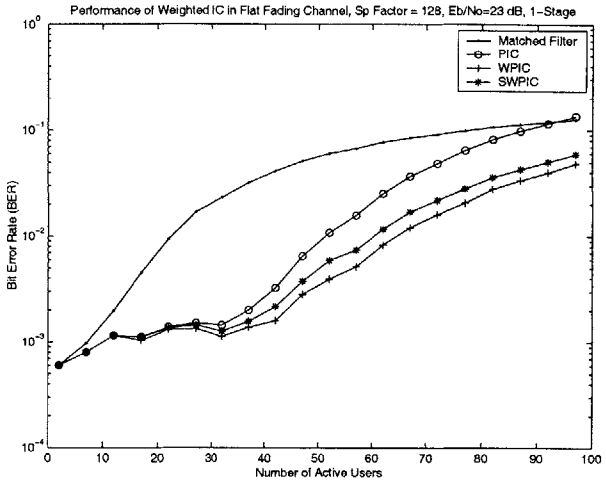

(a)

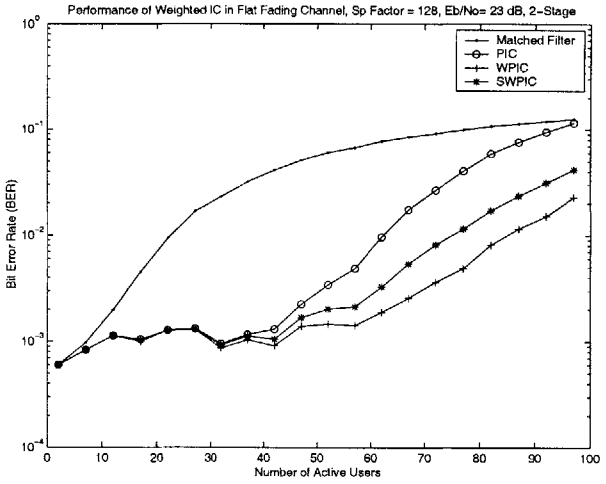

(b)

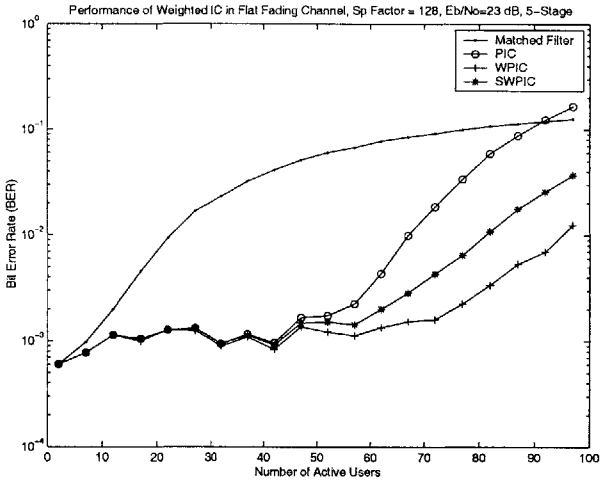

(c)

Figure 3-6: Error probability of weighted PIC vs. the total number of users in Rayleigh Flat-Fading channel: (a) 2 stage, (b) 2 stages, (c) 5 stages

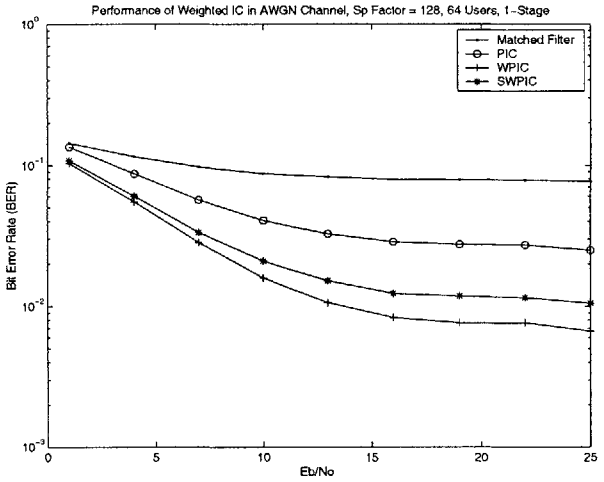

(a)

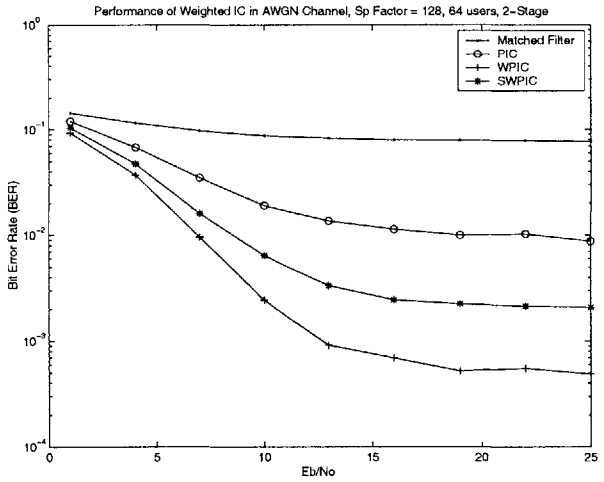

(b)

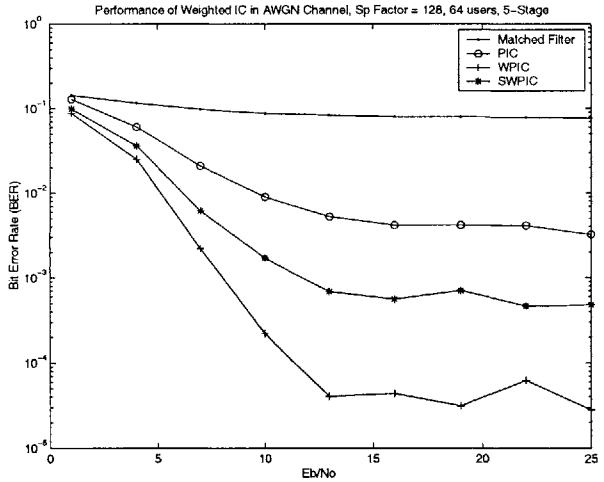

(c)

Figure 3-7: Error probability of weighted PIC vs. $\frac{E_b}{N_0}$ in AWGN channel (64 Users) : (a) 1 stage, (b) 2 stages, (c) 5 stages

3.5 Multistage IC with both feedforward and decision-feedback linear processing

So far, we have developed a class of multistage ICs using MMSE optimized feedback matrix to achieve significant performance improvement over the conventional PIC. Due to its complexity constraint (to be comparable to the conventional PIC), the performance of our receiver is still worse than that of linear joint detectors and is quite far from the single-user performance bound. For the rest of the chapter, we introduce additional complexities to enhance the detector performance. Specifically, we show that by adding a feedforward linear processing unit to the multistage IC and by jointly optimizing the feedforward and the feedback matrix using the MMSE criterion at every stage, we obtain a receiver whose performance not only surpasses that of linear joint detectors but also approaches the single-user performance bound in a few iterations.

3.5.1 Framework of multistage decision-feedback IC with feedforward matrix

Using vector notations developed in section 3.2.1, the structure of a multistage IC with feedforward linear processing module is illustrated in figure 3-8. In the ith stage

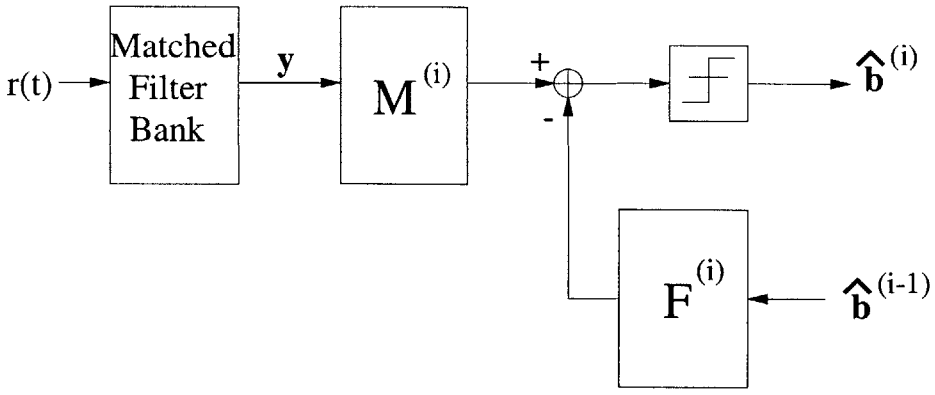

Figure 3-8: A general multistage interference canceller with feedforward processing

of the receiver, the matched-filter output $\mathbf{y}$ is processed by the forward matrix $\mathbf{M}^{(i)}$, while at the same time the feedback matrix $\mathbf{F}^{(i)}$ reconstructs the MAI based on $\hat{\mathbf{b}}^{(i-1)}$. The cancellation output can be expressed as

$$\mathbf{z}^{(i)} = \mathbf{M}^{(i)}\mathbf{y} - \mathbf{F}^{(i)}\hat{\mathbf{b}}^{(i-1)} \tag{3.40}$$

The decision vector $\mathbf{z}^{(i)}$ is processed by minimum-distance (quantization) devices to generate $\hat{\mathbf{b}}^{(i)}$.

Depending on design constraints for $\mathbf{M}$ and $\mathbf{F}$, the formulation in figure 3-8 can lead to different types of joint detectors. For instance, we can assign $\mathbf{M}^{(i)}$ to be the decorrelator or the MMSE detector at the initial stage (i.e. $i = 1$) and identity matrix at subsequent stages, while letting $\mathbf{F}^{(i)} = (\mathbf{R_a} - \mathbf{I})\mathbf{A}$ for $i > 1$, i.e. using full cancellation in all subsequent stages. This yields a multistage IC with decorrelator or MMSE front-end [75, 61]. The main purpose of this type of receiver is to enhance the reliability of symbol estimates at the first stage so that MAI cancellation in subsequent stages are more reliable than using just the matched filter front-end. The drawback with this type of receiver, however, is that the error rate in later stages may not be better than the initial stage, as have been shown in [75], mainly because the cancellation process beyond the initial stage is performed based on the noisy matched-filter output.

Other detectors based on figure 3-8 include MMSE and decorrelator decision feedback interference cancellers [75, 13, 31]. The key idea is to optimize $\mathbf{M}$ and $\mathbf{F}$ with some constraints (such as letting $\mathbf{F}$ to be a lower triangular matrix) to minimize a specific cost function in each stage. For the decorrelator-based decision feedback IC, the goal is completely eliminate MAI at each stage, while for MMSE-based schemes, the goal is to minimize the MSE between the transmitted and received symbols. In addition, [7] derived a class of decision feedback multiuser interference cancellers without assuming perfect MAI reconstruction. Its feedforward and feedback matrices are designed with an attempt to maximize the SIR in every stage. By carefully working out the algebra, this result actually turns out to be a special case of our solution when

the weighting matrix $\mathbf{\Lambda_a}$ is constrained to be diagonal. The performance of these receivers, mostly illustrated through simulations, have been shown to exceed the linear joint detectors in some extent. The assumption of perfect MAI reconstruction and the constraints on $\mathbf{M}$ and $\mathbf{F}$, however, still limits the performance of these detectors.

3.5.2 Multistage IC with MMSE-optimized feedforward and feedback matrices

In this section, we present a multistage IC that is derived via unconstrained joint MMSE optimization for the feedforward and feedback matrices at every stage. The mean-squared error in the ith stage can be denoted as

$$MSE^{(i)} = E[(\mathbf{z}^{(i)} - \mathbf{Ab})^H(\mathbf{z}^{(i)} - \mathbf{Ab})] \tag{3.41}$$

where $\mathbf{z}^{(i)}$ is described in eq. 3.40. Using the fact that the choice of $\mathbf{M}^{(i)}$ and $\mathbf{F}^{(i)}$ that minimizes $MSE^{(i)}$ also minimizes the trace of the covariance matrix (i.e. $cov(\mathbf{z}^{(i)} - \mathbf{Ab})$), we begin our derivation as follows and drop the superscript $^{(i)}$ for notational convenience:

$$\begin{aligned}
cov(\mathbf{z}^{(i)} - \mathbf{Ab}) &= E[(\mathbf{z} - \mathbf{Ab})(\mathbf{z} - \mathbf{Ab})^H] \\
&= E[((\mathbf{MR_a} - \mathbf{I})\mathbf{Ab} - \mathbf{F}\hat{\mathbf{b}} + \mathbf{Mn})((\mathbf{MR_a} - \mathbf{I})\mathbf{Ab} - \mathbf{F}\hat{\mathbf{b}} + \mathbf{Mn})^H] \\
&= E[(\mathbf{MR_a} - \mathbf{I})\mathbf{Abb}^H\mathbf{A}^H(\mathbf{MR_a} - \mathbf{I})^H] + E[\mathbf{Mnn}^H\mathbf{M}^H] \\
&\quad + E[\mathbf{F}\hat{\mathbf{b}}\hat{\mathbf{b}}^H\mathbf{F}^H] - E[(\mathbf{MR_a} - \mathbf{I})\mathbf{Abb}^H\mathbf{F}^H] \\
&\quad - E[\mathbf{F}\hat{\mathbf{b}}\mathbf{b}^H\mathbf{A}^H(\mathbf{MR_a} - \mathbf{I})^H]
\end{aligned}$$

The simplification in the last step comes from the fact that the noise term is uncorrelated with the original symbols and the symbol estimates. To further simplify the covariance matrix, we use the following assumptions that have been stated before, i.e. $E[\mathbf{bb}^H] = \mathbf{I}$, $E[\hat{\mathbf{b}}\hat{\mathbf{b}}^H] = \mathbf{I}$, $E[\mathbf{nn}^H] = \sigma^2\mathbf{R_a}$ $E[\mathbf{b}\hat{\mathbf{b}}^H] = \mathbf{\Lambda_a}$, which can be used to

further reduce the covariance matrix as

$$\begin{aligned}
cov(\mathbf{z}^{(i)} - \mathbf{Ab}) &= (\mathbf{MR_a} - \mathbf{I})\mathbf{AA}^H(\mathbf{MR_a} - \mathbf{I})^H + \sigma^2\mathbf{MR_aM}^H + \mathbf{FF}^H \\
&\quad -(\mathbf{MR_a} - \mathbf{I})\mathbf{A\Lambda_aF}^H - \mathbf{F\Lambda_a}^H\mathbf{A}^H(\mathbf{MR_a} - \mathbf{I})^H \\
&= \mathbf{MR_aUR_a}^H\mathbf{M}^H - \mathbf{MR_aV}^H - \mathbf{VR_a}^H\mathbf{M}^H + \mathbf{A\Lambda_aF}^H + \mathbf{F\Lambda}^H\mathbf{A}^H \\
&\quad +\mathbf{FF}^H + \mathbf{AA}^H \\
&= \mathbf{MR_aUR_a}^H\mathbf{M}^H - \mathbf{MR_aUU^{-1}V}^H - \mathbf{VU^{-1}UR_a}^H\mathbf{M}^H \\
&\quad +\mathbf{VU^{-1}V^H} - \mathbf{VU^{-1}V^H} + \mathbf{A\Lambda_aF}^H + \mathbf{F\Lambda}^H\mathbf{A}^H + \mathbf{FF}^H + \mathbf{AA}^H \\
&= (\mathbf{MR_a} - \mathbf{VU^{-1}})\mathbf{U}(\mathbf{MR_a} - \mathbf{VU^{-1}})^H - \mathbf{VU^{-1}V}^H + \mathbf{A\Lambda_aF}^H \\
&\quad +\mathbf{F\Lambda_a}^H\mathbf{A}^H + \mathbf{FF}^H + \mathbf{AA}^H
\end{aligned}$$

where

$$\mathbf{U} = \mathbf{AA}^H + \sigma^2\mathbf{R_a^{-1}} \tag{3.42}$$

$$\mathbf{V} = \mathbf{AA}^H + \mathbf{F\Lambda}^H\mathbf{A}^H. \tag{3.43}$$

Since the correlation matrix $\mathbf{R_a}$ is symmetric and positive semi-definite, $\mathbf{U}$ is also a positive semi-definite matrix. Therefore, we see that for any feedback matrix $\mathbf{F}$, the choice of feedforward matrix $\mathbf{M}$ that minimizes the mean-squared error is:

$$\begin{aligned}
\mathbf{M} = \mathbf{M}^{opt} &= \mathbf{VU^{-1}R^{-1}} \\
&= (\mathbf{AA}^H + \mathbf{F\Lambda}^H\mathbf{A}^H)(\mathbf{AA}^H + \sigma^2\mathbf{R_a^{-1}})\mathbf{R}^{-1} \\
&= (\mathbf{F\Lambda_a} + \mathbf{A})\mathbf{A}^{-1}(\mathbf{R} + \sigma^2(\mathbf{A}^H\mathbf{A})^{-1})
\end{aligned} \tag{3.44}$$

Now, with $\mathbf{M} = \mathbf{M}^{opt}$, we proceed to find the optimal $\mathbf{F}$ that leads to the minimum MSE. The covariance matrix now becomes

$$\begin{aligned}
cov(\mathbf{z} - \mathbf{Ab}) &= \mathbf{A}\boldsymbol{\Lambda}_\mathbf{a}\mathbf{F}^H + \mathbf{F}\boldsymbol{\Lambda}^H\mathbf{A}^H + \mathbf{F}\mathbf{F}^H + \mathbf{A}\mathbf{A}^H \\
&\quad -(\mathbf{F}\boldsymbol{\Lambda}_\mathbf{a}{}^H + \mathbf{A})(\mathbf{I} + \sigma^2\mathbf{A}^{-1}\mathbf{R}_\mathbf{a}^{-1}(\mathbf{A}^H)^{-1})^{-1}(\mathbf{F}\boldsymbol{\Lambda}_\mathbf{a}{}^H + \mathbf{A})^H \\
&= \mathbf{A}\boldsymbol{\Lambda}_\mathbf{a}\mathbf{F}^H + \mathbf{F}\boldsymbol{\Lambda}^H\mathbf{A}^H + \mathbf{F}\mathbf{F}^H + \mathbf{A}\mathbf{A}^H - (\mathbf{F}\boldsymbol{\Lambda}_\mathbf{a}{}^H + \mathbf{A})G^{-1}(\mathbf{F}\boldsymbol{\Lambda}_\mathbf{a}{}^H + \mathbf{A})^H \\
&= \mathbf{F}(\mathbf{I} - \boldsymbol{\Lambda}_\mathbf{a}{}^H\mathbf{G}^{-1}\boldsymbol{\Lambda}_\mathbf{a})\mathbf{F}^H + \mathbf{A}(\mathbf{I} - \mathbf{G}^{-1})\boldsymbol{\Lambda}_\mathbf{a}(\mathbf{I} - \boldsymbol{\Lambda}_\mathbf{a}{}^H\mathbf{G}^{-1}\boldsymbol{\Lambda}_\mathbf{a})^{-1} \\
&\quad (\mathbf{I} - \boldsymbol{\Lambda}_\mathbf{a}{}^H\mathbf{G}^{-1}\boldsymbol{\Lambda}_\mathbf{a})\mathbf{F}^H + \mathbf{F}(\mathbf{I} - \boldsymbol{\Lambda}_\mathbf{a}{}^H\mathbf{G}^{-1}\boldsymbol{\Lambda}_\mathbf{a})(\mathbf{I} - \boldsymbol{\Lambda}_\mathbf{a}{}^H\mathbf{G}^{-1}\boldsymbol{\Lambda}_\mathbf{a})^{-1} \\
&\quad \boldsymbol{\Lambda}_\mathbf{a}{}^H(\mathbf{I} - \mathbf{G}^{-1})\mathbf{A}^H + \mathbf{A}(\mathbf{I} - \mathbf{G}^{-1})\boldsymbol{\Lambda}_\mathbf{a}(\mathbf{I} - \boldsymbol{\Lambda}_\mathbf{a}{}^H\mathbf{G}^{-1}\boldsymbol{\Lambda}_\mathbf{a})^{-1}\boldsymbol{\Lambda}_\mathbf{a}{}^H(\mathbf{I} - \mathbf{G}^{-1})\mathbf{A}^H \\
&\quad +\mathbf{A}(\mathbf{I} - \mathbf{G}^{-1})(\mathbf{I} - \boldsymbol{\Lambda}_\mathbf{a}(\mathbf{I} - \boldsymbol{\Lambda}_\mathbf{a}{}^H\mathbf{G}^{-1}\boldsymbol{\Lambda}_\mathbf{a})^{-1}\boldsymbol{\Lambda}_\mathbf{a}{}^H(\mathbf{I} - \mathbf{G}^{-1}))\mathbf{A}^H \\
&= (\mathbf{F} - \mathbf{A}(\mathbf{I} - \mathbf{G}^{-1})\boldsymbol{\Lambda}_\mathbf{a}(\mathbf{I} - \boldsymbol{\Lambda}_\mathbf{a}^\mathbf{H}\mathbf{G}^{-1}\boldsymbol{\Lambda}_\mathbf{a})^{-1})(\mathbf{I} - \boldsymbol{\Lambda}_\mathbf{a}{}^H\mathbf{G}^{-1}\boldsymbol{\Lambda}_\mathbf{a}) \\
&\quad (\mathbf{F} - \mathbf{A}(\mathbf{I} - \mathbf{G}^{-1})\boldsymbol{\Lambda}_\mathbf{a}(\mathbf{I} - \boldsymbol{\Lambda}_\mathbf{a}{}^H\mathbf{G}^{-1}\boldsymbol{\Lambda}_\mathbf{a})^{-1})^H \\
&\quad +\mathbf{A}(\mathbf{I} - \mathbf{G}^{-1})(\mathbf{I} - \boldsymbol{\Lambda}_\mathbf{a}(\mathbf{I} - \boldsymbol{\Lambda}_\mathbf{a}{}^H\mathbf{G}^{-1}\boldsymbol{\Lambda}_\mathbf{a})^{-1}\boldsymbol{\Lambda}_\mathbf{a}{}^H(\mathbf{I} - \mathbf{G}^{-1}))\mathbf{A}^H
\end{aligned}$$

where

$$\mathbf{G} = \mathbf{I} + \sigma^2\mathbf{A}^{-1}\mathbf{R}_\mathbf{a}{}^{-1}(\mathbf{A}^H)^{-1}.$$

Since $\mathbf{R}_\mathbf{a}$ is positive semi-definite, $\sigma^2\mathbf{A}^{-1}\mathbf{R}_\mathbf{a}{}^{-1}(\mathbf{A}^H)^{-1}$ is clearly positive semi-definite. Therefore, all eigenvalues of $\mathbf{G}$ is greater than or equal to 1, which means that $(\mathbf{I} - \boldsymbol{\Lambda}_\mathbf{a}{}^H\mathbf{G}^{-1}\boldsymbol{\Lambda}_\mathbf{a})$ is also positive semi-definite. The optimal choice of $\mathbf{F}$ that minimizes the trace of $cov(\mathbf{z} - \mathbf{Ab})$ (and thereby the mean-squared error) can be found as

$$\begin{aligned}
\mathbf{F} = \mathbf{F}^{opt} =& \mathbf{A}(\mathbf{I} - \mathbf{G}^{-1})\boldsymbol{\Lambda}_\mathbf{a}(\mathbf{I} - \boldsymbol{\Lambda}_\mathbf{a}{}^H\mathbf{G}^{-1}\boldsymbol{\Lambda}_\mathbf{a})^{-1} \\
=& \mathbf{A}(\mathbf{I} - (\mathbf{I} + \sigma^2\mathbf{A}^{-1}\mathbf{R}_\mathbf{a}{}^{-1}(\mathbf{A}^H)^{-1})^{-1})\boldsymbol{\Lambda}_\mathbf{a} \\
& (\mathbf{I} - \boldsymbol{\Lambda}_\mathbf{a}{}^H(\mathbf{I} + \sigma^2\mathbf{A}^{-1}\mathbf{R}_\mathbf{a}{}^{-1}(\mathbf{A}^H)^{-1})^{-1}\boldsymbol{\Lambda}_\mathbf{a})^{-1}
\end{aligned} \tag{3.45}$$

The minimum mean-squared error in this case is

$$\begin{aligned} MSE &= tr(\mathbf{A}(\mathbf{I}-\mathbf{G}^{-1})(\mathbf{I}-\mathbf{\Lambda_a}(\mathbf{I}-\mathbf{\Lambda_a}^H\mathbf{G}^{-1}\mathbf{\Lambda_a})^{-1}\mathbf{\Lambda_a}^H(\mathbf{I}-\mathbf{G}^{-1}))\mathbf{A}^H) \\ &= tr(\mathbf{A}((\mathbf{I}-\mathbf{G}^{-1})^{-1}+\mathbf{\Lambda_a}(\mathbf{I}-\mathbf{\Lambda_a}^H\mathbf{\Lambda_a})^{-1}\mathbf{\Lambda_a}^H)^{-1}\mathbf{A}^H) \\ &= tr(\mathbf{A}(\mathbf{I}+\sigma^2\mathbf{A}^H\mathbf{R_a}^H\mathbf{A}+\mathbf{\Lambda_a}(\mathbf{I}-\mathbf{\Lambda_a}^H\mathbf{\Lambda_a})^{-1}\mathbf{\Lambda_a}^H)^{-1}\mathbf{A}^H) \\ &= tr(\mathbf{A}((\mathbf{I}-\mathbf{\Lambda_a}^H\mathbf{\Lambda_a})^{-1}+\sigma^2\mathbf{A}^H\mathbf{R_a}^H\mathbf{A})^{-1}\mathbf{A}^H) \end{aligned}$$

where the simplifications in steps 2, 3, and 4 all uses the matrix inversion lemma introduced in [63]:

$$(\mathbf{A}+\mathbf{BCD})^{-1}=\mathbf{A}^{-1}+\mathbf{A}^{-1}\mathbf{B}(\mathbf{C}^{-1}+\mathbf{DA}^{-1}\mathbf{B})^{-1}\mathbf{DA}^{-1}$$

This completes our derivation.

To summarize, we have obtained the following results from the MMSE optimization of feedforward and feedback matrices:

1. For any feedback matrix $\mathbf{F}^{(i)}$, the choice of $\mathbf{M}^{(i)}$ that minimizes the MSE in stage i is

$$\mathbf{M}^{(i),opt}=(\mathbf{F}^(i)\mathbf{\Lambda_a}^{(i-1)}+\mathbf{A})\mathbf{A}^{(-1)}(\sigma^2\mathbf{A}^H\mathbf{A}^{-1}+\mathbf{R_a})^{-1} \tag{3.46}$$

2. With $\mathbf{M}^{(i)}=\mathbf{M}^{(i),opt}$, the choice of $\mathbf{F}$ that minimizes the MSE in the ith stage is

$$\begin{aligned} \mathbf{F}^{(i)} =&\mathbf{F}^{(i),opt}=\mathbf{A}(\mathbf{I}-(\mathbf{I}+\sigma^2\mathbf{A}^{-1}\mathbf{R_a}^{-1}(\mathbf{A}^H)^{-1})^{-1})\mathbf{\Lambda_a}^{(i-1)} \\ &(\mathbf{I}-\mathbf{\Lambda_a}^{(i-1)H}(\mathbf{I}+\sigma^2\mathbf{A}^{-1}\mathbf{R_a}^{-1}(\mathbf{A}^H)^{-1})^{-1}\mathbf{\Lambda_a}^{(i-1)})^{-1} \end{aligned} \tag{3.47}$$

To gain some insights about this detector, which we name the MMSE Multistage IC with feedforward Processing (MMSEMIC), we look at the initial stage, i.e. $i=1$. In this case, $\mathbf{\Lambda_a}^{(0)}=\mathbf{0}$ (since there are no previous symbol decisions) and thus $\mathbf{F}^{(1)}=\mathbf{0}$. This gives $\mathbf{M}^{(1)}=(\sigma^2\mathbf{A}^{-2}+\mathbf{R})^{-1}$, which is exactly the linear MMSE joint detector. This makes sense, since the MMSE linear joint detector is indeed the feedforward

matrix that minimizes the MSE when there is no feedback cancellation. As the number of stages increases, the symbol estimates become more accurate and $\mathbf{\Lambda_a}^{(i)}$ approaches the identity matrix, we expect the performance of this receiver to surpass that of linear MMSE joint detector.

To implement the proposed receiver in a practical system, we carry out the following procedures at each stage:

1. Estimate the error probability for each user in the last stage either via SIR approximation or interleaved training sequences.

2. Compute $\mathbf{\Lambda_a}^{(i-1)}$ for the current stage (i.e. stage i).

3. Compute feedback matrix $\mathbf{F}^{(i)}$ based on $\mathbf{\Lambda_a}^{(i-1)}$ and reconstruct the MAI using $\hat{\mathbf{b}}^{(i-1)}$ from the last stage.

4. Calculate feedforward matrix $\mathbf{M}^{(i)}$ based on $\mathbf{F}^{(i)}$.

5. Apply $\mathbf{M}^{(i)}$ to linearly transform the matched-filter output and subtract the reconstructed MAI from the transformation output. Send cancellation output to quantization devices to generate symbol decisions for the current stage.

6. Repeat steps 1 through 5 at subsequent stages until BER target is reached.

Note that the main complexity of the algorithm comes from the matrix inversion process involving $\mathbf{\Lambda_a}^{(i-1)}$ at every stage.

3.5.3 Alternative solutions with reduced complexity

Since the proposed receiver already achieves the performance of a standard linear MMSE detector in the initial stage, we expect its performance to exceed all linear joint detectors in later stages. Its complexity, however, also exceeds that of the joint detectors and grows in proportion with the number of stages, primarily due to the fact that matrix inversion, which has a complexity on the order of $O((LK)^3)$, has to be performed at every stage. To lower the complexity, in this section we introduce

two suboptimal solutions that have lower complexities and yet may still outperform the linear joint detectors.

Since the complexity at each stage mainly lies in matrix inversion, we design the suboptimal solution so that the inversion is only performed once throughout the entire cancellation process. One sensible choice is as follows:

$$\mathbf{M}^{(1)} = \begin{cases} (\mathbf{R} + (\mathbf{A}\mathbf{A}^H)^{-1}\sigma^2)^{-1} & \text{if } i = 1 \\ \mathbf{I} & \text{if } i > 1 \end{cases} \tag{3.48}$$

$$\mathbf{F}^{(i)} = (\mathbf{R} - \mathbf{I})\mathbf{A}\boldsymbol{\Lambda}_{\mathbf{a}}{}^{(i-1)} \tag{3.49}$$

In intuitive terms, the resulting receiver, which we call MMSE-Feedback Multistage IC (MMSEFIC), is a weighted multistage IC with linear MMSE detector at the initial stage. In subsequent stages, the MAI are reconstructed and subtracted from the matched-filter output. The cancellation weights are adjusted at each stage to minimize the MSE. In this way, the complexity of the system is similar to that of conventional PIC with MMSE first stage.

In addition, if we do not have estimates for the background noise (which contains thermal noise and intercell interferences) power ready, we may also use the decorrelator at the initial stage instead, which gives the following specification for $\mathbf{M}^{(i)}$ and $\mathbf{F}^{(i)}$:

$$\mathbf{M}^{(i)} = \begin{cases} \mathbf{R}^{-1} & \text{if } i = 1 \\ \mathbf{I} & \text{if } i > 1 \end{cases} \tag{3.50}$$

$$\mathbf{F}^{(i)} = (\mathbf{R} - \mathbf{I})\mathbf{A}\boldsymbol{\Lambda}_{\mathbf{a}}{}^{(i-1)} \tag{3.51}$$

This suboptimal receiver, which we call MMSE-Feedback Multistage IC with decorrelating first-stage (MMSEFICD), has a complexity that is similar to the PIC with decorrelating first stage.

3.6 Performance of MMSE multistage IC with forward and feedback matrices

3.6.1 Asymptotic analysis

In this section we calculate the asymptotic error probability of the proposed MMSE multistage IC with feedforward and feedback matrices for a large system with perfect power-control and random spreading codes. This means that we assume $A_1(1) = A_2(1) = \ ... \ = A_k(l) = A_{k+1}(l) = \ ... \ = A_K(L) = A$, $K \to \infty$, $N \to \infty$ and $\frac{K}{N} = \beta$.

We first look at the minimum MSE of each stage under MMSEMIC, which can be found as

$$\begin{aligned} MSE^{(i)} &= \frac{1}{K}E[tr(\mathbf{A}((\mathbf{I} - \mathbf{\Lambda_a}^H\mathbf{\Lambda_a})^{-1} + \sigma^2\mathbf{A}^H\mathbf{R_a}^H\mathbf{A})^{-1}\mathbf{A}^H)] \\ &= \frac{1}{K}E[\sum_{k=1}^{LK}\lambda_k(\mathbf{A}((\mathbf{I} - \mathbf{\Lambda_a}^H\mathbf{\Lambda_a})^{-1} + \sigma^2\mathbf{A}^H\mathbf{R_a}^H\mathbf{A})^{-1}\mathbf{A}^H)] \\ &= A^2(1-(\Lambda_a^{(i)})^2)E[\frac{1}{1+\frac{A^2(1-\Lambda_a^2)}{\sigma^2}\lambda_k(\mathbf{R_a})}]. \end{aligned}$$

where $\lambda_k(\mathbf{R_a})$ is the kth eigenvalue of $\mathbf{R_a}$. Simplification in the third step is based on the perfect power control and random spreading codes assumption, in which all users should have very similar error performance and thereby all diagonal entries in $\mathbf{\Lambda_a}^{(i)}$ equals to the constant $\Lambda_a^{(i)}$.

Now, to further simplify $MSE^{(i)}$, we use a convergence theorem proved in [75], which shows that for a DS-CDMA system with random spreading codes, correlation matrix $\mathbf{R}$ and $\frac{K}{N} = \beta$,

$$lim_{K\to\infty}E[\frac{1}{1+X^2\lambda_k(\mathbf{R})}] = 1 - \frac{1}{4\beta X^2}F(X^2,\beta) \tag{3.52}$$

where

$$F(u,v) \equiv (\sqrt{u(1+\sqrt{v})^2+1} + \sqrt{u(1-\sqrt{v})^2+1})^2.$$

Thus, we see that as $K \to \infty$,

$$MSE^{(i)} \rightarrow A^2(1-(\Lambda_a^{(i)})^2)(1-\frac{\sigma^2}{4\beta A^2(1-(\Lambda_a^{(i)})^2)}F(\frac{A^2(1-(\Lambda_a^{(i)})^2)}{\sigma^2},\beta))$$

To find the signal-to-interference ratio from $MSE^{(i)}$, we note that it has been shown in [76] that for a perfectly power-controlled system using MMSE detector, if $MSE = E[(\mathbf{z}-\mathbf{Ab})^H(\mathbf{z}-\mathbf{Ab})]$ has the following form:

$$MSE = A_{mse}^2(1-\frac{\sigma^2}{4\beta A_{mse}^2}F(\frac{A_{mse}^2}{\sigma^2},\beta)),$$

then the resulting signal-to-interference ratio is

$$SIR = \frac{A^2}{MSE} - \frac{A^2}{A_{MSE}^2}$$

By careful observation, we recognize that our $MSE^{(i)}$ is exactly in the form of 3.53 with $A_{MSE} = A\sqrt{1-(\Lambda_a^{(i)})^2}$. Hence, the asymptotic signal-to-interference ratio of MMSEMIC can therefore be found as

$$\begin{aligned}
SIR^{MMSEMIC,(i)} &= \frac{A^2}{MSE^{(i)}} - \frac{A^2}{A^2(1-(\Lambda_a^{(i)})^2)} \\
&= \frac{A^2}{A^2(1-(\Lambda_a^{(i)})^2)}(\frac{1}{1-\frac{\sigma^2}{4\beta A^2(1-(\Lambda_a^{(i)})^2)}F(\frac{A^2(1-(\Lambda_a^{(i)})^2)}{\sigma^2},\beta)} - 1) \\
&= \frac{1}{1-(\Lambda_a^{(i)})^2}(\frac{A^2(1-(\Lambda_a^{(i)})^2)}{\sigma^2} - \frac{1}{4}F(\frac{A^2(1-(\Lambda_a^{(i)})^2)}{\sigma^2},\beta)) \\
&= \frac{A}{\sigma^2} - \frac{1}{4(1-(\Lambda_a^{(i)})^2)}F(\frac{A^2(1-(\Lambda_a^{(i)})^2)}{\sigma^2},\beta))
\end{aligned}$$

where simplification in the third step has been shown in [75]. The second term in the last step is basically how far the asymptotic performance of MMSEMIC is from the single-user bound.

The asymptotic error probability of MMSEMIC in stage i can then be approxi-

mated using the standard Gaussian approximation:

$$Pe^{MMSEMIC,(i)} = Q(\sin\frac{\pi}{M}\sqrt{SIR^{MMSEMIC,(i)}}). \tag{3.53}$$

We next analyze the convergence behavior of MMSEMIC using error probabilities calculated based on Gaussian approximation. Since $SIR^{MMSEMIC,(i)}$ is a function of $Pe^{MMSEMIC,(i)}$ through $\Lambda_a^{(i)}$, $Pe^{MMSEMIC,(i)}$ is also a function of $Pe^{MMSEMIC,(i-1)}$ such that $Pe^{MMSEMIC,(i)} = \tilde{H}(Pe^{MMSEMIC,(i-1)})$. To find the error probability at which MMSEMIC reaches convergence, we just need to find out when $Pe^{MMSEMIC,(i)} = Pe^{MMSEMIC,(i-1)}$.

Figures 3-9, 3-10, and 3-11 show the convergence behavior of MMSEMIC as a function of the number of stages for small, large, and over-loaded systems, respectively, assuming BPSK modulation and a signal-to-noise ratio (SNR) of 7dB. The convergence curve for WPIC (i.e. weighted PIC with MMSE optimized feedback matrix) is also plotted for comparison. We see that, in figures 3-9(a) and 3-9(b), which corresponds to a system with load $\beta = 0.5$ and 0.75, respectively, the error floor for MMSEMIC and WPIC are essentially the same, except that it takes MMSEMIC fewer stages to reach convergence. In system with larger load, i.e. $\beta = 1$ and $\beta = 1.25$, which corresponds to figures 3-10(a) and 3-10(b), respectively, we see that the error floors of MMSEMIC starts to be significantly better than WPIC, while MMSEMIC also takes noticeably fewer iterations to reach convergence than WPIC. For overloaded system, i.e. figures 3-11(a), 3-11(b), and 3-11(c), which corresponds to $\beta = 1.5$, 2, and 4, respectively, we see that while WPIC performs poorly, WLIC still exhibits a very low error-rate floor (except for extremely high load, i.e $\beta = 4$), even though its convergence rate has slowed down significantly compared to the earlier cases.

3.6.2 Simulation verification

The performance of the proposed MMSE multistage IC with feedforward and feedback matrix and its suboptimal variations are verified via simulation for an asynchronous

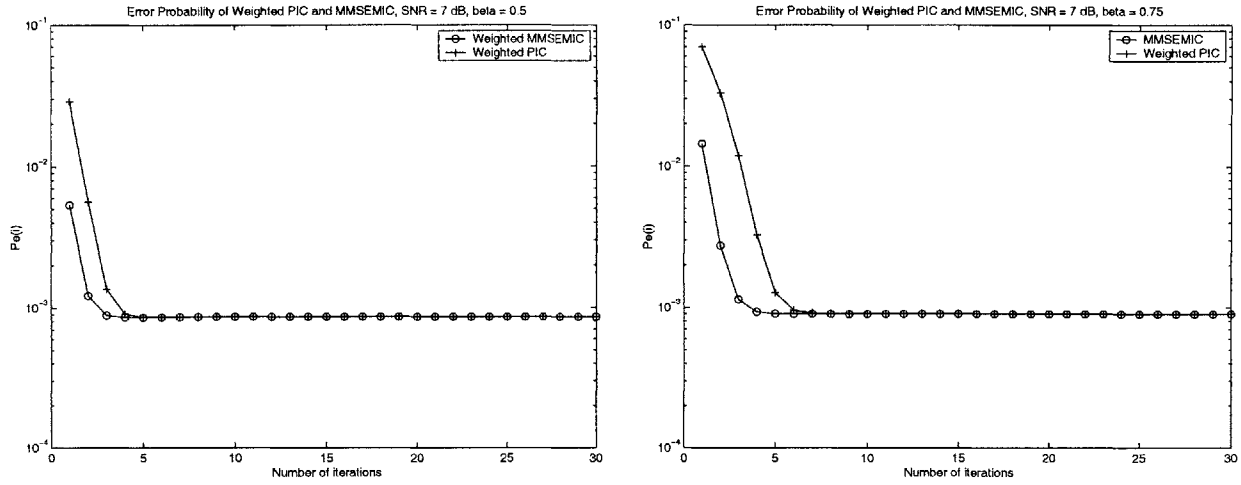

(a) (b)

Figure 3-9: Error probability convergence based on Gaussian approximation for MMSEMIC and WPIC for systems with loading (a) $\beta = 0.5$ and (b) $\beta = 0.75$

BPSK modulated and uncoded DS-CDMA system using random spreading codes with a spreading gain of $N = 128$. The receiver operates on every frame of 800 data symbols, including 12 training symbols for error-rate estimation.

We first look at the bandwidth efficiency of the proposed algorithms. Figures 3-12 (a)-(c) show the bit-error rate (BER) of MMSEMIC, MMSEFIC and MMSEFICD as a function of the number of users in the AWGN channel after two, three and five stages, respectively. The BER of the matched filter, the decorrelator, the linear MMSE detector and the single-user performance bound are also plotted for comparison. The amplitude of each user is fixed such that the individual $\frac{E_b}{N_0}$ is 7 dB, which resembles perfect power control. To simulate a more realistic channel, the corresponding performances in the frequency non-selective Rayleigh fading channel with average $\frac{E_b}{N_0} = 10dB$ are shown in figures 3-13(a)-(c) for two-, three- and five stage performances, respectively.

From these plots, we observe that the proposed algorithms (including the sub-optimal techniques) clearly outperforms the linear joint detectors. Furthermore, we observe that after three stages, the BER of the MMSEMIC is very close to the single-user performance bound. What else is interesting is that after three stages, the

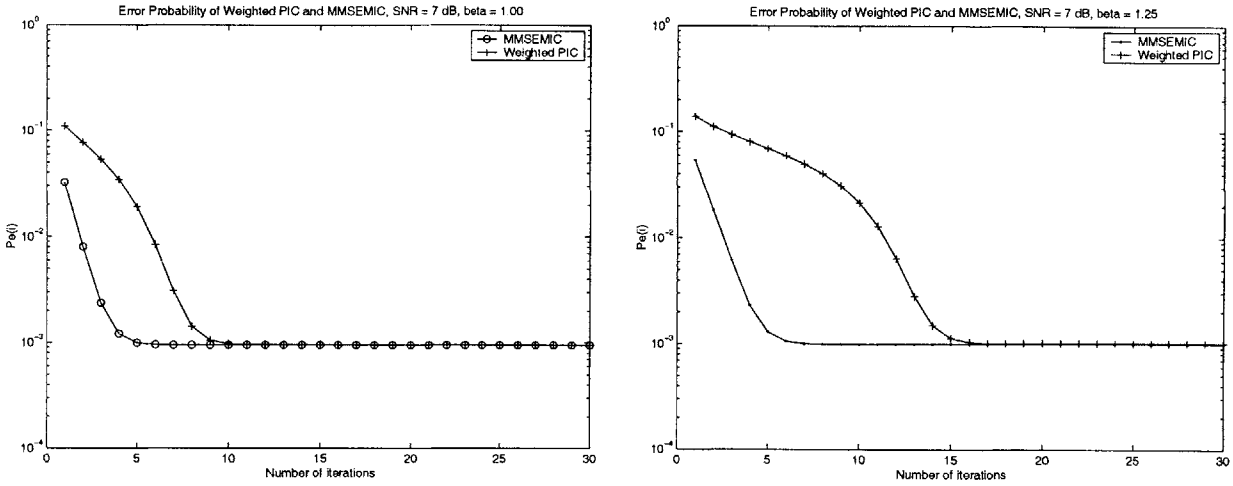

Figure 3-10: Error probability convergence based on Gaussian approximation for MMSEMIC and WPIC for systems with loading (a) $\beta = 1.0$ and (b) $\beta = 1.25$

performance of the MMSEMIC becomes somewhat insensitive to the MAI, as the error rate does not seem to increase proportionally with the number of users in the system. The BER gap between the MMSEMIC and the single-user bound may be contributed by the background noise enhancement caused by the linear transformation procedure at every stage. In addition, note that at early stages the performances of the proposed suboptimal schemes (MMSEFIC and MMSEFICD) are far from that of MMSEMIC. At later stages, however, the BER of these schemes, particularly MMSEFIC, approaches that of the MMSEMIC and the single-user bound.

We next look at the energy efficiency of the proposed algorithms. Figures 3-14(a)-(c) show the BER vs. $\frac{E_b}{N_0}$ for the proposed algorithms in a system with 75% load (96 users). We see that the energy efficiency of the proposed algorithms significantly outperforms the linear joint detectors. After 3 stages, the performance of MMSEMIC is very close to the single-user bound. Among the proposed suboptimal techniques, the power efficiency of MMSEFIC becomes very close to that of MMSEMIC and single-user bound at later stages.

3.7 Chapter summary

In this chapter, we have presented two effective multistage parallel interference cancellation algorithms that are derived using stage-by-stage MMSE optimization. The key difference between our detection schemes and the conventional approaches is that, instead of assuming the symbol estimates in previous stages to be completely accurate, we incorporate a weighting matrix into the detection process. The weighting matrix is an approximate measure of the correlation between symbol estimates in the previous stage and the true transmitted symbols. Our first algorithm applies decision-feedback to cancel the MAI and has a complexity that is comparable to that of the conventional PIC. Its performance significantly surpasses that of conventional and partial PIC for both AWGN and fading channels. Our second algorithm uses both feedforward and feedback matrices to suppress MAI, and its complexity is on the same order as that of linear joint detection. The performance of this detector not only surpasses that of our first scheme and the linear joint detectors but also approaches the single-user performance bound in a small number of iterations.

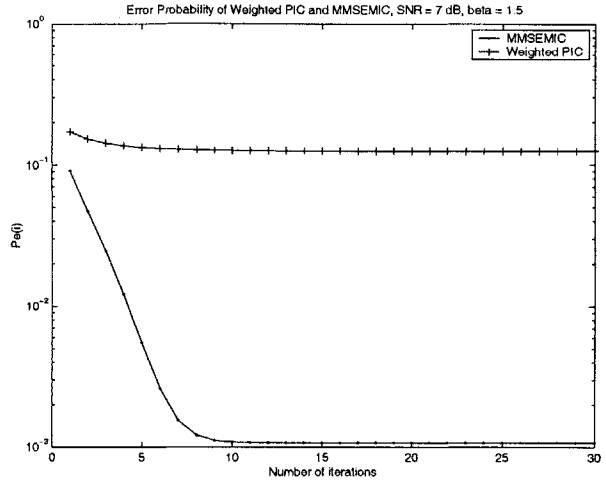

(a)

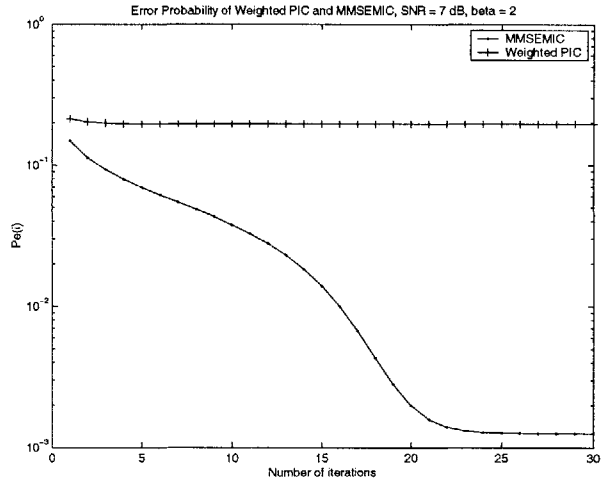

(b)

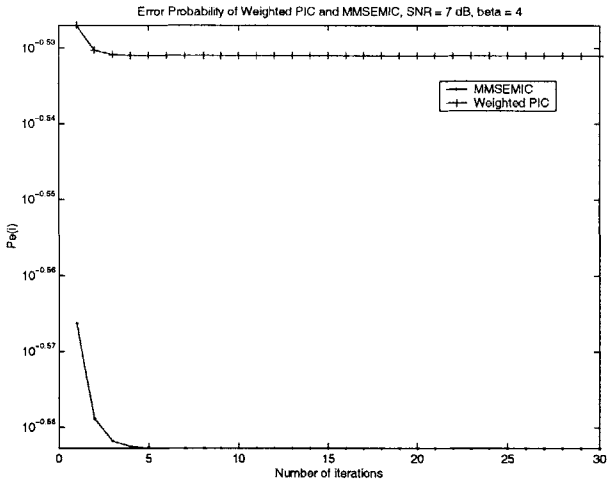

(c)

Figure 3-11: Error probability convergence based on Gaussian approximation for MMSEMIC and WPIC for systems with loading (a) $\beta = 1.5$, (b) $\beta = 2$, and (c) $\beta = 4$

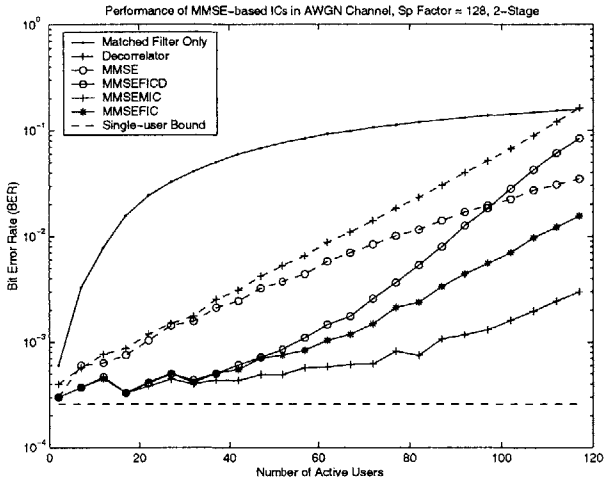

(a)

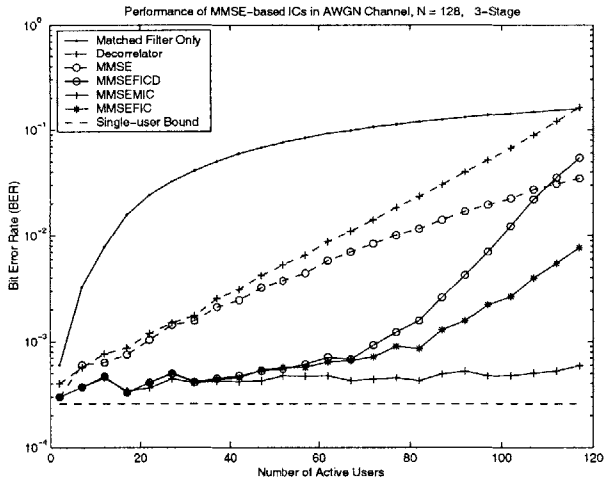

(b)

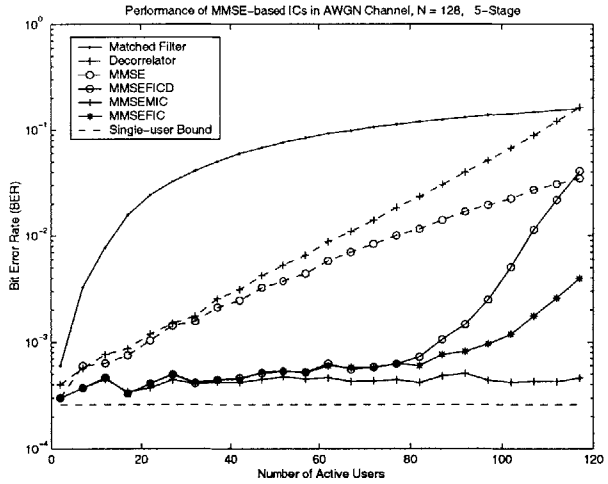

(c)

Figure 3-12: Error probability of multistage MMSE IC vs. the total number of users in AWGN channel: (a) 1 stage, (b) 2 stages, (c) 5 Stages

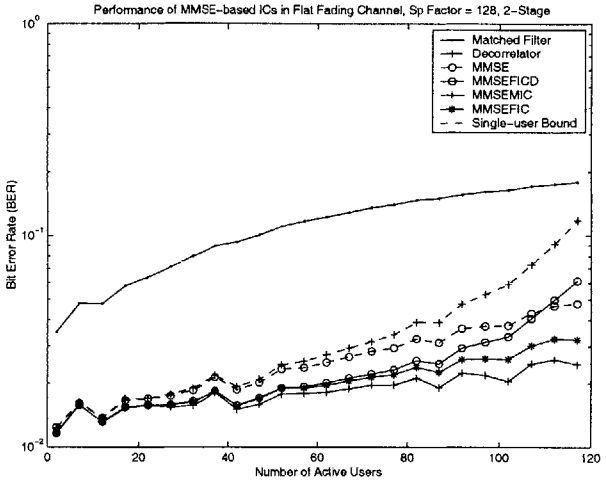

(a)

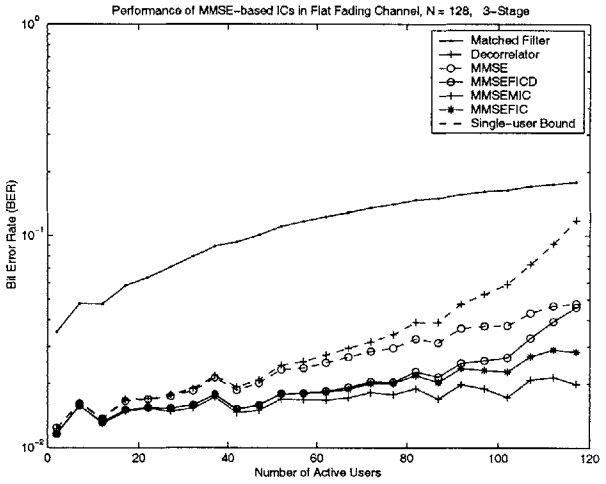

(b)

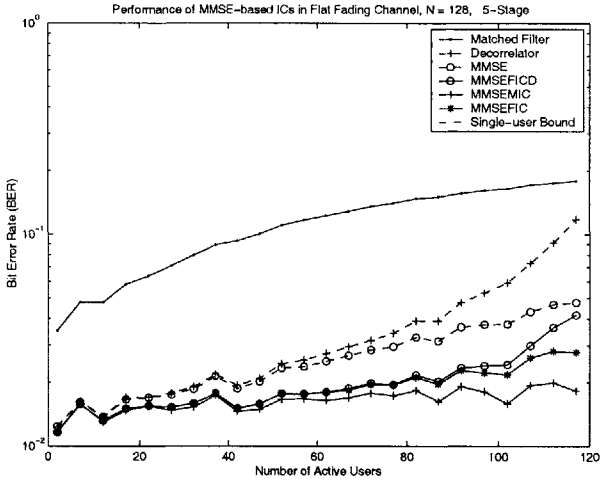

(c)

Figure 3-13: Error probability of multistage MMSE IC vs. the total number of users in flat-fading channel: (a) 1 stage, (b) 2 stages, (c) 5 stages

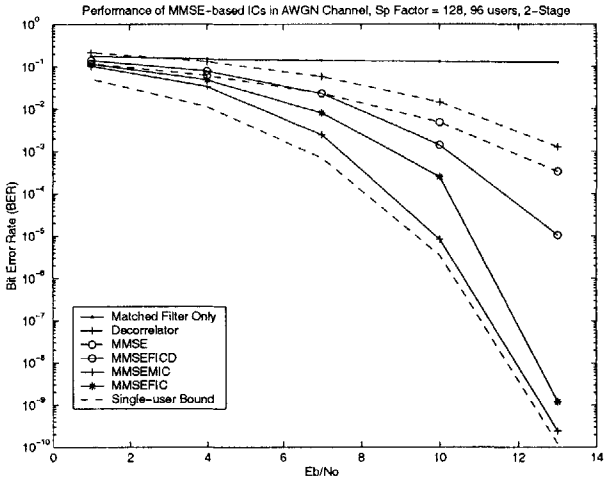

(a)

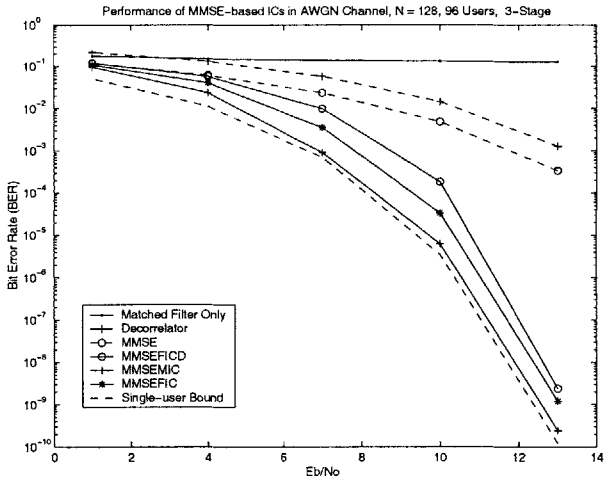

(b)

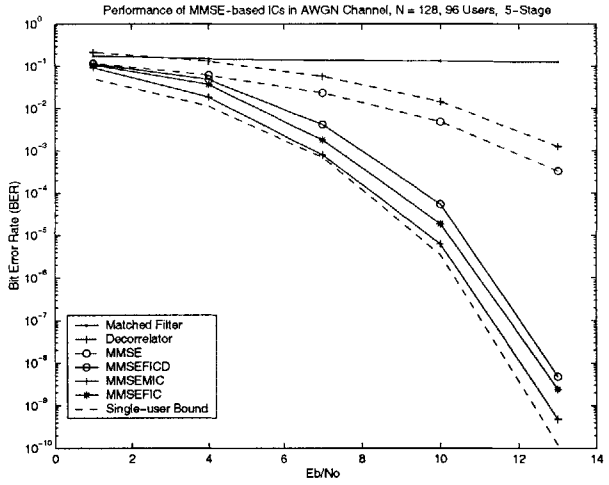

(c)

Figure 3-14: Error probability of multistage MMSE IC vs. $\frac{E_b}{N_0}$ in AWGN channel (96 Users): (a) 1 stage, (b) 2 stages, (c) 5 stages

Chapter 4

A Dual-mode Linear Multiuser Receiver

In this chapter, we investigate the detection problem in receiver design for the uplink a direct-sequence code-division multiple access (DS-CDMA) system. The design objective is to minimize the system computational complexity while meeting the quality of service (QoS) requirements (such as bit-error rate(BER), throughput, and delay constraint) of the users. Specifically, we focus on linear joint detection. We introduce a dual-mode multiuser detector that dynamically switches its detection mode between matched filter and decorrelator operations based on the channel characteristics. This detector significantly reduces the overall computational requirement while maintaining similar performance as that of the decorrelator. The switching mechanism of our dual-mode detector is designed by exploiting the performance-complexity tradeoff between the decorrelator and the matched filter.

4.1 Motivations and background

The spectral efficiency of a conventional DS-CDMA system that employs single-user matched-filter detection suffers from multiple-access interference (MAI), or user-to-user interference caused by non-zero cross-correlation between the spreading code waveforms of different subscribers. Multiuser joint detector has emerged as a promis-

ing technique to suppress MAI. Unlike the single-user detector that performs detection for each user individually and treats other users' signals as additive white noise, the joint detector incorporates the information of other subscribers into consideration while recovering data for the desired user.

The multiuser detector that leads to jointly optimal error probabilities for all users was proposed by [74] using a maximum likelihood sequence estimation approach. The complexity of this detector, however, grows exponentially with the number of users and is thus unsuitable for practical implementation. Since then, most of the research efforts in joint detection focus on the design of suboptimal algorithms that yield good performance-complexity tradeoff [33, 42, 24, 46, 75, 84, 85]. There are grossly two classes of suboptimal joint detectors: linear and non-linear detectors. The linear detectors basically perform a linear transformation on the matched-filter output to tune out the interferences, but the nonlinear detectors typically employs decision-feedback interference cancellation.

In this chapter, we consider the class of linear multiuser detectors, which has been shown to perform significantly better than the matched filter and is yet much simpler to implement than a maximal likelihood (ML) detector [55, 75] (which is optimal in terms of performance). In particular, we focus on a specific linear multiuser detector called decorrelator, the operations of which do not require accurate estimation of the amplitudes of the users' received signals and the background noise power. The asymptotic performance of the decorrelator has been extensively studied in the context of asymptotic multiuser efficiency, bit-error rate (BER), effective bandwidth, and user capacity [32, 54, 67, 76].

Previous studies have demonstrated that the decorrelator in general is more effective than the single-user matched filter in suppressing MAI. Its performance, however, may not exceed that of the matched filter in certain cases due to its inherent noise enhancement problem [76]. In particular, when the background interferences, such as intercell interferences and thermal noise, are excessively high compared to the MAI, the decorrelator is likely to perform worse than the matched filter. Moreover, the decorrelator has a much higher computational complexity than the matched fil-

ter [34]. Even though these facts are well-known, little seem to have been done to incorporate them into system design considerations. By exploiting this performance-complexity tradeoff between the decorrelator and the matched filter, we propose a new design for implementing a decorrelator-based multiuser receiver.

The main feature of our dual-mode detector is that it dynamically switches between the decorrelator and the matched-filter operations based on the interference characteristics. Our receiver is capable of significantly reducing the consumption of computational resources while maintaining similar performance as that of the decorrelator. A key element in this technique is the switching criterion, i.e. when to switch from one mode to the other. We obtain this switching criterion by comparing the analytical performance between the decorrelator and the matched filter. The effectiveness of our dual-mode detector is illustrated via simulations.

This chapter is organized as follows. We begin by briefly introducing the basic models and structures of the decorrelator and the matched filter in section 2. We propose our dual-mode detector in section 3 and then derive the switching threshold in section 4 by comparing the signal-to-interference ratio of the decorrelator and the matched filter. We present simulation results in section 5 to verify the receiver performance. Chapter summary is given in section 6.

4.2 System model

We begin with a mathematical description of a single-cell DS-CDMA system. Assuming K users employing antipodal signals for transmission over a frequency non-selective additive white Gaussian noise (AWGN) channel, the received baseband signal can be expressed as

$$r(t) = \sum_{k=1}^{K} A_k s_k(t-\tau_k) d_k(t-\tau_k) + n(t), \tag{4.1}$$

where A_k and τ_k are the received amplitude and delay of user k, respectively. The function $d_k(t)$ denotes the user data waveform, where $d_k(t) = \sum_{i=-\infty}^{\infty} d_{k,i} rect(t - iT_b)$,

with T_b being the symbol interval, $d_{k,i} \in \{-1, 1\}$ being the ith transmitted symbol of user k, and $rect(t)$ being the rectangular pulse of width T_b and unit amplitude. The background additive white Gaussian noise (AWGN) with one-sided density power density $2N_p$ is denoted by $n(t)$, which consists of thermal noise as well as intercell interference, i.e. interferences from users in other cells. The function $s_k(t)$ denotes the spreading signature waveform of user k and can be expressed as

$$s_k(t) = \sum_{i=-\infty}^{\infty} \sum_{j=1}^{N} c_{k,j} g(t - jT_c - iT_b), \tag{4.2}$$

where $c_{k,j} \in \{-1, 1\}$ is the value of the jth chip of user k's spreading sequence; N is the spreading factor; T_c is the chip interval, i.e. $T_b = NT_c$; $g(t)$ is the chip pulse, which is assumed to be rectangular for the convenience of analysis and simulation; The energy of $g(t)$ has been normalized such that $\int_{Tb} |s_k(t)|^2 dt = 1$.

First we look at linear joint detection for a symbol-synchronous DS-CDMA system, i.e. τ_k is zero for all k. This model applies to the uplink with very tight timing control, an example of which is the time-division synchronous CDMA (TD-SCDMA) system developed for 3rd generation wireless system in China [66]. To detect the ith symbol of the kth user, the receiver first performs matched filtering for user k over the interval $[iT_b, (i+1)T_b]$. The detection for the ith symbol for all users is thus equivalent to passing $r(t)$ through a bank of matched filters. The output of this filter bank, which we denote as $\mathbf{y} = [y_1 \ y_2 \ ... \ y_K]^T$, forms a set of sufficient statistics for the detector decision on the received symbols. Each element of $\mathbf{y}$ can be found as

$$\begin{aligned} y_k &= \int_{iTb}^{(i+1)T_b} r(t) s_k(t) dt \\ &= A_k d_{k,i} + \sum_{j=1, j\neq k}^{K} \rho_{k,j} A_j d_{j,i} + n_k, \end{aligned} \tag{4.3}$$

where n_k is the projection of $n(t)$ on $s_k(t)$ and $\rho_{k,j} = \int_{iTb}^{(i+1)T_b} s_k(t) s_j(t) dt$ is the cross-correlation between the kth and jth users' signature waveforms. The middle term of y_k is the MAI from other users on user k, which is clearly caused by the nonzero

cross-correlations between the users' signature waveforms. Furthermore, we see that

$$\mathbf{y} = \mathbf{RAd} + \mathbf{n}, \tag{4.4}$$

where $\mathbf{R}$ is a K-by-K correlation matrix with elements $R_{k,j} = \rho_{k,j}$, $\mathbf{A}$ is a diagonal matrix with $A_{k,k} = A_k$, $\mathbf{d} = [d_{1,i}\ d_{2,i}\ ...\ d_{K,i}]^T$ is the data vector, and $\mathbf{n} = [n_1\ n_2\ ...\ n_K]^T$ is the noise vector.

With linear multiuser detection and hard-limited decision, the output decision for user k's symbol is made as $\hat{d}_{k,i} = sgn(z_k)$ where

$$\mathbf{z} = \mathbf{Ly}, \tag{4.5}$$

$\mathbf{L}$ is a linear transformation matrix depending on the type of detector that is used. For the conventional matched-filter detector, $\mathbf{L}$ is a K by K identity matrix. For the decorrelator, $\mathbf{L} = \mathbf{R}^+$, where $\mathbf{R}^+$ denotes the Moore-Penrose pseudo-inverse of $\mathbf{R}$. When $\mathbf{R}$ is nonsingular, $\mathbf{R}^+$ equals to $\mathbf{R}^{-1}$. The decorrelator essentially performs a linear transformation with the intention to completely eliminate MAI. It has been shown that the decorrelator achieves the optimal near-far resistance as long as $\mathbf{R}$ is nonsingular, i.e. user signature waveforms are linearly independent of each other [75].

We now develop a similar model for an asynchronous CDMA network, which is applicable to the uplink of a cellular system without timing control. In contrast to the symbol-synchronous case, user k's delay, τ_k, is no longer zero but a real number that is distributed between zero and T_b and is independent of the timing of other users. To minimize the decision delay, we look at one-shot detectors, which means that the detection of the ith bit of user k is based only on the received signal over the interval $[\tau_k + iT_b, \tau_k + (i+1)T_b]$. The one-shot detection is optimal for the matched-filter detection but suboptimal for the decorrelator detection [75].

Without loss of generality, we consider the detection of the ith bit of user 1, and we assume that $\tau_1 = 0$. We therefore want to look at interval $[iT_b, (i+1)T_b]$ for $\hat{d}_{1,i}$. Due to the assumed asynchronism, the interference caused by each user may contribute in multiple dimensions. We subsequently rewrite $r(t)$ over the time interval of interest

as

$$r(t) = \sum_{k=1}^{2K-1} A_k \tilde{d}_{k,i} \tilde{s}_k(t), \quad t \in [iT_b, (i+1)T_b], \tag{4.6}$$

where $\tilde{d}_{1,i} = d_{1,i}$, $\tilde{s}_1(t) = s_1(t)$, and for $k \neq 1$

$$\begin{aligned}
\tilde{d}_{2k,i} &= d_{k,i-1}, \quad \tilde{d}_{2k+1,i} = d_{k,i} \\
\tilde{s}_{2k}(t) &= \begin{cases} s_k(t-\tau_k), & t \in [iT_b, iT_b + \tau_k] \\ 0 & otherwise \end{cases} \\
\tilde{s}_{2k+1}(t) &= \begin{cases} s_k(t-\tau_k), & t \in [iT_b + \tau_k, (i+1)T_b] \\ 0 & otherwise \end{cases}.
\end{aligned}$$

A set of sufficient statistics for the one-shot detection over the interval $[iT_b, (i+1)T_b]$ is $\tilde{\mathbf{y}} = [\tilde{y}_1 \ \tilde{y}_2 \ ... \ \tilde{y}_{2K-1}]^T$ where

$$\tilde{y}_k = \int_{iTb}^{(i+1)T_b} r(t)\tilde{s}_k(t)dt.$$

We see that, similar to the synchronous case,

$$\tilde{\mathbf{y}} = \tilde{\mathbf{R}}\mathbf{A}\mathbf{d} + \mathbf{n}, \tag{4.7}$$

where now $\tilde{\mathbf{R}}$ is a $(2K-1)$ by $(2K-1)$ correlation matrix with elements $\tilde{R}_{k,j} = \tilde{\rho}_{k,j} = \int_{iTb}^{(i+1)T_b} \tilde{s}_k(t)\tilde{s}_j(t)dt$.

The estimate of the ith symbol of user 1 is obtained as $\hat{d}_{1,i} = sgn(\tilde{z}_i)$ where

$$\tilde{\mathbf{z}} = \mathbf{L}\tilde{\mathbf{y}}, \tag{4.8}$$

where $\mathbf{L}$ is an identity matrix for the matched-filter detection, and $\mathbf{L} = \tilde{\mathbf{R}}^+$ for the decorrelator. Here, again, we see that the decorrelator can completely eliminate MAI for user 1 as long as the one-shot cross-correlation matrix $\tilde{\mathbf{R}}$ is nonsingular.

4.3 Architecture of the dual-mode detector

Even though the decorrelator is able to effectively suppress MAI, its performance suffers from a problem known as noise enhancement. The reason is that during the linear transformation process, the noise component in the received signal is also being scaled by the inverse of the correlation matrix. This has been shown to result in a greater noise power [75]. Consequently, in the case where the background noise is stronger than MAI, the decorrelator is likely to perform worse than the matched filter. In particular, [76] showed that for a DS-CDMA system with random spreading codes and an optimal choice of spreading gain, the spectral efficiency of the decorrelator is greater than that of the matched filter only if the average $\frac{E_b}{N_o}$ of all users in the system exceeds 5.2 dB.

In terms of computational complexity, the decorrelator operation requires significantly more computational resources beyond the matched filtering. It is shown in [34] that for a standard implementation of the full-decorrelator in an asynchronous CDMA system, the total number of operations required beyond the matched filtering is at least on the order of cubic of the number of users. It is therefore inefficient to apply the decorrelator in an environment where it does not significantly outperform the matched filter.

These observations prompt us to propose a dual-mode multiuser detector that dynamically switches the detection mode between the decorrelator and the matched-filter operations. The overall architecture and operations of this dual-mode detector can be easily understood by examining figure 1. The receiver first processes the incoming signal with a bank of matched filters. Next, it performs certain necessary estimations using the output of the matched filter. These estimates are then used to decide whether to perform multiuser detection (MUD). If so, the decorrelator transformation will be performed. Otherwise, the receiver bypasses the decorrelator operations, and the output of the matched filter is used for the symbol decision. The detection mode is decided on a symbol-by-symbol basis for each user.

The key idea here is that the decorrelator operation for all users will be performed

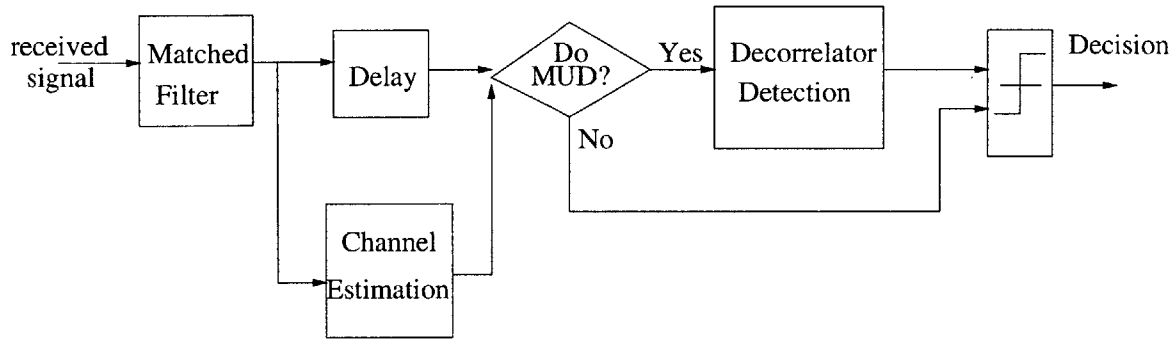

Figure 4-1: Structure of the dynamic dual-mode linear multiuser receiver

only if the MAI dominates other background interferences for a significant number of users. Note that in a realistic cellular system, the background interferences for each user come not only from the thermal noise but also from other sources such as inter-cell interferences, which can be quite strong at times. Also, due to multipath fading, the amplitude of the received signal of each user may vary over time significantly. We thus expect that there would be a significant portion of time during which the decorrelator does not outperform the matched filter. The use of this dual-mode detector therefore has the potential of significantly reducing the computational requirement while maintaining similar performance as that of the decorrelator, if not better.

4.4 Switching criterion

In this section, we describe how to make decisions about the detection mode, which is the key element of this dual-mode receiver. We first analyze and compare the performance of the one-shot decorrelator and the matched filter, based on which we then decide our design parameters for the switching block that determines the detector mode.

We first look at the performance of the decorrelator, which has been extensively studied[32, 67, 72, 75, 76, 77]. Most of the existing works focus on the asymptotic behavior of the decorrelator by letting the spreading factor N and the number of users K go to infinity while fixing the ratio between N and K at a finite value. Here,

instead of analyzing the asymptotic behavior, we derive a performance bound on the output signal-to-interference ratio (SIR) of the one-shot decorrelator detector for finite K and N.

We first look at a two user synchronous system. In this case, the matched-filter output for users 1 and 2 can be explicitly expressed as

$$\begin{aligned} y_1 &= A_1 b_1 + A_2 \rho b_2 + n_1 \\ y_2 &= A_2 b_2 + A_1 \rho b_2 + n_2 \end{aligned}$$

where we let $\rho = \rho_{1,2}$ to denote the cross-correlation between the spreading codes of users 1 and 2. If we express the matched-filter output into vector form $\mathbf{y} = \mathbf{RAb} + \mathbf{n}$, the correlation matrix is

$$\mathbf{R} = \begin{bmatrix} 1 & \rho \\ \rho & 1 \end{bmatrix}$$

The inverse of $\mathbf{R}$ can be found as

$$\mathbf{R}^{-1} = \frac{1}{1-\rho^2} \begin{bmatrix} 1 & -\rho \\ -\rho & 1 \end{bmatrix}$$

The output of the decorrelator transformation is $\mathbf{z} = \mathbf{R}{-}1\mathbf{y} = [z_1 z_2]^T$, the elements of which can be found as

$$\begin{aligned} z_1 &= A_1 b_1 + \frac{n_1 - \rho n_2}{1-\rho^2} \\ z_2 &= A_2 b_2 + \frac{n_2 - \rho n_1}{1-\rho^2} \end{aligned}$$

Without loss of generality, we look at the performance of user 1. We see that before decorrelator, the signal-to-interference ratio (SIR) of user 1 is

$$SIR_1^{mf} = \frac{A_1^2}{A_2^2 \rho^2 + N_p} \tag{4.9}$$

After decorrelator, the SIR becomes

$$\begin{aligned} SIR_1^{decorr} &= \frac{A_1^2}{E[(\frac{n_1-\rho n_2}{1-\rho^2})^2]} \\ &= \frac{A_1^2(1-\rho^2)^2}{E[n_1^2]+E[n_2^2]\rho-2\rho E[n_1 n_2]} \\ &= \frac{A_1^2(1-\rho^2)^2}{N_p+N_p\rho^2-2\rho N_p} \\ &= \frac{A_1^2(1-\rho^2)}{N_p} \end{aligned} \tag{4.10}$$

The tradeoff here is that even though the MAI has been eliminated, the back ground noise has been enhanced by a factor of $1-\rho^2$. Or equivalent, we can say that the user pay a penalty of $1-\rho^2$ in the signal power for using decorrelator.

If we compare SIR_1^{mf} and SIR_1^{decorr}, we see that the decorrelator will benefit user 1 in terms of SIR only if

$$\frac{A_1^2(1-\rho^2)}{N_p} > \frac{A_1^2}{A_2^2\rho^2+N_p}$$

Or equivalently

$$\frac{A_2^2}{N_p} > \frac{1}{1-\rho^2}$$

which means that the decorrelator outperforms matched filter in terms of SIR only if the signal-to-background-noise ratio (SNR) of user 2 exceeds $\frac{1}{1-\rho^2}$.

Using similar procedure, we can show that user 2 will benefit from decorrelator detection only if

$$\frac{A_1^2}{N_p} > \frac{1}{1-\rho^2}.$$

We now extend the analysis to a system with K users. Without loss of generality and for notational convenience, we again analyze the SIR for user 1. We state our main results in this section and present the proof in appendix B. Let us first consider a synchronous CDMA system with nonsingular correlation matrix $\mathbf{R}$. The soft output

of the decorrelator detector for user 1 in this case is

$$z_1 = A_1 d_1 + \sum_{k=1}^{K} R_{1,k}^{-1} n_k, \tag{4.11}$$

where n_k is the kth element of the noise vector. The following theorem gives a lower bound on the SIR of any user:

Theorem 4.1 *Let SIR_1^{decorr} denote the output SIR of the decorrelator receiver for user 1 in a symbol-synchronous CDMA system where the spreading sequences of all users are linearly independent of each other. Then*

$$SIR_1^{decorr} \geq \eta_1 = \frac{A_1^2 \sigma_{min}^2(\mathbf{R})}{N_p}, \tag{4.12}$$

where $\sigma_{min}(\mathbf{R})$ is the minimum singular value of $\mathbf{R}$, the correlation matrix of the user signature sequences, and N_p is the noise power.

Similarly, for an asynchronous CDMA system using the one-shot decorrelator detection, we obtain the following corollary:

Corollary 4.1 *Let $\tilde{S}IR_1^{decorr}$ denote the output SIR of the one-shot decorrelator receiver for user 1 in an asynchronous CDMA system. Assuming that the one-shot correlation matrix $\tilde{\mathbf{R}}$ is nonsingular, then*

$$\tilde{S}IR_1^{decorr} \geq \tilde{\eta}_1 = \frac{A_1^2 \sigma_{min}^2(\tilde{\mathbf{R}})}{N_p}. \tag{4.13}$$

The interpretation of theorem 4.1 and corollary 4.1 is that even though the decorrelator has eliminated MAI completely, its performance is now limited by the noise enhancement, and the worst-case noise enhancement factor is the inverse of the minimum singular value of the cross-correlation matrix.

So far, we have assumed that the cross-correlation matrix involved in the detection process is nonsingular. This condition can be maintained for a synchronous

CDMA system as long as the number of users is less than the spreading factor. For an asynchronous CDMA system, however, the non-singularity of the one-shot cross-correlation matrix is not guaranteed even if the number of users is less than the spreading gain [75]. This is because each user in such a system is capable of contributing interferences in multiple dimensions. Theorem 4.2 subsequently gives a lower bound for the decorrelator SIR in the case where the one-shot correlation matrix is singular.

Theorem 4.2 *Let* $\tilde{SIR}_1^{decorr}$ *denote the SIR of the one-shot decorrelator receiver for user 1 in an asynchronous CDMA system with singular one-shot correlation matrix* $\tilde{\mathbf{R}}$. *Then*

$$\tilde{SIR}_1^{decorr} \geq \tilde{\gamma}_1 = \frac{A_1^2 M_{1,1}^2}{\sum_{j=2}^{K} M_{1,j}^2 A_j^2 + \frac{(N_p)}{\hat{\sigma}_{min}^2(\tilde{\mathbf{R}})}}, \tag{4.14}$$

where $\hat{\sigma}_{min}(\tilde{\mathbf{R}})$ *is the minimum nonzero singular value of* $\tilde{\mathbf{R}}$. $M_{i,j} = \mathbf{v_i}'\mathbf{v_j}$, *where* $\mathbf{v_i}'$ *is the transpose of* $\mathbf{v_i}$, *which is a length-L vector that contains the first L components of the ith right singular vector of* $\tilde{\mathbf{R}}$ [1], *where L is the number of nonzero singular values in* $\tilde{\mathbf{R}}$.

The bound in theorem 4.2 leads to another fundamental insight on the decorrelator. It shows that when the correlation matrix is singular, the decorrelator's performance suffers not only from the noise enhancement but also from the residual MAI and an attenuation on its own signal power. It is widely believed that the decorrelator generally performs worse than the matched filter in this case [76].

We now look at user 1's SIR if only the matched-filter detection is used. This SIR can be expressed as

$$SIR_1^{mf} = \frac{A_1^2}{\sum_{j=2}^{K} \rho_{1,j}^2 A_j^2 + N_p} \tag{4.15}$$

[1] *The ith right singular vector refers to the ith row of* $\mathbf{V}$, *where* $\mathbf{R} = \mathbf{V\Sigma V^T}$ *is the singular decomposition of* $\mathbf{R}$.

for synchronous user transmissions and

$$\widetilde{SIR}_1^{mf} = \frac{A_1^2}{\sum_{j=2}^{2K-1} \widetilde{\rho}_{1,j}^2 A_j^2 + N_p} \tag{4.16}$$

for an asynchronous system.

The question is: when does the decorrelator perform significantly better than the matched filter? The answer varies from user to user and depends on a wide variety of factors such as the correlation properties of the user signature sequences, the propagation environment, and the strength of the background interferences. We use the criteria that the decorrelator significantly outperforms the matched filter for each user only if 1) the cross-correlation matrix is nonsingular, and 2) the worst case SIR of the decorrelator is greater than the SIR of the matched filter. Even though these criteria seem to favor the use of the matched filter over the decorrelator, they nonetheless simplify the process of deciding the switching method for the dual-mode detector.

Using the above specified criteria, the decorrelator detection is favorable for user 1 only if

$$\eta_1 > SIR_1^{mf} = \frac{A_1^2}{\sum_{j=2}^{K} \rho_{1,j}^2 A_j^2 + N_p} \tag{4.17}$$

for synchronous systems and

$$\tilde{\eta}_1 > \tilde{SIR}_1^{mf} = \frac{A_1^2}{\sum_{j=2}^{2K-1} \widetilde{\rho}_{1,j}^2 A_j^2 + N_p} \tag{4.18}$$

for asynchronous systems. Equations 4.17 and 4.18 can be further reduced to eq. 4.19 and 4.20 below, respectively.

$$\frac{N_p}{\sigma_{min}^2(\mathbf{R})} < \sum_{j=2}^{K} \rho_{1,j}^2 A_j^2 + N_p. \tag{4.19}$$

$$\frac{N_p}{\sigma^2_{min}(\tilde{\mathbf{R}})} < \sum_{j=2}^{2K-1} \tilde{\rho}^2_{1,j} A_j^2 + N_p. \tag{4.20}$$

Eqns. 4.19 and 4.20, together with the non-singularity constraint on the correlation matrix, can subsequently be used for our switching criteria so that the decorrelator detection will be performed only if the corresponding criteria are met. The intuition here is that the decorrelator detection should be performed only if the worst-case noise enhancement incurring from the decorrelator operation is less than the total interferences before the decorrelator detection.

There is, however, one problem for using eqs. 4.19 and 4.20 as the switching criteria. As mentioned before, this decision somewhat favors the use of the matched filter over the decorrelator, as we are comparing the worst case SIR of the decorrelator with the exact SIR of the matched filter. To address this problem, we modify eqs. 4.19 and 4.20 by replacing the minimum singular value of the correlation matrix with reciprocal of the average of all singular values of $\mathbf{R^{-1}}$. This average can be computed as the average of the reciprocals of the singular values of the correlation matrix $\mathbf{R}$. Since $\mathbf{R}$ is symmetric and positive semi-definite, singular-value decomposition here is identical to eigen decomposition [63]. The average singular value of $\mathbf{R^{-1}}$ can therefore be found by averaging over the reciprocals of the eigen-values of the correlation matrix $\mathbf{R}$. Eqns. 4.21 and 4.22 show the modified criterion that we eventually use for our dual-mode detector in synchronous and asynchronous CDMA systems, respectively.

$$\frac{N_p(trace(\mathbf{R^{-1}}))^2}{K^2} < \sum_{j=2}^{K} \rho^2_{1,j} A_j^2 + N_p, \tag{4.21}$$

$$\frac{N_p(trace(\tilde{\mathbf{R}}^{-1}))^2}{(2K-1)^2} < \sum_{j=2}^{2K-1} \tilde{\rho}^2_{1,j} A_j^2 + N_p, \tag{4.22}$$

where $trace(\mathbf{R^{-1}})$ is the sum of all diagonal elements in the inverse of $\mathbf{R}$, which can

be found as

$$trace(\mathbf{R^{-1}}) = \sum_{i=1}^{rank(R)} \frac{1}{\lambda_i(\mathbf{R})}, \tag{4.23}$$

where $rank(R)$ is the rank of matrix $\mathbf{R}$ and $\lambda_i(\mathbf{R})$ is the ith eigenvalue of $\mathbf{R}$.

Even though the average eigenvalue of correlation matrix can be readily estimated with the knowledge of the spreading waveforms and the transmission delays of all users, the process is as complicated as finding $\mathbf{R}^{-1}$ or $\tilde{\mathbf{R}}^{-1}$. This defeats the purpose of the dual-mode detector. Fortunately, we can use the following proposition to further simplify our decision process for a system with random spreading codes, which apply to realistic DS-CDMA system using long pseudorandom spreading codes, such as in the IS-95 and CDMA2000 reverse link. This proposition has been proved in [6] and can be stated as:

Proposition 4.1 *Suppose that K users employ direct-sequence spread-spectrum waveforms with N chips per symbol. Let*

$$\lim_{K\to\infty} \frac{K}{N} = \beta \in (0, \infty)$$

Suppose that the choice of signature sequences is completely random: the sequences assigned to each user are independent, and all binary sequences are equally likely. Then, the percentage of the K eigenvalues of $\mathbf{R}$ that lie below x converges (as $K \to \infty$) to the cumulative distribution function of the probability density function

$$f_\beta(x) = [1 - \beta^{-1}]^+ \delta(x) + \frac{\sqrt{[x-a]^+[b-x]^+}}{2\pi\beta x},$$

where

$$[z]^+ = \max\{0, z\},$$

and

$$\begin{aligned} a &= (1-\sqrt{\beta})^2 \\ b &= (1+\sqrt{\beta})^2 \end{aligned}$$

Moreover, if $\beta \leq 1$, the smallest eigenvalue converges almost surely to a.

Using this lemma, we proceed to simplify the process of finding average eigenvalues of $\mathbf{R}$ for $\beta < 1$ in a large system as follows:

$$\begin{aligned} E[\frac{1}{\lambda_i(\mathbf{R})}] &\rightarrow \int_0^\infty \frac{1}{x} f_\beta(x)dx \\ &= \int_a^b \frac{\sqrt{(x-a)(b-x)}}{2\pi\beta x^2}dx \\ &= \frac{1}{1-\beta} \end{aligned}$$

where the explicit express for the definite integral can be verified using [22] for $\beta < 1$.

Hence, for a system using pseudorandom (PN) spreading code that has period longer than the spreading factor, we consider decorrelator operation to be desirable for user 1 if

$$N_p(\frac{1}{1-\beta})^2 < \sum_{j=2}^{K} \rho_{1,j}^2 A_j^2 + N_p \tag{4.24}$$

for synchronous system and

$$N_p(\frac{1}{1-\beta})^2 < \sum_{j=2}^{2K-1} \widetilde{\rho}_{1,j}^2 A_j^2 + N_p \tag{4.25}$$

for one-shot detection in asynchronous system, where $\beta = \frac{K}{N}$.

Furthermore, for a system with random spreading codes, we have shown earlier in chapters that $\sum_{j=2}^{K} E[\rho_{j,k}^2] = \frac{K-1}{N}$ for all $j \neq k$ in a synchronous system and that $\sum_{j=2}^{2K-1} E[\widetilde{\rho}_{1,j}^2] = \frac{K-1}{N}$ for all $j \neq k$ for a symbol asynchronous but chip synchronous system. In addition, if we employ perfect power control, we have $A_1 = A_2 = \ldots =$

$A_K = A$. In this case, i.e. with perfect power control and random spreading, we can further simplify our threshold for performing decorrelator to be

$$\begin{aligned} N_p(\frac{1}{1-\beta})^2 &< \frac{K-1}{N}A^2 + N_p \approx \beta A^2 + N_p \\ \longrightarrow \frac{A^2}{N_p} &> \frac{2-\beta}{(1-\beta)^2} \end{aligned} \tag{4.26}$$

for both synchronous and asynchronous system. This threshold actually echoes with our results for the two-user system earlier. It means that decorrelator detection should be performed only if the signal-to-background-noise ratio of each user is larger than a certain threshold, in which case the noise enhancement does not create as much degradation as MAI. In addition, the non-singularity constraint on the correlation matrix, which translates to $\beta < 1$, should also be satisfied for performing decorrelator detection.

In addition to the average eigenvalue, two additional parameters may need to be estimated for the dual-mode detector: the total MAI and the background interference power, which includes thermal noise and intercell interferences. Assuming that we have a method to obtain a rough estimate of the signal amplitudes for each user (such as via a pilot signal [2]), MAI and background interference powers can be estimated as follows. Since the receiver knows the pair-wise cross-correlations among all users, we can use these correlation values and the amplitude estimates to calculate the total MAI power for the user of interest. We can also find the total interference powers at the output of the matched filter by using our amplitude estimates. Then, we can subtract the the MAI power from the estimated overall interference power to estimate the background interference power. Note that in order to decide the detection mode, we do not need very high accuracy in the estimation of amplitudes and interferences.

To summarize, for a system with imperfect power control and random spreading codes, we can use eqs. 4.24 and 4.25 to decided if decorrelator detection is suitable for a particularly user. For a perfect power controlled system, eq. 4.26 can be employed for both synchronous and asynchronous systems. If the receiver finds that decorrelator detection is favorable for over half of the user population, then its operation will be

performed. Otherwise, the symbol decision for each user will be based on the matched filter output.

4.5 Performance verification

Numerical simulations have been performed for an uncoded system (i.e. no channel coding) with BPSK modulation to verify that the proposed detector with our derived decision criterion can achieve similar performance as that of a full decorrelator detector while minimizing the overall complexity. We use a frequency-nonselective and slow-fading channel model, which means each user's signal arrive at the receiver via a single-path with Rayleigh distributed attenuation. We also assume that the receiver for every user has perfect knowledge of the signature waveforms, delays, and amplitudes of all users in the system. All users are spread by a factor of 64 with random spreading codes. The background interferences are modeled as additive white Gaussian noise with varying power over time such that the nominal signal-to-noise ratio for every user is uniformly distributed between 0 and 12 dB. The variations in the background interference power mainly intend to model the intercell interferences from the neighboring cells with different loadings over time.

Figures 4-2 and 4-3 compare the error performances between the dual-mode detector, the one-shot decorrelator, and the matched filter for synchronous and asynchronous CDMA systems, respectively. The bit-error rate (BER) averaged over all users is plotted against the number of users in the system. Each point is averaged over 1000 trials, and within each trial each user transmits 100 symbols continuously. We see that the performance of the dual-mode detector is very close to that of the decorrelator using our decision criterion. Also, for the asynchronous case, because the one-shot correlation matrix occasionally becomes singular, the dual-mode detector actually performs much better than the decorrelator in some cases. Furthermore, it is worth noting that throughout the entire simulation, the dual-mode detector only operates in decorrelator mode 40% of the time, which is a significant saving in processing power.

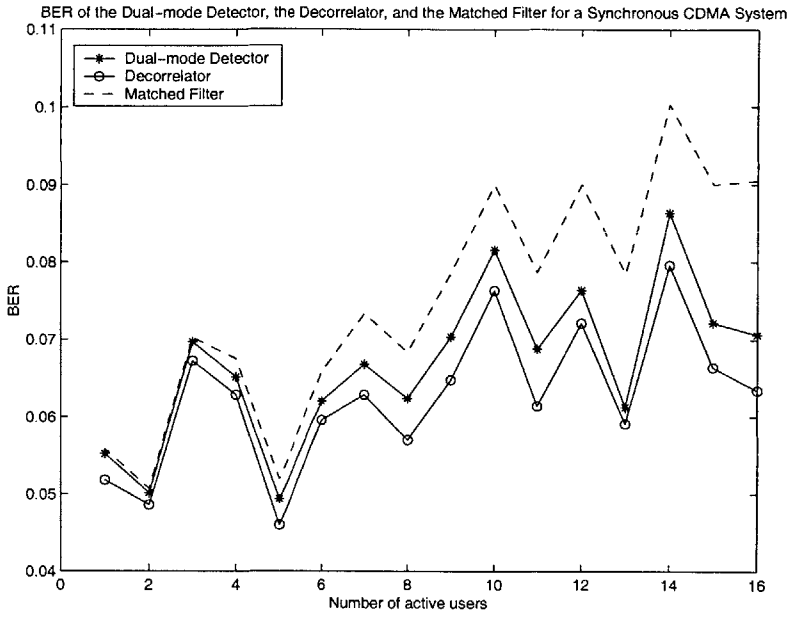

Figure 4-2: Comparison of BER between the dual-mode detector, the decorrelator and the matched filter in a synchronous CDMA system

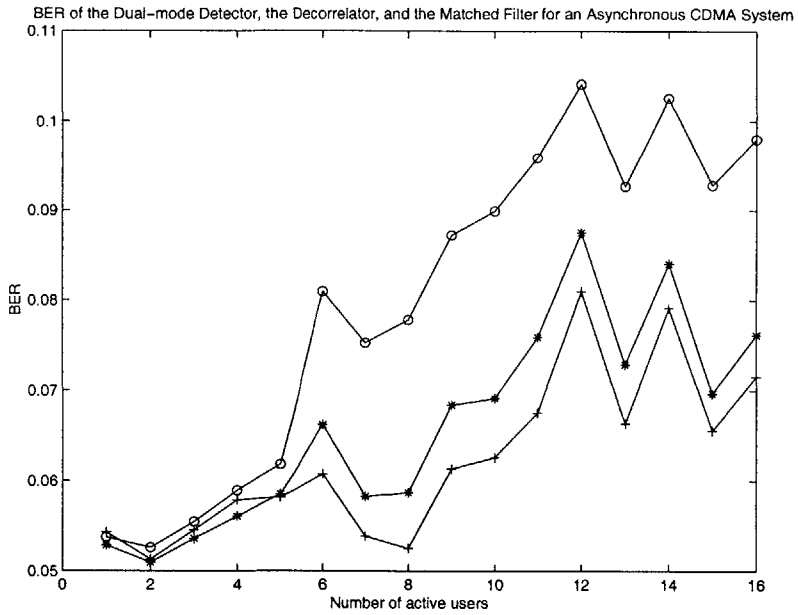

Figure 4-3: Comparison of BER between the dual-mode detector, the decorrelator and matched filter in an asynchronous CDMA system

Nonetheless, we note that there are still small differences between the BER curves of the dual-mode detector and the decorrelator. This gap may be further narrowed by using a switching method that favors more decorrelator operations. The subsequent performance increase, however, will come at the expense of higher computational complexity.

4.6 Chapter summary

In this chapter, we designed a dual-mode linear joint detector that dynamically switches its detection mode between the matched filter and the decorrelator. Our switching criterion is obtained by comparing the error performance of the decorrelator with that of the matched filter. We showed through simulation that the error performance of the proposed receiver is capable of approaching the bit-error rate of the decorrelator while only performing the decorrelating operation 40% of the time.

Chapter 5

Summary and Future Research Directions

Overall, this thesis has addressed three topics. First, we have analyzed and compared the error performances of two promising variable-rate DS-CDMA transmission techniques, namely MCD- and VSG-CDMA for AWGN, flat- and multipath-fading channels. Second, we have derived a class of parallel multistage interference cancellers that exhibits superior performance under the given complexity constraints. Third, we have presented a dual-mode linear multiuser detector that achieves the performance of a decorrelator while consuming significantly less processing power. In this chapter, we briefly summarize the results and point out future research directions for each of the three areas.

5.1 Multirate DS-CDMA transmission techniques

5.1.1 Summary

In this thesis, we compared the error performance of multicode (MCD) and variable-spreading gain (VSG) transmission in the uplink of a DS-CDMA system for a dual-rate system with one high-rate user and multiple low-rate users. We showed that for AWGN channel, at moderately high signal-to-noise ratio, the VSG high-rate user

has a lower error probability than the MCD user when the number of low-rate users is small. In a flat-fading channel, however, VSG and MCD high-rate users exhibit identical error rate, since fading smoothes their interference distributions. For a multipath fading channel, we showed that if the delay spread of the channel is small, then the SIR of the VSG user is worse than that of the MCD user. The reverse is true for channels with large delay spread. We also showed that while for a two-path channel the SIR is a good indication of tradeoffs in error probability, in channels with three or more paths a better SIR does not imply a lower bit-error rate. This phenomenon is mainly due to the asymmetric distribution of the correlated multipath interferences in channels with more than three paths.

5.1.2 Potential follow-up studies

There are a number of future research possibilities to follow-up our study. First, we did not make a definite conclusion on the exact difference between the bit-error rates of MCD and VSG user for channels with three or more paths. Instead we observed that in this case the Gaussian approximation of error probability using SIR may significantly deviates from the exact error probability in some cases. A derivation for the general expression of the exact error rate of MCD and VSG user in multipath channels would nicely complement our research.

Second, in the thesis, we assumed that the user signature sequences are random. The comparison outcomes can significantly change if this assumption has been modified. For instance, it has been shown that if the MCD user only uses Walsh codes but no random code scrambling, its performance in multipath channels will be significantly worse due to the poor autocorrelation property of Walsh codes [18]. It is also possible that the use of certain deterministic sequences with better auto- and cross-correlation properties, such as the ones proposed in [64], can provide MCD users better performance than VSG users.

Third, we assumed the user interferences from other cells to be additive background noise and did not consider interactions between neighboring cells in detail. In reality, a subscriber at cell edge would cause a lot more interferences to the neighbor-

ing cells than one that is near the cell center. Thus, it would be interesting to study the spectral efficiency of MCD and VSG for a general cellular network (i.e. from a multicell perspective) by taking into account both large-scale and small-scale propagation effects. In addition, our error-rate analysis can be extended to systems with more than two rate classes, which is likely to happen in practical multirate CDMA networks.

5.2 Multistage parallel interference cancellation

5.2.1 Summary

In the area of nonlinear multiuser joint detection, we presented two effective multistage weighted parallel interference cancellation algorithms based on stage-by-stage MMSE optimization. The first algorithm is equivalent to a conventional PIC concatenated with a weighting matrix and has a complexity that is on the same order as that of a conventional PIC. Its error performance significantly surpasses that of the conventional PIC, particularly for systems with large user population. The weighting matrix provides an approximate measure on correlations between the previous-stage symbol estimates and the true transmitted symbols. Our second algorithm is more complex than the first technique such that it uses a feedforward matrix and a feedback matrix to suppress the MAI together. Both matrices are derived to jointly minimize the mean-squared cancellation error in each stage. We show that the performance of this algorithm is not only significantly better than our first algorithm but also approaches the single-user performance bound using just a few stages. Its complexity is only on the order of what is required for linear joint detection.

5.2.2 Future research possibilities

While our first algorithm and its suboptimal variations are simple and can be readily implemented in practice using today's technology, the complexity of our second technique is still quite high for practical implementation. To reduce the complexity,

adaptive algorithms can be used to derive the feedback and feedforward processing parameters. However, simple adaptive algorithms, such as the well-known least-mean-square (LMS) algorithm, have slow convergence and can become unstable when the operating condition suddenly changes. For instance, we observed from simulations that if the LMS algorithm is applied in the feedback, its robustness is very sensitive to the number of users. If the coefficients of the LMS is tuned for a system with a large number of users, then its performance will be poor when the number of users becomes small (due to excessive background noise enhancement). The search for a class of reliable and cost-efficient adaptive implementation for both feedforward and feedback matrices is therefore an interesting topic to pursue.

Another interesting idea that can be explored is to apply multistage interference cancellation to coded systems, in which case we can use the output from the channel decoder as previous stage data estimates. In this case, the error probability of the previous stage data bits may be smaller than the corresponding symbol error rate in a uncoded system. A challenge here is to develop a solution that designs the interference cancellation process and the decoder structure jointly to optimize the error performance while maintaining a reasonable complexity.

In addition, we assume the symbol decision devices (after the joint detector) output hard-decision symbols in each stage. It has been shown that using soft-decision quantizers with partial PIC can gain significant performance improvement compared to the coupling of partial PIC and hard-decision estimates[62, 81]. For our proposed receivers, we can also apply soft-decision quantizers to decide the symbol estimates in each stage and use this condition to re-derive the MMSE feedforward and/or feedback matrices to obtain further performance improvement.

5.3 Dual-mode linear multiuser detector

5.3.1 Summary

Finally, this thesis introduced a dual-mode linear multiuser detector for the base-station receiver that dynamically switches its detection mode between the matched filter and the decorrelator. We derived a set of switching criterion and showed through simulation that this receiver is capable of approaching the performance of a decorrelator but using much less processing power. With firmware and DSP implementation, this detector is capable of leading to efficient resource sharing at the base-station receiver.

5.3.2 Future research possibilities

Two follow-up studies can be done for this dual-mode receiver. First, the threshold that we used in this thesis is not necessarily optimal. It is possible to find other simpler or more effective switching criteria that can push the performance of this detector even closer to that of the decorrelator without significantly increasing the complexity. Second, the same philosophy can be extended to other types of detectors such as the linear MMSE detector or even the nonlinear interference cancellers to reduce complexity. Furthermore, we can develop a nonlinear interference canceller that dynamically switches between successive interference cancellation (SIC) and parallel interference cancellation (PIC) according to differences in the user's received power to take advantage of both detection schemes. The benefit in this case is error-performance optimization rather than complexity reduction.

Appendix A

Derivation of the weighting matrix for MMSE-based Multistage Interference Cancellers

In this appendix, we derive the weighting matrix $\mathbf{\Lambda_a}^{(i)}$ for a DS-CDMA system using M-ary phase-shift-keying (M-PSK) modulation, where M is a power of 2. Following our derivation of the MMSE feedback matrix in chapter 3, we see that at stage i, the weighting matrix used in the cancellation process is

$$\mathbf{\Lambda_a}^{(i-1)} = E[\mathbf{b}\hat{\mathbf{b}}^{(i-1)H}]. \tag{A.1}$$

where, as specified in section 5.2, $\mathbf{b}$ is the vector of transmitted symbols and $\hat{\mathbf{b}}^{(i-1)}$ is the vector of the corresponding detected symbols at stage $i-1$. We solve for the diagonal and off-diagonal terms of $\mathbf{\Lambda_a}^{(i)}$ separately. First, assuming all symbols in the M-PSK constellation are transmitted with equal probability, we evaluate the diagonal terms, i.e. $\Lambda_a^{(i)}(m,m)$, as follows:

$$\Lambda_a^{(i)}(m,m) = E[b_m \hat{b}_m^{(i)H}] = \sum_{n=0}^{M-1} \frac{1}{M} E[b_m \hat{b}_m^{(i)H} | b_m = e^{j\frac{2n\pi}{M}}]$$

To find $E[b_m\hat{b}_m^{(i)H}|b_m = e^{j\frac{2n\pi}{M}}]$, we look at the decision regions for M-PSK constellation as shown in figure A-1. For any transmitted symbol b_m, if it is detected correctly, $b_m\hat{b}_m^{(i)H} = 1$. If a mistake is made, however, the detector output has most likely moved into the decision regions of b_m's closest neighbors. The symbol estimate $\hat{b}_m^{(i)}$ will therefore most likely be decoded as $b_m e^{j\frac{2\pi}{M}}$ or $b_m e^{-j\frac{2\pi}{M}}$. It is also possible for $\hat{b}_m^{(i)}$ to be decoded as other symbols besides b_m, $b_m e^{j\frac{2\pi}{M}}$, and $b_m e^{-j\frac{2\pi}{M}}$, but we assume the probability of such event happening to be zero, since in reality, the probability that the detector output falls outside the closest neighbors of b_m is extremely small. In addition, We assume that if an error is made, the detector falls into the two closest (neighboring) decision regions with equal probability. Thus, we evaluate $E[b_m\hat{b}_m^{(i)H}|e^{j\frac{2n\pi}{M}}]$ as

$$\begin{aligned} E[b_m\hat{b}_m^{(i)H}|b_m = e^{j\frac{2n\pi}{M}}] &\approx b_m b_m^H Pr(\hat{b}_m^{(i)} = b_m) + b_m b_m^H e^{j\frac{2\pi}{M}}\frac{1}{2}Pr(\hat{b}_m^{(i)} \neq b_m) \\ &\quad + b_m b_m^H e^{-j\frac{2\pi}{M}}\frac{1}{2}Pr(\hat{b}_m^{(i)} \neq b_m) \\ &= Pr(\hat{b}_m^{(i)} = b_m) + \frac{1}{2}Pr(\hat{b}_m^{(i)} \neq b_m)(e^{j\frac{2\pi}{M}} + e^{-j\frac{2\pi}{M}}) \\ &= 1 - (1 - \cos\frac{2\pi}{M})Pr(\hat{b}_m^{(i)} \neq b_m) \end{aligned}$$

Since $E[b_m\hat{b}_m^{(i)H}|b_m = e^{j\frac{2n\pi}{M}}]$ does not depend on n, we see that

$$\begin{aligned} \Lambda_a^{(i)}(m,m) &= \sum_{n=0}^{M-1}\frac{1}{M}E[b_m\hat{b}_m^{(i)H}|b_m = e^{j\frac{2n\pi}{M}}] \\ &= \frac{1}{M}\sum_{n=0}^{M-1} 1 - (1 - \cos\frac{2\pi}{M})Pr(\hat{b}_m^{(i)} \neq b_m) \\ &= 1 - (1 - \cos\frac{2\pi}{M})Pr(\hat{b}_m^{(i)} \neq b_m) \end{aligned}$$

Since $Pr(\hat{b}_m^{(i)} \neq b_m)$ is basically the error probability for b_m, we can estimate this term on a user-by-user basis. Among the diagonal terms of $\mathbf{\Lambda_a}^{(i)}$, the first K terms measure the reliability the first symbol estimate for users 1 through K, the second K terms measure the accuracy of the users' second symbol estimates, and so on. Therefore, if we let $b_k(l)$ denote the lth symbol transmitted by user k, we have $\Lambda_a^{(i)}(m,m) =$

$E[b_k(l)\hat{b}_k(l)^{(i-1)}]$ for $m = (K-1)l + k$. It is reasonable to assume that $Pr(\hat{b}_k(l)^{(i)} \neq b_k(l)) = Pe_k^{(i)}$ for all l, where $Pe_k^{(i)}$ is the error probability of user k is stage i. Subsequently, we find the diagonal terms of the weighting matrix as

$$\Lambda_a^{(i)}(m,m) = 1 - (1 - \cos\frac{2\pi}{M})Pe_k^{(i)},\ m = K(l-1) + k,\ l, k \in \{1,\ 2,\ ...\ L\}. \quad \text{(A.2)}$$

or equivalently

$$diag(\mathbf{\Lambda_a}) = [\mathbf{w}^{(i)T}\mathbf{w}^{(i)T}\ ...\ \mathbf{w}^{(i)T}]^T$$

where $\mathbf{w}^{(i)} = 1 - (1 - \cos\frac{2\pi}{M})\mathbf{P}^{(i)}$ such that $\mathbf{P}^{(i)} = [Pe_1^{(i)},\ Pe_2^{(i)},\ ...\ Pe_K^{(i)}]^T$.

We proceed to derive the off-diagonal terms. To make the derivation process clear, let's first consider a synchronous CDMA system where each user transmits one symbol only, i.e. $L = 1$ and $\rho_{k,m}^{(0)}(l) = \rho_{k,m}^{(0)}$. In this case, $\mathbf{\Lambda_a}^{(i)}$ becomes a K-by-K matrix, and its diagonal vector equals to $\mathbf{w}^{(i)}$. Each off-diagonal term of $\mathbf{\Lambda_a}^{(i)}$ can be found as

$$\Lambda_a^{(i)}(m,k) = E[b_m\hat{b}_k^{(i)H}],\ m \neq k$$

which measures the effect of user m's symbol on user k's detector output. We see that such effect is caused by the MAI from user m on user k. For $i > 1$, i.e. after at least one cancellation, the effect of MAI becomes small for sufficiently accurate symbol estimates. Thus, for $i > 1$, we approximate $\Lambda_a^{(i)}(m,k)$ to be 0 for all $m \neq k$, $k, m \in \{1,\ 2,\ ...\ K\}$. For the initial stage, i.e. stage 1, where the symbol decisions are made solely based on the matched filter output, the effect of MAI can be quite strong. In this case we choose to compute $\Lambda_a^{(1)}(m,k)$ as follows.

First, we consider the case $M = 2$, i.e. a binary phase-shift-keying (BPSK) modulated system. Assume the transmitted symbols are equally likely being 1 or -1,

we have

$$\begin{aligned}\Lambda_a^{(1)}(m,k) &= E[b_m \hat{b}_k^{(1)H}] \\ &= \frac{1}{2}E[b_m \hat{b}_k^{(1)}|b_k = 1] + \frac{1}{2}E[b_m \hat{b}_k^{(1)}|b_k = -1]\end{aligned}$$

Due to symmetry in the constellation, $E[b_m \hat{b}_k^{(1)}|b_k = 1] = E[b_m \hat{b}_k^{(1)}|b_k = -1] = E[b_m \hat{b}_k^{(1)}]$, it is therefore sufficient to evaluate $E[b_m \hat{b}_k^{(1)}|b_k = 1]$, which can be expressed as

$$E[b_m \hat{b}_k^{(1)}|b_k = 1] = \frac{1}{2}E[\hat{b}_k^{(1)}|b_k = 1, b_m = 1] - \frac{1}{2}E[\hat{b}_k^{(1)}|b_k = 1, b_m = -1]$$

where we solve the first term on the right hand side as

$$\begin{aligned}E[\hat{b}_k^{(1)}|b_k = 1, b_m = 1] &= Pr(\hat{b}_k^{(1)} = b_k|b_k = 1, b_m = 1) \\ &\quad -Pr(\hat{b}_k^{(1)} = -b_k|b_k = 1, b_m = 1) \\ &= 1 - 2Q(\frac{A_k + A_n\rho_{k,m}^{(0)}}{\sqrt{\sigma^2 + MAI_k - (A_n\rho_{k,m}^{(0)})^2}})\end{aligned}$$

where

$$MAI_k = \sum_{m=1, m\neq k}^{K} ((A_m(l)\rho_{k,m}^{(0)})^2.$$

Note that in calculating the error probability for b_k, we applied standard Gaussian approximation to treat the MAI from all users other than user n as white Gaussian noise, which is valid for a system with large spreading gain, perfect power control, and random spreading codes. Similarly, we find that

$$\begin{aligned}E[\hat{b}_k^{(1)}|b_k = 1, b_m = -1] &= Pr(\hat{b}_k^{(1)} = b_k|b_k = 1, b_m = -1) \\ &\quad -Pr(\hat{b}_k^{(1)} = -b_k|b_k = 1, b_m = -1) \\ &= 1 - 2Q(\frac{A_k - A_n\rho_{k,m}^{(0)}}{\sqrt{\sigma^2 + MAI_k - (A_n\rho_{k,m}^{(0)})^2}})\end{aligned}$$

To put the terms together, we find that

$$\begin{aligned}
\Lambda_a^{(1)}(m,k) &= E[b_m \hat{b}_k^{(1)H}] = E[b_m \hat{b}_k^{(1)} | b_k = 1] \\
&= \frac{1}{2}(1 - 2Q(\frac{A_k + A_n \rho_{k,m}^{(0)}}{\sqrt{\sigma^2 + MAI_k - (A_n \rho_{k,m}^{(0)})^2}})) \\
&\quad -\frac{1}{2}(1 - 2Q(\frac{A_k - A_n \rho_{k,m}^{(0)}}{\sqrt{\sigma^2 + MAI_k - (A_n \rho_{k,m}^{(0)})^2}})) \\
&= Q(\frac{A_k - A_n \rho_{k,m}^{(0)}}{\sqrt{\sigma^2 + MAI_k - (A_n \rho_{k,m}^{(0)})^2}}) - Q(\frac{A_k + A_n \rho_{k,m}^{(0)}}{\sqrt{\sigma^2 + MAI_k - (A_n \rho_{k,m}^{(0)})^2}})
\end{aligned}$$

which completes our derivation for the weighting matrix for BPSK modulated systems with synchronous transmission.

To extend the result to a general M-PSK system where M is a power of 2, we evaluate ${\Lambda_a}^{(1)}(m,k)$ as

$$\begin{aligned}
\Lambda_a^{(1)}(m,k) &= E[b_m \hat{b}_k^{(1)H}] \\
&= \sum_{k=0}^{M-1} \frac{1}{M} E[b_m \hat{b}_k^{(1)H} | b_k = e^{j\frac{2k\pi}{M}}]
\end{aligned}$$

An example of M-PSK constellation is shown in figure A-1 for $M = 8$. Due to sym-

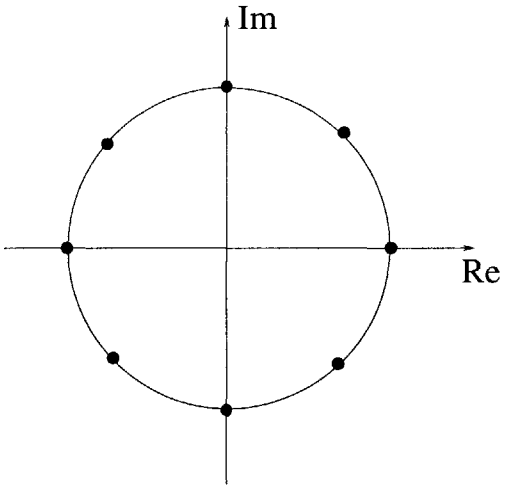

Figure A-1: M-PSK signal constellation for M=8

metry of the constellation and the conjugate symmetric product in the expectation, we see that $E[b_m \hat{b}_k^{(1)H} | b_k = e^{j\frac{2k\pi}{M}}]$ is the same for all $k \in \{0, 2, \ldots M-1\}$. Thus, without loss of generality, we evaluate $E[b_m \hat{b}_k^{(1)H} | b_k = 1]$, which corresponds to $k = 0$ and can be evaluated as:

$$\begin{aligned} E[b_m \hat{b}_k^{(1)H} | b_k = 1] &= \sum_{m=0}^{M-1} e^{j\frac{2m\pi}{M}} E[\hat{b}_k^{(1)H} | b_m = e^{j\frac{2m\pi}{M}}, b_k = 1] \\ &\approx \sum_{m=0}^{M-1} e^{j\frac{2m\pi}{M}} (Prob[\hat{b}_k^{(1)H} = 1 | b_m = e^{j\frac{2m\pi}{M}}, b_k = 1] \\ &\quad + e^{-j\frac{2\pi}{M}} Prob[\hat{b}_k^{(1)H} = e^{j\frac{2\pi}{M}} | b_m = e^{j\frac{2m\pi}{M}}, b_k = 1] \\ &\quad + e^{j\frac{2\pi}{M}} Prob[\hat{b}_k^{(1)H} = e^{-j\frac{2\pi}{M}} | b_m = e^{j\frac{2m\pi}{M}}, b_k = 1]) \end{aligned} \tag{A.3}$$

where the approximation in the second step assumes that, if a symbol error is made, it is most likely for the received signal to fall into the decision regions of the two closest neighboring constellations.

The key to evaluate $E[b_m \hat{b}_k^{(1)H} | b_k = 1]$ lies in finding the three probability terms in eq. (A.3). The first term, $Prob[\hat{b}_k^{(1)H} = 1 | b_m = e^{j\frac{2m\pi}{M}}, b_k = 1]$, is just the probability of correct detection for user k. The second and third terms, i.e. $Prob[\hat{b}_k^{(1)H} = 1 | b_m = e^{j\frac{2m\pi}{M}}, b_k = 1]$ and $Prob[\hat{b}_k^{(1)H} = 1 | b_m = e^{j\frac{2m\pi}{M}}, b_k = 1]$, are the probabilities that the received signal for user k falls into the decision regions of upper and lower closest neighbors, respectively. To evaluate these terms, we first review a fairly accurate geometric approximation for calculating the probability of error for detecting M-PSK signals in a single-user system using matched filter.

Let's consider a single-user communication system operating in an additive white Gaussian noise (AWGN) channel. The matched filter output for each symbol can be expressed as

$$y = Ab + n = |\Xi_y| e^{j\phi_y}$$

where A is the signal amplitude, b is the current transmitted symbol, and n is the noise term modeled as Gaussian random variable with variance σ^2; Ξ_y and ϕ_y are the

amplitude and phase of matched filter output y. Assuming all symbols in the M-PSK signal-set have equal probability of being transmitted, the probability of error using minimum distance detection can be found as

$$\begin{aligned} Pe &= \sum_{m=0}^{M} \frac{1}{M} Prob[error|b = e^{j\frac{2m\pi}{M}}] \\ &= \sum_{m=0}^{M-1} \frac{1}{M} (Prob[\phi_y > \frac{(2m+1)\pi}{M}|b = e^{j\frac{2m\pi}{M}}] \\ &\quad + Prob[\phi_y < \frac{(2m-1)\pi}{M}|b = e^{j\frac{2m\pi}{M}}]) \end{aligned}$$

Due to symmetry in the constellation, $Pr[error|b = e^{j\frac{2m\pi}{M}}]$ is the same for all $m \in \{0, 1, ... M\}$. Therefore, without loss of generality, we consider the case $b = 1$, i.e. $m = 0$, the error probability in which can be expressed as

$$Pr[error|b = 1] = Prob[\phi_y > \frac{\pi}{M}] + Prob[\phi_y < -\frac{\pi}{M}]$$

In order to obtain the exact value of these probability terms, we need to first find the probability density function of y via integration in two-dimensional Gaussian field and then integrate this density function over all possible phase values. This has been done in a number of text books [58, 55, 75]. This procedure, however, gives tedious results that do not yield clear insights. Here, instead of using such an analytical approach, we calculate the error probability using an approximation based on signal-detection geometry.

The geometric representation for detecting y given $b = 1$ is shown in figure A-2. We see that if the signal-to-noise ratio is large enough, i.e. $A \gg \sigma$, the arc distance from point A, which is the mean of the received signal, to the line corresponding to $\frac{\pi}{M}$ is approximately $A \sin \frac{\pi}{M}$. The probability that the phase of y will be greater than $\frac{\pi}{M}$ given $b = 1$ is the same as the probability that the received signal will fall above the line corresponding to $\frac{\pi}{M}$ given the center of gravity is at Ab, which can be evaluated as the error probability in one-dimensional Gaussian detection with minimum distance

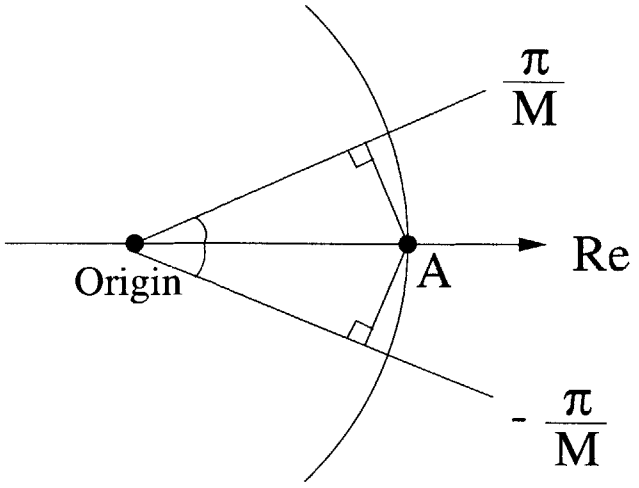

Figure A-2: Geometric representation for M-PSK signal detection in AWGN channel

equals to $A \sin \frac{\pi}{M}$ and can be expressed as

$$Prob[\phi_y > \frac{\pi}{M}] = Q(\frac{A}{\sigma} \sin \frac{\pi}{M}).$$

Similarly, the probability that y will be smaller than $-\frac{\pi}{M}$ can be approximated in the same way as

$$Prob[\phi_y < -\frac{\pi}{M}] = Q(\frac{A}{\sigma} \sin \frac{\pi}{M}).$$

The probability of error for M-PSK modulation in AWGN channel is then

$$Pe^{M-PSK} = 2Q(\frac{A}{\sigma} \sin \frac{\pi}{M}) = 2Q(\sqrt{\gamma} \sin \frac{\pi}{M})$$

where $\gamma = \frac{A^2}{\sigma^2}$ is the signal-to-noise ratio (SNR). This result has also been obtained in an alternative method in [55] via approximations in numerical integration. The accuracy of the approximation increases as M and γ increases. The case where this approximation leads to the most error is for BPSK modulation, i.e $M = 2$. Using the approximation, we have $Pe = 2Q(\sqrt{\gamma})$ whereas in reality, the error probability is $Pe = Q(\sqrt{\gamma})$. They differ by a factor of 2 because in approximation, we assume each

symbol has two closest neighboring constellations, while for BPSK modulation, there is only one neighbor.

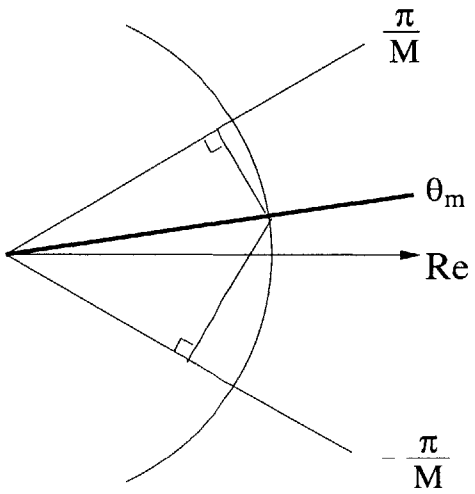

Figure A-3: Geometric representation for M-PSK signal detection with MAI in AWGN channel

Now, we use the same technique to evaluate $E[b_m \hat{b}_k^{(1)H} | b_k = 1]$. Recall from eq. (A.3) that

$$\begin{aligned} E[b_m \hat{b}_k^{(1)H} | b_k = 1] \approx \sum_{m=0}^{M-1} & e^{j\frac{2m\pi}{M}} (Prob[\hat{b}_k^{(1)} = 1 | b_m = e^{j\frac{2m\pi}{M}}, b_k = 1] \\ & + e^{-j\frac{2\pi}{M}} Prob[\hat{b}_k^{(1)} = e^{j\frac{2\pi}{M}} | b_m = e^{j\frac{2m\pi}{M}}, b_k = 1] \\ & + e^{j\frac{2\pi}{M}} Prob[\hat{b}_k^{(1)} = e^{-j\frac{2\pi}{M}} | b_m = e^{j\frac{2m\pi}{M}}, b_k = 1]) \end{aligned} \tag{A.4}$$

We first evaluate $Prob[\hat{b}_k^{(1)} = e^{j\frac{2\pi}{M}} | b_m = e^{j\frac{2m\pi}{M}}, b_k = 1]$ by approximating MAI suffered by user k from all other users, i.e. other than user m, as additive white Gaussian noise. In this case, we note that detecting user k's data given $b_k = 1$ and user m's data $b_m = e^{j\frac{2m\pi}{M}}$ is equivalent to the following detection scenario in AWGN channel:

$$\begin{aligned} y_k &\approx A_k b_k + A_m b_m \rho_{k,m}^{(0)} + \tilde{n} \\ &= A_k + A_m \rho_{k,m}^{(0)} (\cos\frac{2m\pi}{M} + j \sin\frac{2m\pi}{M}) + \tilde{n} \end{aligned}$$

where $\tilde{n}$ is a circularly symmetric complex Gaussian random variable with variance equal to $MAI_k - A_m^2(\rho_{k,m}^{(0)})^2 + \sigma^2$. The geometric representation for the detection process is shown in figure A-3. We see that this case differs from single-user detection in AWGN such that the mean of the phase of y has been tilted by $\theta_{m,k}$, where

$$\theta_{m,k} = \tan^{-1} \frac{A_m \rho_{k,m}^{(0)} \sin \frac{2m\pi}{M}}{A_k + A_m \rho_{k,m}^{(0)} \cos \frac{2m\pi}{M}} \tag{A.5}$$

At the same time, the signal-to-noise ratio of y has become

$$\begin{aligned} \gamma_{m,k} &= \frac{(A_k + A_m \rho_{k,m}^{(0)} \cos \frac{2m\pi}{M})^2 + (A_m \rho_{k,m}^{(0)} \sin \frac{2m\pi}{M})^2}{MAI_k - A_m^2(\rho_{k,m}^{(0)})^2 + \sigma^2} \\ &= \frac{A_k^2 + A_m^2(\rho_{k,m}^{(0)})^2 + 2A_k A_m \rho_{k,m}^{(0)} \cos \frac{2m\pi}{M}}{MAI_k - A_m^2(\rho_{k,m}^{(0)})^2 + \sigma^2} \end{aligned}$$

instead of just $\frac{A_k^2}{\sigma^2}$. Using this model and figure A-3, we can apply the same geometric approximation to evaluate $Prob[\hat{b}_k^{(1)} = e^{j\frac{2\pi}{M}} | b_m = e^{j\frac{2m\pi}{M}}, b_k = 1]$ as in the M-PSK single-user detection case:

$$Prob[\hat{b}_k^{(1)} = e^{j\frac{2\pi}{M}} | b_m = e^{j\frac{2m\pi}{M}}, b_k = 1] \approx Q(\sin(\frac{\pi}{M} - \theta_{m,k})\sqrt{\gamma_{m,k}})$$

Using similar method, we evaluate the second error probability term in A.4 as

$$Prob[\hat{b}_k^{(1)} = e^{-j\frac{2\pi}{M}} | b_m = e^{j\frac{2m\pi}{M}}, b_k = 1] \approx Q(\sin(\frac{\pi}{M} + \theta_{m,k})\sqrt{\gamma_{m,k}})$$

Therefore, the probability of correct detection, i.e. $Prob[\hat{b}_k^{(1)} = 1 | b_m = e^{j\frac{2m\pi}{M}}, b_k = 1]$, can be approximated as

$$\begin{aligned} P_c &= Prob[\hat{b}_k^{(1)} = 1 | b_m = e^{j\frac{2m\pi}{M}}, b_k = 1] \\ &= 1 - Prob[\hat{b}_k^{(1)} = e^{j\frac{2\pi}{M}} | b_m = e^{j\frac{2m\pi}{M}}, b_k = 1] - Prob[\hat{b}_k^{(1)} = e^{-j\frac{2\pi}{M}} | b_m = e^{j\frac{2m\pi}{M}}, b_k = 1] \\ &\approx 1 - Q(\sin(\frac{\pi}{M} - \theta_{m,k})\sqrt{\gamma_{m,k}}) - Q(\sin(\frac{\pi}{M} + \theta_{m,k})\sqrt{\gamma_{m,k}}) \end{aligned}$$

Now we are ready to evaluate $E[b_m \hat{b}_k^{(1)H}]$, which can be expressed as

$$\begin{aligned}
E[b_m \hat{b}_k^{(1)H}] &= E[b_m \hat{b}_k^{(1)H} | b_k = 1] \\
&= \sum_{m=0}^{M-1} \frac{1}{M} e^{j\frac{2m\pi}{M}} (Prob[\hat{b}_k^{(1)} = 1 | b_m = e^{j\frac{2m\pi}{M}}, b_k = 1] \\
&\quad + e^{-j\frac{2\pi}{M}} Prob[\hat{b}_k^{(1)H} = e^{j\frac{2\pi}{M}} | b_m = e^{j\frac{2m\pi}{M}}, b_k = 1] \\
&\quad + e^{j\frac{2\pi}{M}} Prob[\hat{b}_k^{(1)H} = e^{-j\frac{2\pi}{M}} | b_m = e^{j\frac{2m\pi}{M}}, b_k = 1]) \\
&= \frac{1}{M} \sum_{m=0}^{M-1} e^{j\frac{2\pi m}{M}} (1 - Q(\sin(\frac{\pi}{M} - \theta_{m,k})\sqrt{\gamma_{m,k}}) - Q(\sin(\frac{\pi}{M} + \theta_{m,k})\sqrt{\gamma_{m,k}}) \\
&\quad + e^{-j\frac{2\pi}{M}} Q(\sin(\frac{\pi}{M} - \theta_{m,k})\sqrt{\gamma_{m,k}}) + e^{j\frac{2\pi}{M}} Q(\sin(\frac{\pi}{M} + \theta_{m,k})\sqrt{\gamma_{m,k}})) \\
&= \frac{1}{M} \sum_{m=0}^{M-1} e^{j\frac{2m\pi}{M}} (Q(\sin(\frac{\pi}{M} - \theta_{m,k})\sqrt{\gamma_{m,k}})(e^{-j\frac{2\pi}{M}} - 1) \\
&\quad + Q(\sin(\frac{\pi}{M} + \theta_{m,k})\sqrt{\gamma_{m,k}})(e^{j\frac{2\pi}{M}} - 1))
\end{aligned}$$

where simplification in the first step is due to constellation and conjugate symmetry and simplification in the last step is due to the fact that $\sum_{m=0}^{M-1} e^{j\frac{2m\pi}{M}} = 0$.

The accuracy of the approximation is similar to that in M-PSK detection, i.e. the larger the M and A_k are, the more accurate the approximation. Furthermore, let's look at the accuracy of the approximation for the case of BPSK, i.e. $M = 2$. If we assume that $A_k > A_m \rho_{k,m}^{(0)}$, which is usually the case in a system with good power control, we see from the expression in eq. (A.5) that $\theta_{m,k} = 0$ since $\sin m\pi = 0$. In this case, the signal-to-interference ratio becomes:

$$\gamma_{m,k} = \begin{cases} \frac{A_k + A_m \rho_{k,m}^{(0)}}{MAI_k - A_m^2 (\rho_{k,m}^{(0)})^2 + \sigma^2} & \text{if } m = 0 \\ \frac{A_k - A_m \rho_{k,m}^{(0)}}{MAI_k - A_m^2 (\rho_{k,m}^{(0)})^2 + \sigma^2} & \text{if } m = 1 \end{cases}$$

In this setting, we find $E[b_m \hat{b}_k^{(1)H}]$ as

$$\begin{aligned}
E[b_m \hat{b}_k^{(1)H}] &= \frac{1}{2}(-4Q(\gamma_{0,k}) + 4Q(\gamma_{1,k})) \\
&= 2(Q(\frac{A_k - A_m \rho_{k,m}^{(0)}}{MAI_k - A_m^2 (\rho_{k,m}^{(0)})^2 + \sigma^2}) - Q(\frac{A_k + A_m \rho_{k,m}^{(0)}}{MAI_k - A_m^2 (\rho_{k,m}^{(0)})^2 + \sigma^2}))
\end{aligned}$$

which is exactly a factor of 2 from the exact correlation value of $E[b_m \hat{b}_k^{(1)H}]$ for BPSK, which we calculated earlier in this section. This factor of 2 difference is again contributed by the fact that we have considered two closest neighbors in the approximation rather than one.

Finally, we obtain the expression for the off-diagonal terms in $\mathbf{\Lambda_a^{(1)}}$, i.e. $\Lambda_a^{(1)}(m,k)$ for $n \neq k$, as

$$\begin{aligned}
\Lambda_a^{(1)}(m,k) &= E[b_m \hat{b}_k^{(1)H}] \\
&= \frac{1}{M} \sum_{m=0}^{M-1} e^{j\frac{2m\pi}{M}} (Q(\sin(\frac{\pi}{M} - \theta_{m,k})\sqrt{\gamma_{m,k}})(e^{-j\frac{2\pi}{M}} - 1) \\
&\quad + Q(\sin(\frac{\pi}{M} + \theta_{m,k})\sqrt{\gamma_{m,k}})(e^{j\frac{2\pi}{M}} - 1))
\end{aligned}$$

The derivation of $\mathbf{\Lambda_a^{(1)}}$ for synchronous DS-CDMA system using multistage detection is now complete.

To extend our derivation to the asynchronous case, we first take a look at the structure of $\mathbf{\Lambda_a^{(1)}}$ that spans over L symbols, which can be expressed as

$$\mathbf{\Lambda_a}^{(1)} = \begin{bmatrix}
\mathbf{\Lambda}^{(1),0}(1) & \mathbf{\Lambda}^{(1),1}(1) & \mathbf{0} & \dots & \dots & \mathbf{0} \\
\mathbf{\Lambda}^{(1),-1}(2) & \mathbf{\Lambda}^{(1),0}(2) & \mathbf{\Lambda}^{(1),0}(2) & \mathbf{0} & \dots & \mathbf{0} \\
\dots & \dots & \dots & \dots & \dots & \dots \\
\mathbf{0} & \dots & \dots & \mathbf{0} & \mathbf{\Lambda}^{(1),-1}(L) & \mathbf{\Lambda}^{(1),0}(L)
\end{bmatrix}$$

where

$$\begin{aligned}
\mathbf{\Lambda}^{(1),0}(l) &= E[\mathbf{b}(l)\hat{\mathbf{b}}^{(1)H}(l)] \\
\mathbf{\Lambda}^{(1),-1}(l) &= E[\mathbf{b}(l)\hat{\mathbf{b}}^{(1)H}(l-1)] \\
\mathbf{\Lambda}^{(1),1}(l) &= E[\mathbf{b}(l)\hat{\mathbf{b}}^{(1)H}(l+1)]
\end{aligned}$$

The zero terms in the matrix is due to the fact that $E[\mathbf{b}(j)\hat{\mathbf{b}}^{(1)H}(k) = 0$ for $|j-k| > 1$ because for any pair of users, the current symbol of one user does not have an impact through MAI on the symbol of the other user that is transmitted more than one

symbol interval before and after. In other words, each symbol of the desired user are only going to be affected by two symbols from each of the other users, one in the current symbol interval, and one either in the immediate past of future depending on the delay offset.

Our remaining task is to evaluate $\mathbf{\Lambda}^{(1),0}(l)$, $\mathbf{\Lambda}^{(1),-1}(l)$ and $\mathbf{\Lambda}^{(1),1}(1)$. We first look at $\mathbf{\Lambda}^{(1),0}(l) = E[\mathbf{b}(l)\hat{\mathbf{b}}^{(1)H}(l)]$, which is a K-by-K matrix with off-diagonal entries found using our approximation method as

$$\begin{aligned}
\Lambda^{(1),0}(l)_{m,k} &= E[b_m(l)\hat{b}_k^{(1)H}(l)] \\
&= \frac{1}{M}\sum_{m=0}^{M-1} e^{j\frac{2m\pi}{M}}(Q(\sin(\frac{\pi}{M}-\theta_{m,k}(l))\sqrt{\gamma_{m,k}(l)})(e^{-j\frac{2\pi}{M}}-1) \\
&\quad +Q(\sin(\frac{\pi}{M}+\theta_{m,k}(l))\sqrt{\gamma_{m,k}(l)})(e^{j\frac{2\pi}{M}}-1))
\end{aligned}$$

where $m \neq k$ and

$$\begin{aligned}
\theta_{m,k}(l) &= \tan^{-1}\frac{A_m(l)\rho_{k,m}^{(0)}(l)\sin(\frac{2m\pi}{M}+\phi_m-\phi_k)}{A_k(l)+A_m(l)\rho_{k,m}^{(0)}(l)\cos(\frac{2m\pi}{M}+\phi_m-\phi_k)} \\
\gamma_{m,k} &= \frac{A_k(l)^2+A_m(l)^2(\rho_{k,m}^{(0)}(l))^2+2A_k(l)A_m(l)\rho_{k,m}^{(0)}(l)\cos(\frac{2m\pi}{M}+\phi_m-\phi_k)}{MAI_k(l)-A_m^2(l)(\rho_{k,m}^{(0)}(l))^2+\sigma^2}
\end{aligned}$$

where

$$\begin{aligned}
MAI_k(l) &= \sum_{m=1,m\neq k}^{K}((A_m(l)\rho_{k,m}^{(0)}(l))^2 \\
&+ (A_m(l-1)\rho_{k,m}^{(-1)}(l))^2u(\tau_m-\tau_k)+(A_m(l+1)\rho_{k,m}^{(1)}(l))^2u(\tau_k-\tau_m)).
\end{aligned}$$

We next calculate $\mathbf{\Lambda}^{(1),1}(l) = E[\mathbf{b}(l)\hat{\mathbf{b}}_{\mathbf{k}}^{(1)H}(l+1)]$. The diagonal entries of this matrix, i.e. $E[b_m(l)\hat{b}_m^{(1)}(l+1)]$, are all zero because successive transmitted symbols of the same user are independent. For off-diagonal terms, we see that $E[b_m(l)\hat{b}_k^{(1)}(l+1)] =$

0 for all $\tau_m \geq \tau_k$. For the case where $\tau_m \leq \tau_k$, we find that

$$\begin{aligned} E[b_m(l)\hat{b}_k^{(1)}(l+1)] &= \frac{1}{M}\sum_{m=0}^{M-1} e^{j\frac{2m\pi}{M}}(Q(\sin(\frac{\pi}{M}-\tilde{\theta}_{m,k}(l+1))\sqrt{\tilde{\gamma}_{m,k}(l+1)})(e^{-j\frac{2\pi}{M}}-1) \\ &\quad +Q(\sin(\frac{\pi}{M}+\tilde{\theta}_{m,k}(l+1))\sqrt{\tilde{\gamma}_{m,k}(l+1)})(e^{j\frac{2\pi}{M}}-1)) \end{aligned}$$

where

$$\begin{aligned} \tilde{\theta}_{m,k}(l+1) &= \tan^{-1}\frac{A_m(l)\rho_{k,m}^{(-1)}(l+1)\sin(\frac{2m\pi}{M}+\phi_m-\phi_k)}{A_k(l+1)+A_m(l)\rho_{k,m}^{(-1)}(l+1)\cos(\frac{2m\pi}{M}+\phi_m-\phi_k)} \\ \tilde{\gamma}_{m,k} &= \frac{A_k(l+1)^2+A_m(l)^2(\rho_{k,m}^{(-1)}(l+1))^2+2A_k(l+1)A_m(l)\rho_{k,m}^{(-1)}(l+1)\cos(\frac{2m\pi}{M}+\phi_m-\phi_k)}{MAI_k(l+1)-A_m^2(l)(\rho_{k,m}^{(-1)}(l+1))^2+\sigma^2} \end{aligned}$$

Thus, we can express the entries of $\mathbf{\Lambda}^{(1),1}(l)$ as

$$\begin{aligned} \Lambda^{(1),1}(l)_{m,k} &= u(\tau_m-\tau_k)\frac{1}{M}\sum_{m=0}^{M-1} e^{j\frac{2m\pi}{M}}(Q(\sin(\frac{\pi}{M}-\tilde{\theta}_{m,k}(l))\sqrt{\tilde{\gamma}_{m,k}(l)})(e^{-j\frac{2\pi}{M}}-1) \\ &\quad +Q(\sin(\frac{\pi}{M}+\tilde{\theta}_{m,k}(l))\sqrt{\tilde{\gamma}_{m,k}(l)})(e^{j\frac{2\pi}{M}}-1)) \end{aligned}$$

Using similar method, we can find the entries of $\mathbf{\Lambda}^{(1),-1}(l)$ as

$$\begin{aligned} \Lambda^{(1),-1}(l)_{m,k} &= E[b_m(l)\hat{b}_k^{(1)}(l-1)] \\ &= u(\tau_k-\tau_m)\frac{1}{M}\sum_{m=0}^{M-1} e^{j\frac{2m\pi}{M}}(Q(\sin(\frac{\pi}{M}-\bar{\theta}_{m,k}(l-1))\sqrt{\bar{\gamma}_{m,k}(l-1)})(e^{-j\frac{2\pi}{M}}-1) \\ &\quad +Q(\sin(\frac{\pi}{M}+\bar{\theta}_{m,k}(l-1))\sqrt{\bar{\gamma}_{m,k}(l-1)})(e^{j\frac{2\pi}{M}}-1)) \end{aligned}$$

where

$$\begin{aligned} \bar{\theta}_{m,k}(l-1) &= \tan^{-1}\frac{A_m(l)\rho_{k,m}^{(1)}(l-1)\sin(\frac{2m\pi}{M}+\phi_m-\phi_k)}{A_k(l-1)+A_m(l)\rho_{k,m}^{(1)}(l-1)\cos(\frac{2m\pi}{M}+\phi_m-\phi_k)} \\ \bar{\gamma}_{m,k} &= \frac{A_k(l-1)^2+A_m(l)^2(\rho_{k,m}^{(1)}(l-1))^2+2A_k(l-1)A_m(l)\rho_{k,m}^{(1)}(l-1)\cos(\frac{2m\pi}{M}+\phi_m-\phi_k)}{MAI_k(l-1)-A_m^2(l)(\rho_{k,m}^{(1)}(l-1))^2+\sigma^2} \end{aligned}$$

To summarize, we have derived the weighting matrix $\mathbf{\Lambda_a}^{(1)}$ to be used in multistage interference cancellation with MMSE-based feedback matrix for K users (each of

which transmits L symbols) as

$$\mathbf{\Lambda_a}^{(i)} = \begin{bmatrix} \mathbf{\Lambda}^{(i),0}(1) & \mathbf{\Lambda}^{(i),1}(1) & \mathbf{0} & \dots & \dots & \mathbf{0} \\ \mathbf{\Lambda}^{(i),-1}(2) & \mathbf{\Lambda}^{(1),0}(2) & \mathbf{\Lambda}^{(i),0}(2) & \mathbf{0} & \dots & \mathbf{0} \\ \dots & \dots & \dots & \dots & \dots & \dots \\ \mathbf{0} & \dots & \dots & \mathbf{0} & \mathbf{\Lambda}^{(i),-1}(L) & \mathbf{\Lambda}^{(i),0}(L) \end{bmatrix}$$

where

$$\Lambda^{(i),0}(l)_{m,k} = \begin{cases} 1-(1-\cos\frac{2\pi}{M})Pe_k^{(1)} & \text{if } k=m \\ \frac{1}{M}\sum_{m=0}^{M-1} e^{j\frac{2m\pi}{M}}(Q(\sin(\frac{\pi}{M}-\theta_{m,k}(l))\sqrt{\gamma_{m,k}(l)})(e^{-j\frac{2\pi}{M}}-1) & \\ +Q(\sin(\frac{\pi}{M}+\theta_{m,k}(l))\sqrt{\gamma_{m,k}(l)})(e^{j\frac{2\pi}{M}}-1)) & \text{if } k\neq m \text{ and } i=1 \\ 0 & \text{if } k\neq m \text{ and } i>1 \end{cases}$$

$$\begin{aligned} \Lambda^{(i),1}(l)_{m,k} &= u(\tau_m-\tau_k)u(2-i)\frac{1}{M}\sum_{m=0}^{M-1} e^{j\frac{2m\pi}{M}}(Q(\sin(\frac{\pi}{M}-\tilde{\theta}_{m,k}(l))\sqrt{\tilde{\gamma}_{m,k}(l)})(e^{-j\frac{2\pi}{M}}-1) \\ &\quad +Q(\sin(\frac{\pi}{M}+\tilde{\theta}_{m,k}(l))\sqrt{\tilde{\gamma}_{m,k}(l)})(e^{j\frac{2\pi}{M}}-1)) \end{aligned}$$

$$\begin{aligned} \Lambda^{(i),-1}(l)_{m,k} &= u(\tau_k-\tau_m)u(2-i)\frac{1}{M}\sum_{m=0}^{M-1} e^{j\frac{2m\pi}{M}}(Q(\sin(\frac{\pi}{M}-\bar{\theta}_{m,k}(l))\sqrt{\bar{\gamma}_{m,k}(l)})(e^{-j\frac{2\pi}{M}}-1) \\ &\quad +Q(\sin(\frac{\pi}{M}+\bar{\theta}_{m,k}(l))\sqrt{\bar{\gamma}_{m,k}(l)})(e^{j\frac{2\pi}{M}}-1)) \end{aligned}$$

where $u(t)$ equals 1 if $t > 0$ and equals 0 otherwise. This completes our derivation for $\mathbf{\Lambda_a}^{(i)}$.

Now we look at the convergence behavior of $\mathbf{\Lambda_a}^{(i)}$ in a system with random spreading codes, perfect power control and stationary channel (i.e. $A_1(1) = A_2(1) = \dots = A_K(L) = A$) as $K \to \infty$ and $N \to \infty$ while keeping $\frac{K}{N} = \beta$. The expression for the diagonal terms of $\mathbf{\Lambda_a}^{(1)}$ are clearly unaffected, since they only depend on the modulation format and the error probability of each user in the previous stage. The off-diagonal terms, however, are going to vanish, which we show next.

We first examine the asymptotic behavior of $\theta_{m,k}(l)$. Due to perfect power control, we have

$$\begin{aligned}\theta_{m,k}(l) &= \tan^{-1}\frac{A\rho_{k,m}^{(0)}(l)\sin(\frac{2m\pi}{M}+\phi_m-\phi_k)}{A+A\rho_{k,m}^{(0)}(l)\cos(\frac{2m\pi}{M}+\phi_m-\phi_k)} \\ &= \tan^{-1}\frac{\rho_{k,m}^{(0)}(l)\sin(\frac{2m\pi}{M}+\phi_m-\phi_k)}{1+\rho_{k,m}^{(0)}(l)\sin(\frac{2m\pi}{M}+\phi_m-\phi_k)}\end{aligned}$$

For random spreading codes, it has been shown in [56] that $E[\rho_{k,m}^{(0)}(l)] = 0$ and $E[(\rho_{k,m}^{(0)}(l))^2] \propto \frac{1}{N}$. Therefore, as $N \to \infty$, $\rho_{k,m}^{(0)}(l)$ converges to zero in mean-square sense. This means that $\theta_{m,k}(l) \to 0$ as $N \to \infty$. Similar arguments can be made to show that $\tilde{\theta}_{m,k}(l)$ and $\bar{\theta}_{m,k}(l)$ also converge to zero in mean-square sense as the spreading factor becomes infinitely large.

Next, we look at the asymptotic behavior of $\gamma_{k,m}(l)$. As $K \to \infty$, $(A_m\rho_{k,m}^{(0)})^2$ is going to be negligible compared to MAI_k. We therefore can express $\gamma_{k,m}(l)$ as

$$\begin{aligned}\gamma_{k,m}(l) &\to \frac{A^2(1+(\rho_{k,m}^{(0)}(l))^2+2\rho_{k,m}^{(0)}(l)\cos(\frac{2m\pi}{M}+\phi_m-\phi_k))}{MAI_k(l)+\sigma^2} \\ &\to \frac{A^2}{MAI_k(l)+\sigma^2}\end{aligned}$$

where the convergence in the second step is due to the asymptotic behavior of $\rho_{k,m}^{(0)}(l)$ as $N \to \infty$.

Using asymptotic behaviors of $\theta_{m,k}(l)$ and $\gamma_{m,k}$, we see that

$$\begin{aligned}\Lambda^{(1),0}(l)_{m,k} &= E[b_m(l)\hat{b}_k^{(1)H}(l)] \\ &\approx \frac{1}{M}\sum_{m=0}^{M-1} e^{j\frac{2m\pi}{M}}(Q(\sin(\frac{\pi}{M})\sqrt{\frac{A^2}{MAI_k+\sigma^2}})(e^{-j\frac{2\pi}{M}}-1) \\ &\quad +Q(\sin(\frac{\pi}{M})\sqrt{\frac{A^2}{MAI_k+\sigma^2}})(e^{j\frac{2\pi}{M}}-1)) \\ &= \frac{1}{M}Q(\sin(\frac{\pi}{M})\sqrt{\frac{A^2}{MAI_k+\sigma^2}})(e^{-j\frac{2\pi}{M}}+e^{j\frac{2\pi}{M}}-2)\sum_{m=0}^{M-1} e^{j\frac{2m\pi}{M}} \\ &= 0\end{aligned}$$

Using similar procedure, we can also show that

$$\begin{aligned} \Lambda^{(1),1}(l)_{m,k} &\approx 0 \\ \Lambda^{(1),-1}(l)_{m,k} &\approx 0 \end{aligned}$$

Therefore, in a system with perfect power control and random spreading codes, as K and N both approach infinity, $\mathbf{\Lambda_a}^{(i)}$ can be approximated as

$$\mathbf{\Lambda_a}^{(i)} \approx \begin{bmatrix} \mathbf{W^{(i)}} & \mathbf{0} & \mathbf{0} & \ldots & \ldots & \mathbf{0} \\ \mathbf{0} & \mathbf{W^{(i)}} & \mathbf{0} & \mathbf{0} & \ldots & \mathbf{0} \\ \ldots & \ldots & \ldots & \ldots & \ldots & \ldots \\ \mathbf{0} & \ldots & \ldots & \mathbf{0} & \mathbf{0} & \mathbf{W^{(i)}} \end{bmatrix}$$

where $\mathbf{W^{(i)}}$ is a K-by-K diagonal matrix that can be evaluated depending on modulation format of b_k. For a M-PSK modulated system, we found previously that

$$W^{(i)}(k,k) \approx 1 - Pe_k^{(i)}(1 - \cos\frac{2\pi}{M}).$$

Appendix B

Proof of Theorem 4.1 and 4.2

In this appendix, we derive theorems 4.1 and 4.2 by finding a lower bound on the decorrelator SIR for a particular user (w.l.o.g. user 1) in terms of the singular value of the correlation matrix. We first prove theorem 4.1, assuming linear independence between the spreading codes of different users.

Following the decorrelator detector model in section 2, we express $\mathbf{z}$, the soft output vector that contains detection statistics for all users from decorrelator detection, as follows:

$$\begin{aligned} \mathbf{z} &= \mathbf{R}^{+}\mathbf{y} \\ &= \mathbf{R}^{-1}(\mathbf{RAd} + \mathbf{n}) \\ &= \mathbf{Ad} + \mathbf{R}^{-1}\mathbf{n} \end{aligned}$$

Since the detection decision for the data bit of user 1 is made as $\hat{d}_1 = sgn(\mathbf{z}_1)$, the SIR for user 1 with decorrelator detection is

$$\beta_1^{decorr} = \frac{A_1^2}{E[|(\mathbf{R}^{-1}\mathbf{n})_1|^2]}$$

where $(\mathbf{R}^{-1}\mathbf{n})_1$ is the first element in vector $\mathbf{R}^{-1}\mathbf{n}$. The derivation of the lower bound

then proceeds as follows:

$$\begin{aligned}
\beta_1^{decorr} &= \frac{A_1^2}{E[|(\mathbf{R}^{-1}\mathbf{n})_1|^2]} \\
&\geq \frac{A_1^2}{E[|(\|\mathbf{R}^{-1}\|\mathbf{n})_1|^2]} \\
&= \frac{A_1^2}{\|\mathbf{R}^{-1}\|^2 E[n_1^2]} \\
&= \frac{A_1^2}{\sigma_{max}^2(\mathbf{R}^{-1})N_p} \\
&= \frac{A_1^2\sigma_{min}^2(\mathbf{R})}{N_p} \\
&= \eta_{1,sync,ind}
\end{aligned}$$

where $\|\mathbf{R}^{-1}\|$ is the induced 2-norm of $\mathbf{R}^{-1}$ [12].

We now show that this lower bound is obtainable for some noise vector $\mathbf{n}$. Suppose that the singular decomposition of the symmetric matrix $\mathbf{R}$ is $\mathbf{R} = \mathbf{V}\mathbf{\Sigma}\mathbf{V}^T$, the worst case of noise amplification happens when $\mathbf{n} = \mathbf{v}_k$, where $\mathbf{v}_k$ is the singular vector corresponding to the minimum singular value of $\mathbf{R}$ (or the singular vector corresponding to the maximum singular value of $\mathbf{R}^{-1}$). Also note that since $\mathbf{R}$ is symmetric, its singular values equal to the eigen values. Since the noise is white, any subspace orientation for the vector $\mathbf{n}$ is possible. Therefore the lower-bound in theorem 4.1 is achievable. Hence the proof for theorem 4.1 is complete.

Now we use the same approach to prove theorem 4.2 by assuming that the one-shot cross-correlation matrix $\tilde{\mathbf{R}}$ is singular. In this case, the expression of the output vector $\tilde{\mathbf{z}}$ from decorrelator detection is then:

$$\begin{aligned}
\tilde{\mathbf{z}} &= \tilde{\mathbf{R}}^{+}\tilde{\mathbf{R}}\tilde{\mathbf{A}}\tilde{\mathbf{d}} + \tilde{\mathbf{R}}^{+}\mathbf{n} \\
&= \mathbf{V}\begin{bmatrix} \mathbf{\Sigma}^{-1} & \mathbf{0} \\ \mathbf{0} & \mathbf{0} \end{bmatrix}\mathbf{V}^T\mathbf{V}\begin{bmatrix} \mathbf{\Sigma} & \mathbf{0} \\ \mathbf{0} & \mathbf{0} \end{bmatrix}\mathbf{V}^T\tilde{\mathbf{A}}\tilde{\mathbf{d}} + \tilde{\mathbf{R}}^{+}\mathbf{n} \\
&= \mathbf{V}\begin{bmatrix} \mathbf{I} & \mathbf{0} \\ \mathbf{0} & \mathbf{0} \end{bmatrix}\mathbf{V}^T\tilde{\mathbf{A}}\tilde{\mathbf{d}} + \tilde{\mathbf{R}}^{+}\mathbf{n} \\
&= \mathbf{M}\tilde{\mathbf{A}}\tilde{\mathbf{d}} + \tilde{\mathbf{R}}^{+}\mathbf{n}
\end{aligned}$$

where $\mathbf{V}\begin{bmatrix} \mathbf{\Sigma} & \mathbf{0} \\ \mathbf{0} & \mathbf{0} \end{bmatrix}\mathbf{V}^T$ is the singular value decomposition (SVD) of $\tilde{\mathbf{R}}$, with $\mathbf{\Sigma}$ being a L-by-L diagonal matrix containing the L non-zero singular values of $\tilde{\mathbf{R}}$ on the diagonal, where $L < 2K-1$. The matrix $\mathbf{M}$ has elements

$$M_{i,j} = \begin{bmatrix} v_{i,1} & v_{i,2} & \cdots & v_{i,L-1} & v_{i,L} \end{bmatrix} \begin{bmatrix} v_{j,1} & v_{j,2} & \cdots & v_{j,L-1} & v_{j,L} \end{bmatrix}^T$$

where $v_{i,l}$ is the lth element of the ith right singular vector of $\mathbf{R}$. Note that because $\mathbf{V}$ is a $2K-1$-by-$2K-1$ orthogonal matrix, $M_{i,i}$ is always less than or equal to 1.

Now we can express the SIR of decorrelator in this case as:

$$\begin{aligned} \tilde{\beta}_1^{decorr} &= \frac{M_{1,1}^2 A_1^2}{\sum_{i=2}^{K} M_{1,i}^2 A_i^2 + E[|(\tilde{\mathbf{R}}^{-1}\mathbf{n})_1|^2]} \\ &\geq \frac{M_{1,1}^2 A_1^2}{\sum_{i=2}^{K} M_{1,i}^2 A_i^2 + \frac{1}{\tilde{\sigma}_{min}(\tilde{\mathbf{R}})} N_p} \\ &= \tilde{\gamma}_1 \end{aligned}$$

where the inequality follows from the same reason as in the proof of theorem 4.1. The lower bound can be achieved by the same manner as in theorem 4.1. The proof for theorem 4.2 is thus complete.

Bibliography

[1] V. Veeravalli and B. Aazhang, "On the Coding-Spreading Tradeoff in CDMA Systems," *Proc. 1996 Conf. Inform. Sci. Syst.*, Princeton University, Princeton, NJ, Mar. 1996, p. 1136-1141.

[2] F. Adachi, M. Sawahashi, and H. Suda, "Wideband DS-CDMA for Next Generation Mobile Communications Systems," *IEEE Communications Magazine*, Sept. 1998, p. 56-69.

[3] P. Agin and F. Gourgue, "Comparison Between Multicode with Fixed Spreading and Single Code with Variable Spreading Options in UTRA/TDD," *2nd IEEE Workshop on Signal Processing Advances in Wireless Communications, 1999.* p 325-328.

[4] K. Araki, "Fundamental Problems of Nationwide Mobile Radio-telephone System," NTT Rev. Elec. Comm. Lab., 1968.

[5] D. Ayyagari and A. Ephremides, "Cellular Multicode CDMA Capacity for Integrated (Voice and Data) Services," *IEEE Journal on Selected Areas in Communications*, Vol. 17, No. 5, May 1999, p. 928-938.

[6] Z. D. Bai and Y. Q. Yin, "Limit of the smallest eigenvalue of a large dimensional sample covariance matrix," *IEEE Trans. Infor. Theory*, 20:284-287, Mar. 1974.

[7] N. Chan, "Multipath Propagation Effects on a CDMA Cellular System," *IEEE Trans. Veh. Technol.*, vol. 43, Nov., 1994, p. 848-855.

[8] A. Chan and G. Wornell, "A Class of Asymptotically Optimum Iterated-Decision Multiuser Detectors," *Proc. Int. Conf. Acost, Speech, Signal Processing (ICASSP-2001)*, Salt Lake City, UT, May 2001.

[9] K. Cheun, "Performance of Direct-sequence Spread-spectrum RAKE Receivers with Random Spreading Sequences," *IEEE Trans. Commun.*, vol. 45, Sept 1997, p. 1130-1143.

[10] T. Cover and J. Thomas, *Elements of Information Theory*, John Wiley and Sons, Inc., 1991.

[11] E. Dahlman and K. Jamal, "Wide-band Services in a DS-CDMA based FPLMTS System," *Proc. Vehic. Tech. Conf.'96,* Atlanta, GA, May 1996, p. 1656-1660.

[12] M. Dahleh, M. Dahleh, and G. Verghese, "Lectures on Dynamic Systems and Control", Dept. of Elec. Eng. and Comp. Sci., Mass. Inst. Tech., 2000.

[13] A. Duel-Hallen, "Decorrelating Decision-feedback Multiuser Detector for Synchronous CDMA," *IEEE Trans. Commun.,* Vol. 41, pp. 285-290, Feb. 1993.

[14] EIA/TIA Interim Standard, "Cellular System Dual Mode Mobile Station – Land Station Compatibility Specifications," IS-54, *Electronic Industries Association,* May 1990.

[15] M. Fan and K.-Y. Siu, "Weighted Multistage Interference Cancellation Based on Constrained MMSE Optimization," to be submitted to *IEEE J. Select. Area. Comm.*

[16] P.Z. Fan, N. Suehiro, N. Kuroyanagi and X. M. Deng, " Class of binary sequences with zero correlation zone", it IEEE Electronic Letters, vol: 35, issue: 10, May 1999, pp. 777-779.

[17] W. Feller, *An Introduction to Probability Theory and Its Applications,* vol. 1 & 2, Wiley, New York, 1966.

[18] M. Fong, V. K. Bhargava and Q. Wang, "Concatenated Orthogonal/PN Spreading Sequences and Their Application to Cellular DS-CDMA Systems with Integrated Traffic," *IEEE Journal on Selected Areas in Communications.*, Vol. 14, No. 3, April 1996, p. 547-558.

[19] G.D. Forney, "Modulation and Coding for Linear Gaussian Channels," *IEEE Trans. Infor. Theory*, vol. 44, no. 6, October, 1998, pp. 2384-2414.

[20] R. Frenkiel, "A High-capacity Mobile Radio-telephone System," *IEEE Trans. Veh. Tech.*, 1970.

[21] K. S. Gilhousen, *et. al.*, "On the Capacity of a Cellular CDMA System," *IEEE Trans. Veh. Technol.*, vol. 40, May 1991, p. 303-311

[22] I. Gradshteyn and I. Ryzhik, *Table of Integrals, Series, and Products.* Academic Press, San Diego, CA, 1980.

[23] H. Harashima and H. Miyakawa, "A Method of Code Conversion for A Digital Communication Channel with Intersymbol Interference," *IEEE Trans. Comm.*, vol. COM-20, Aug. 1972, p. 774-780.

[24] M. Honig, U. Madhow and S. Verdu, "Blind Adaptive Multiuser Detection," *IEEE Trans. Infor. Theory*, vol. 41, No. 4, July 1995, p. 944-960.

[25] S. Ramakrishna and J. Holtzman, "A Comparison between Single Code and Multiple Code Transmission Schemes in a CDMA System", In *Proceedings of VTC'98*, pages 791-795, Vol. 2, 1998.

[26] J. Holtzman, "A Simple, Accurate Method to Calculate Spread-spectrum Multiple-Access Error Probabilities", *IEEE Transactions on Communications*, Vol. 40, No. 3, March 1992, p. 461-464.

[27] C-L. I and R. D. Gitlin, "Multi-code CDMA wireless personal communication networks," *ICC'95* Seattle, WA, Vol. 2, Page(s): 1060 -1064, June 1995.

[28] C-L. I. and R. D. Gitlin, "Variable Spreading Gain CDMA," *AT&T Lab Notebook*, pp. 9-11, August 1993.

[29] W. Jang, B. Vojcic and R. Pickholtz, "Joint Transmitter-Receiver Optimization in Synchronous Multiuser Communications over Multipath Channels," *IEEE Trans. Comm.*, vol. 46, no. 2, Feb. 1998, p. 269-278.

[30] A. Johansson and A. Svensson, "Analysis of Successive Interference Cancellation Scheme in Multiple Data Rate DS/CDMA Systems," *Technical Report No. 15*, Department of Information Theory, Chalmers University of Technology, Gothenburg, Sweden, August 1995.

[31] M. Kavehrad and J. Salz, "Cross-polarization Cancellation and Equalization in Digital Transmission over Dually Polarized Multipath Fading Channels," *AT&T Technical Journal*, Vol. 64, pp. 2211-2245, Dec. 1985.

[32] Kiran and D. N. C. Tse, " Effective Interference and Effective Bandwidth of Linear Multiuser Receivers in Asynchronous CDMA Systems," *IEEE Trans. Inform. Theory*, vol. 46, July, 2000, p. 1426-1447.

[33] A. Klein, G. Kaleh, and P. Baier, "Zero-Forcing and Minimum Mean-Square-Error Equalization for Multiuser Detection in Code-Division Multiple-Access Channels," *IEEE Trans. Vehicular Technology*, Vol. 45, No. 2, May 1996, p. 276-287.

[34] E. L. Kuan, L. Hanzo, "Joint Detection CDMA Techniques for Third-Generation Transceivers," *Proc. ACTC Mobile Communications Summit*, Rhodes, Greece, June 1998, pp. 727-732.

[35] K. C. Hwang and K. B. Lee, "Performance analysis of low processing gain DS/CDMA systems with random spreading sequences," *IEEE Commun. Lett.*, Vol. 2, No. 12, pp. 315-317, Dec. 1998.

[36] E. Lee and D.G. Messerschmitt, *Digital Communication*, second edition, Kluwer Academic Publishers, ISBN 0-7923-9391-0.

[37] W. C. Lee, "Overview of Cellular CDMA," *IEEE Trans. Vehicular Technology*, Vol. 40, No. 2, May 1991, p. 291-302.

[38] W. Lee, *Mobile Communications Engineering: Theory and Applications*, 2nd ed., New York: McGraw-Hill, 1998.

[39] S. J. Lee, H. W. Lee, and D. K. Sung, "Capacities of Single-code and Multicode DS-CDMA Systems Accommodating Multiclass Services," *IEEE Trans. Vehic. Tech.*, Vol. 48, No. 2, March 1999, p. 376-384.

[40] R. K. Morrow and J. S. Lehnert, "Bit-to-bit Error Dependence in Slotted DS/SSMA Pakcet Systems with Random Signature Sequences," *IEEE Trans Commun.*, Vol. COM-37, pp. 1052-1061, Oct. 1989.

[41] W. C. Y. Lee, "The most spectrum-efficient duplexing system: CDD," *IEEE Commun. Magazine,* vol. 40, no. 3, Mar. 2000, pp. 163-166.

[42] U. Madhow and M. L. Honig, "MMSE Interference Suppression for Direct-Sequence Spread-Spectrum CDMA," *IEEE Trans. Comm.*, Vol. 42, December 1994, p. 3178-3188.

[43] P. Shamain and L. Milstein, "Using Higher Order Constellations with Minimum Mean Square Error (MMSE) Receiver for Severe Multipath CDMA Channel," *Personal, Indoor and Mobile Radio Communications, 1998. The Ninth IEEE International Symposium on*, Vol. 3, 1998, p. 1035-1039.

[44] T. Minn and K.-Y. Siu, "Variable Chip Rate CDMA," *Proc. VTC2000*, May 2000, p. 2267-2271.

[45] T. Minn and K. Y. Siu, "Dynamic assignment of orthogonal variable spreading factor codes in W-CDMA," *IEEE J. Selected Areas Commun.,*, vol. 18, pp. 1429-1440, Aug 2000. Special Issue in Wideband CDMA.

[46] S. Moshavi, "Multi-user Detection for DS-CDMA Communications," *IEEE Communications Magazine*, Oct. 1996, p. 124-136.

[47] M. Mouly and M. Pautet, *The GSM System for Mobile Communication*, ISBN: 2-9507190-0-7, 1992.

[48] T. Ojanpera, R. Prasad, *Wideband CDMA for Third Generation Mobile Communications*, London: Arctech House, 1998.

[49] T. Ottoson and A. Svensson, "Multi-Rate Schemes in DS/CDMA Systems," *Proc. IEEE Vehic. Tech. Conf.,* Chicago, IL, July 25-28, 1995, p. 1006-1010.

[50] T. Ottosson and A. Svensson, "Multi-Rate Performance in DS/CDMA Systems," Technical Report No. 14, Dept. of Information Theory, Chalmers University of Technology, Goteborg, Sweden, 1995.

[51] P. Patel and J. Holtzman, "Analysis of a simple successive interference cancellation scheme in DS/CDMA system," *IEEE J. Select Areas Commun.*, vol. 12, pp. 796-807, June 1994.

[52] R. Pickholtz, D. Schilling and L. Milstein, "Theory of Spread-spectrum Communications–A Tutorial," *IEEE Transactions on Communications,* Vol. COM-30, No. 5, May 1982, p. 855-884.

[53] "Performance of Multirate Techniques in DS-CDMA Systems", http://perth.mit.edu/.

[54] H. V. Poor and S. Verdu, "Probability of Error in MMSE Multiuser Detection," *IEEE Trans. Information Theory*, Vol. 43, No. 3, May 1997, p. 858-871.

[55] J. G. Proakis, *Digital Communications*, 3rd ed., New York: McGraw-Hill, 1995.

[56] D. V. Sarwate, M. B. Pursley, "Partial Correlation Effects in Direct-Sequence Spread-Spectrum Multiple-Access Communication Systems," *IEEE. Trans. Comm.*, Vol. Com-32, May, 1984, p. 567-573.

[57] M. B. Pursley, "Performance Evaluation for Phase-coded Spread-spectrum Multiple-access Communication – Part I: System Analysis," *IEEE Trans. Comm.,* Vol. COM-25, pp. 795-799, Aug. 1977.

[58] T. Rappaport, *Wireless Communications: Principles and Practice.* Upper Saddle River, N.J.: Prentice Hall, 1996.

[59] R.A. Scholtz, "The origins of spread-spectrum communications," *IEEE Trans. Commun.*, Vol. COM-30, No. 5, May 1982, pp. 822-854.

[60] N. Seidl, I. Howitt and J. Richie, "Blind Adaptive Linear Multiuser Detection for Multirate CDMA Systems," *Proc. VTC 2000*, Sept. 2000, p. 1296-1303.

[61] B. Zhu, N. Ansari and Z. Siveski, "Convergence and stability analysis of a synchronous adaptive CDMA receiver" *IEEE Trans. Commun.*, Vol. 43, pp. 3073-3079, Dec. 1995.

[62] D. Divsalar, M. Simon and D. Raphaeli, "Improved Parallel Interference Cancellation for CDMA," *IEEE Trans. Commun.*, Vol. 46, No. 2, pp. 258-268, Feb. 1998.

[63] G. Strang, *Linear Algebra*, Wellesley, MA: Wellesley-Cambridge Press, 1993.

[64] N. Suehiro, "A signal design without co-channel interference for approximately synchronized CDMA systems," *IEEE Journ. Select. Area. Comm.*, vol. 12, no. 5, 1994, pp. 837-841.

[65] TIA/EIA Interim Standard-95, "Mobile station - base station compatibility standard for dual-mode wideband spread spectrum cellular system," July 1993.

[66] CATT, "TD-SCDMA Radio Transmission Technology for IMT-2000 candidate submission", *Proposal to ITU for G3 RTT*, September, 1998.

[67] D. N. C. Tse and S. V. Hanly, "Linear multiuser receivers: Effective interference, effective bandwidth and user capacity," *IEEE Trans. Inform. Theory*, vol. 45, Mar, 1999, p. 641-657.

[68] Y. Chang, D. Tse and D. G. Messerschmitt, "Multimedia CDMA Wireless Network Design: the Link Layer Perspective," *VTC'96.*

[69] G. Turin, "Introduction to Spread-Spectrum Antimultipath Techniques and Their Applications to Urban Digital Radio," *Proceedings of the IEEE*, Vol. 68, No. 3, March 1980, p. 328-353.

[70] M. K. Varanasi and B. Aazhang, "Multistage Detection in Asynchronous Code-division Multiple Access Communications," *IEEE Trans. Commun.*, Vol. 38, pp. 509-519, Apr. 1990.

[71] M. Varanasi, "Group Detection for Synchronous Gaussian Code-division Multiple Access Channels," *IEEE Trans. Infor. Theory*, vol. 41, No. 4, July 1995, p. 1083-1096.

[72] V. V. Veeravalli, "The Role of Coding in CDMA Systems with Multiuser Detection," *1997 IEEE International Conference on Personal Wireless Communications*, p. 470-474.

[73] S. Vembu and A. J. Viterbi, "Two Different Philosophies in CDMA - A Comparison," *IEEE Vehicular Technology Conference, 1996*, Vol. 2, p. 869-873.

[74] S. Verdu, "Minimum Probability of Error For Asynchronous Gaussian Multiple Access Channels," *IEEE Trans. Information Theory*, Vol. IT-32, No.1, Jan. 1986, p. 85-96.

[75] S. Verdu, *Multiuser Detection*, New York: Cambridge University Press, 1998.

[76] S. Verdu and S. Shamai, "Spectral Efficiency of CDMA with Random Spreading," *IEEE Trans. Information Theory*, Vol. 45, No. 2, Mar. 1999, p. 622-639.

[77] P. Viswanath, V. Anantharam, D. Tse, "Optimal Sequences, Power Control, and User Capacity of Synchronous CDMA Systems with Linear MMSE Multiuser Receivers," *IEEE Trans. Infor. Theory*, vol. 45, no. 6, Sept, 1999, p. 1968-1983.

[78] A. J. Viterbi, *CDMA: Principles of Spread Spectrum Communications*, Reading, Massachusetts: Addison-Wesley Publishing Company, 1995.

[79] B. Vojcic and W. Jang, "Transmitter Precoding in Synchronous Multiuser Communications," *IEEE Trans. Comm.*, vol. 46, no. 10, Oct. 1998, p. 1346-1355.

[80] T. Wada, T. Yamazato, M. Katayama, and A. Ogawa, "A Constant Amplitude Coding for Orthogonal Multi-code CDMA Systems," *IEICE Trans. Fundamentals,* Vol. E80-A, No. 12, December 1997, p. 2477-2483.

[81] N. Correal, R. Buehrer and B. Woerner, "A DSP-based DS-CDMA Multiuser Receiver Employing Partial Interference Cancellation," *IEEE J. Select. Areas Commun.*, Vol. 17, No. 4, pp. 613-630, April, 1999.

[82] T. Wong and T. Lok, "Transmitter Adaptation in Multicode DS-CDMA Systems," *IEEE JSAC*, vol. 19, No. 1, Jan. 2001, p. 69-82.

[83] G. Wu, A. Jalali and P. Mermelstein, "On Channel Model Parameters for Microcellular CDMA Systems," *IEEE Trans. Veh. Technol.*, vol. 44, No. 3, August 1995, p. 706-711.

[84] Z. Xie, R. T. Short, and C. K. Rushforth, "A Family of Suboptimum Detectors for Coherent Multi-User Detectors," *IEEE JSAC*, Vol. 8, No. 4, May 1990, pp. 683-90.

[85] K. Yao, "Error Probability of Asynchronous Spread Spectrum Multiple Access Communication Systems," *IEEE Trans Commun.*, vol. COM-25, pp. 802-809, Aug. 1977.

[86] Y. C. Yoon, R. Kohno, and H. Imai, "Cascaded Co-channel Interference Cancelling and Diversity Combining for Spread-spectrum Multi-access Over Multipath Fading Channels," *Symp. Information Theory and its Applications (SITA'92)*, Minakami, Japan, Sept., 1992.

[87] Young, W.R., "Advanced Mobile Phone Service: Introduction, Background, and Objectives," *Bell Systems Technical Journal*, Vol. 58, pp. 1-14, January 1979.

[88] R. Zhang, T. Tihung, H. Zhang and P. He, "BER Performance Comparison of Single Code and Multicode DS/CDMA Channelization Schemes for High Rate Data Transmission," *IEEE Commun. Letters*, vol. 5, No. 2, Feb. 2001, p. 67-69.

3521-18